AD NUMBER

AD905524

NEW LIMITATION CHANGE

TO

Approved for public release, distribution unlimited

FROM

Distribution authorized to U.S. Gov't. agencies only; Test and Evaluation; JUL 1972. Other requests shall be referred to Air Force Materials Command, Wright-Patterson AFB, OH 45433.

AUTHORITY

AFML ltr, 13 Sep 1974

AFML-TR-72-168

INDUCTION MELTING AND CASTING OF TITANIUM ALLOY AIRCRAFT COMPONENTS

THOMAS S. PIWONKA
CHARLES R. COOK
TRW Inc.

TECHNICAL REPORT AFML-TR-72-168
JULY 1972

AIR FORCE MATERIALS LABORATORY
AIR FORCE SYSTEMS COMMAND
WRIGHT-PATTERSON AIR FORCE BASE, OHIO 45433

NOTICES

When Government drawings, specifications, or other data are used for any purpose other than in connection with a definitely related Government procurement operation, the United States Government thereby incurs no responsibility nor any obligation whatsoever; and the fact that the government may have formulated, furnished, or in any way supplied the said drawings, specifications, or other data, is not to be regarded by implication or otherwise as in any manner licensing the holder or any other person or corporation, or conveying an rights or permission to manufacture, use, or sell any patented invention that may in any way be related thereto.

Copies of this report should not be returned unless return is required by security considerations, contractual obligations, or notice on a specific document.

INDUCTION MELTING AND CASTING OF TITANIUM ALLOY AIRCRAFT COMPONENTS

Thomas S. Piwonka

Charles R. Cook

FOREWORD

This Final Technical Report covers the work performed under Contract F33615-70-C-1409 from March 1970 to July 1972. The manuscript was released by the author in July, 1972 for publication.

This contract with TRW Inc., Cleveland, Ohio was initiated under Manufacturing Methods Project 164-0. The work was administered under the technical direction of Mr. W.T. O'Hara and Mr. K.L. Love, AFML/LTM of the Manufacturing Technology Division, Air Force Materials Laboratory, Wright-Patterson Air Force Base, Ohio 45433.

Mr. C.R. Cook, Section Manager, Materials Development Department, TRW Equipment Group, was responsible for program management. Dr. T.S. Piwonka and Mr. E. M. Grala were project engineers responsible for the execution of the technical effort. The authors acknowledge the contributions of Mr. W. H. Schweikert, General Electric Company, Evendale, Ohio for the mold production effort.

This project was accomplished as part of the Air Force Manufacturing Methods program, the primary objective of which is to implement, on a timely basis, manufacturing processes, techniques, and equipment for use in economical production of USAF material and components.

Your comments are solicited on the potential utilization of the information contained herein as applied to your present and future production programs. Suggestions concerning additional manufacturing methods required on this or other subjects will be appreciated.

This technical report has been reviewed and is approved.

H. A. JOHNSON
Chief, Metals Branch
Manufacturing Technology Division

ABSTRACT

Induction melting of titanium alloys using a semi-levitation technique and bottom pouring in a graphite crucible was evaluated for four titanium alloys, Ti-6Al-4V, Ti-6Al-2Sn-4Zr-2Mo, Ti-3Al-8V-6Cr-4Mo-4Zr (Beta C), and Ti-11Mo-4.5Sn-6Zr (Beta III). Precision investment (lost wax) casting molds coated with pyrolytic graphite were used with the melting technique to make castability, tensile specimen, and bearing housing segment castings. Castability and tensile properties of the alloys were characterized. Bearing housing segments were subject to porosity, which was extensively studied. Process capabilities and limitations were investigated for induction melting and the pyrolytic graphite coated mold . Properties of castings were determined, and weldability of the four cast alloys evaluated. Effects of the casting process on microstructure were investigated.

TABLE OF CONTENTS

TABLE OF CONTENTS (cont'd)

LIST OF FIGURES

LIST OF FIGURES (cont'd)

LIST OF FIGURES (cont'd)

LIST OF TABLES

I INTRODUCTION

As demands on aircraft engine performance have increased during the past two decades, efforts have been intensified to produce power plants with improved thrust-to-weight ratios. One of the techniques by which this may be accomplished is through the use of low density materials in engine components. Because of its high strength-to-weight ratio, good medium temperature properties, and corrosion resistance, titanium is an attractive material for aircraft engine parts. Designers have made wide use of forgings of titanium alloys both as rotating and as structural members of engine assemblies. The forging process lacks, however, the versatility of metal casting, and there is thus great interest in expanding the use of titanium through the application of titanium castings in engines.

Titanium castings have not been widely used to date because of processing problems which have both limited the quality and resulted in high production costs of castings. The high reactivity of molten titanium and its alloys has hindered full utilization of this metal in its cast form. The difficulty of melting and holding a titanium alloy in a crucible, without dissolving the crucible, has led to the development and use of cold-crucible melting techniques, such as consumable electrode, and electron beam melting systems. To these has recently been added electroslag processes and non-consumable electrode methods.

Currently, the bulk of titanium castings are produced by melting in a consumable electrode skull furnace. This method has the advantage of avoiding contamination of the melt with crucible materials. However, it also has a number of serious disadvantages, some technical, some economic. For instance, high operator skill is required to control the melt, which limits heat reproducibility.

There is also the difficulty of achieving melt superheat temperatures and the difficulty of controlling power input. Because the liquid metal is in contact with metal frozen against the skull, superheating is limited. When the arc is turned off to permit pouring, the bath begins to freeze immediately in the crucible, necessitating a fast pour, which can cause erosion of the mold and resultant inclusions in the casting. The addition of electron beam guns to superheat the bath does not affect the temperature gradient in the crucible. This gradient is a problem itself, for it means that the hottest metal is poured into the mold first, while the last metal poured, which goes into the riser, is the coldest, defeating attempts to set up favorable temperature gradients for directional solidification in the casting.

Electron beam melting of titanium also uses a skull to prevent contamination of the melt. Its main advantage lies in the fact that superheat temperatures can be achieved and scrap can be reprocessed without welding into an electrode. Its main disadvantages are the large power requirements, longer melt cycles, higher vacuums, and more expensive control equipment. In addition, the very high temperature of the electron beam volatilizes low melting point alloy constituents (such as aluminum), requiring adjustments in charge composition.

In an attempt to overcome the inherent deficiencies of cold wall melting techniques, TRW developed a crucible melting process for titanium alloys. The demonstration of this process as a commercial production method was one of the objectives of this program.

A second objective of the program was the demonstration of a mold material suitable for titanium casting. Molds used for titanium castings must be adaptable to precision investment casting methods; they must be able to be preheated to temperatures high enough to permit filling of thin sections; they must be able to resist the attack of liquid titanium long enough to permit favorable thermal gradients to be set up; and, they should cause no case to form on the casting as a result of chemical attack. Three approaches have been taken:

1) use of a very stable oxide mold,

2) use of carbonaceous mold, and

3) use of a refractory metal interface on the surface of the mold.

The oxide mold approach requires a chemical milling operation to remove a surface case. The refractory metal mold requires expensive equipment and processing steps to avoid oxidation of the mold during mold forming and firing. So far, this mold has not demonstrated the ability to be heated to temperatures above 700-800°F prior to pouring without causing mold defects.

For these reasons, neither oxide nor refractory metal molds were used in this study. Instead, the molds used in this work were pyrolytic graphite coated ceramic, provided by the General Electric Company. These molds are prepared by making a conventional lost wax ceramic shell mold, employing ceramic materials and techniques usually used in lost wax casting technology, and then coating its interior with pyrolytic graphite to form a nonreactive barrier between the molten titanium and the mold ceramic.

II EXPERIMENTAL PROGRAM

A. Melting Point Determinations

Information on liquidus and solidus temperatures of titanium alloys is generally unknown. Thus information on the range of mushy zone, which influences such items as alloy castability and shrinkage porosity must be guessed at by foundrymen, hindering their efforts to produce sound castings. For this reason, TRW undertook to determine the liquidus and solidus temperatures of the four alloys used in this program.

1. Method

The method used is that of Cadoff and Nielson (1), in which a 0.375" cube of the alloy in question is placed on a niobium plate within a test chamber. The plate is heated by resistance and it in turn heats the specimen cube. The cube is viewed optically, and its temperature is monitored by an optical pyrometer. The solidus temperature is taken as that temperature at which the corners begin to round, and the liquidus temperature as that temperature when the specimen slumps and runs along the niobium strip.

The specimens were melted in a dry argon atmosphere (argon was dried by passing over titanium chips at 1600°F). Twenty minutes was required to melt each specimen. Their appearance after melting is shown in Figure 1. Temperature measurements were made by a Pyro-Eye two-color optical automatic reading pyrometer. This instrument is a product of Instrument Development Laboratories of Attleboro, Massachusetts; its accuracy at 3000°F is ± 35°F.

2. Results

Results are given in Table I. The beta alloys have lower liquidus and solidus temperatures and shorter mushy zones than the alpha-beta alloys investigated. Chemical analyses for these alloys are shown in Table II.

A note of caution should be added on interpretation of the temperature data. The affinity of liquid titanium for all other materials is well known. Thus there was some alloying found with the niobium plate, as shown in Figure 2, which gives electron beam microprobe photos above, at, and below the interface between the strip and the cube. Although these photos are only qualitative, they show that there has been Nb diffusion into the titanium alloy sample. Nb is expected to raise the alloy liquidus and solidus temperatures (2).

As a further check on the accuracy of the measurements, the melting point of pure titanium was determined using the above method. It was found to be 2900 ± 35°F, which compares quite well with the value reported recently by Reed (3) of 2930 ± 18°F.

Figure 1. Appearance of Melting Point Determination Specimen.

TABLE I

Melting Temperature Determinations

		Ti-6Al-4V	Ti-6Al-2Sn-4Zr-2Mo	Beta C	Beta III
Liquidus Temperature, °F	Average (No. Detmn.)	3205 (2)	3120 (2)	3000 (2)	3073 (3)
" "	Range	3200-3210	3080-3160	2940-3060	2980-3120
Solidus Temperature, °F	Average (No. Detmn.)	2914 (4)	2890 (4)	2829 (4)	2863 (3)
" "	Range	2890-2940	2860-2935	2815-2850	2850-2880
Average Liquidus - Solidus Range °F		293	230	171	212

TABLE II

Chemical Analyses of Titanium Alloy Melt Stock

Alloy	Heat No.	Chemical Composition w/o										
		Al	V	Sn	Zr	Cr	Mo	Fe	O	N	H	C
Ti-6Al-4V[a]	Futura Titanium G-7571	6.3	4.2					.12	.16	.009	.009	.022
Ti-6Al-2Sn-4Zr-2Mo[b]	RMI 303487	6.2		2.0	4.2		1.8	.06	.124	.008	.0052	.02
Ti-3Al-8V-6Cr-4Mo-4Zr	RMI 303973	3.3	8.1		3.9	5.9	4.2	.07	.094	.010	.0046	.03
Beta III Titanium[c]	Cruc. K 50654			4.5	6.0		11.0	.05	.15	.01	.0041	.02

(a) Purchased to AMS 4928D

(b) Purchased to AMS 4975

(c) Purchased to AMS 4977

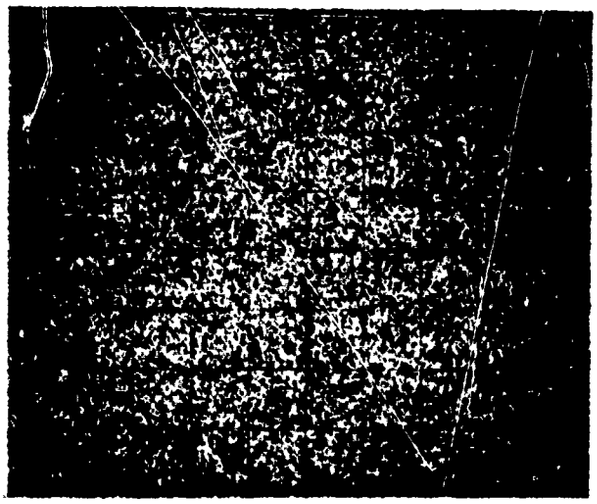

Ti alloy sample,
.04 inches above
interface

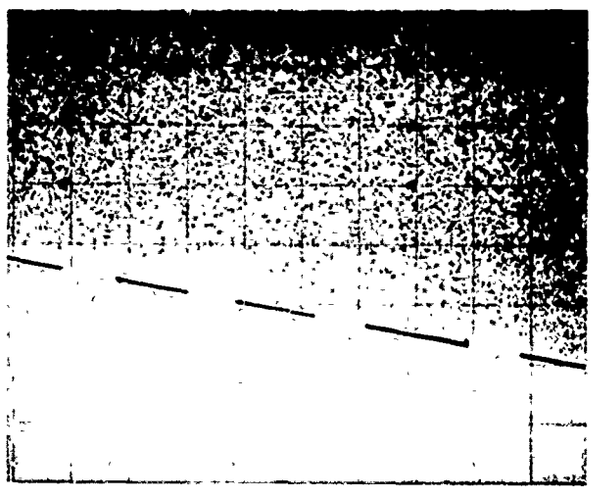

Interface

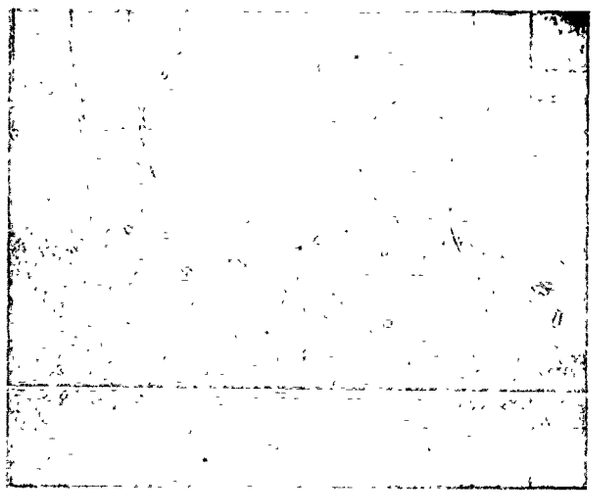

Cb strip
.05 inches below
interface

Figure 2. Columbium Fluorescence above, at, and below Cb-Ti Alloy Interface in Melting Determination. 500X

B. Casting Process

1. TRW Melting Technique

a. Melting Furnace and Procedure

TRW has developed a system which permits induction melting and pouring of titanium-base alloys. In view of the history of unsuccessful attempts (4-6) to find a truly non-reactive crucible, and the inherent limitations of levitation melting (7), we have developed a melting method which permits a controlled amount of crucible contamination, but limits this by making use of levitation forces generated during induction melting, in much the same way as did Ahearn (8,9), in earlier work at Watertown Arsenal.

The TRW technique minimizes the time which the molten metal is in contact with a graphite crucible, and provides a rapid direct pour into the mold. A schematic sketch of the process is shown in Figure 3.

The salient features of the process are:

1) the titanium is brought to a temperature just below the melting point of the alloy and soaked at this temperature for several minutes.

2) at this point the power input is markedly increased to melt the charge,

3) the molten titanium melts the bottom melt-out disc. (This normally occurs within approximately one minute of the time the power is increased) resulting in a direct pour of superheated metal into the mold.

The charge is suspended from a titanium rod within a machined high purity graphite crucible. The crucible wall thickness is kept below 0.100" to minimize its effect as a susceptor of the induction field. Crucibles are machined from extruded tubes of Graphitite G, a product of the Carborundum Co. This material is a high density, fully graphitized, small particle size (.008") graphite. It was selected for its combination of purity, density, machinability, and high strength (9500 psi). Power is applied at about 1/3 - 1/2 maximum melt power to heat the charge to the incipient melting point, whereupon full power is applied. The charge melts very rapidly and drops off onto the disc. Because of the high power inputs, (approximately 10 kw per pound of charge) the melt is violently stirred and is partially levitated during melting, and thus does not rest against the crucible walls. The levitation effect is visibly enhanced by the presence of the suspension rod.

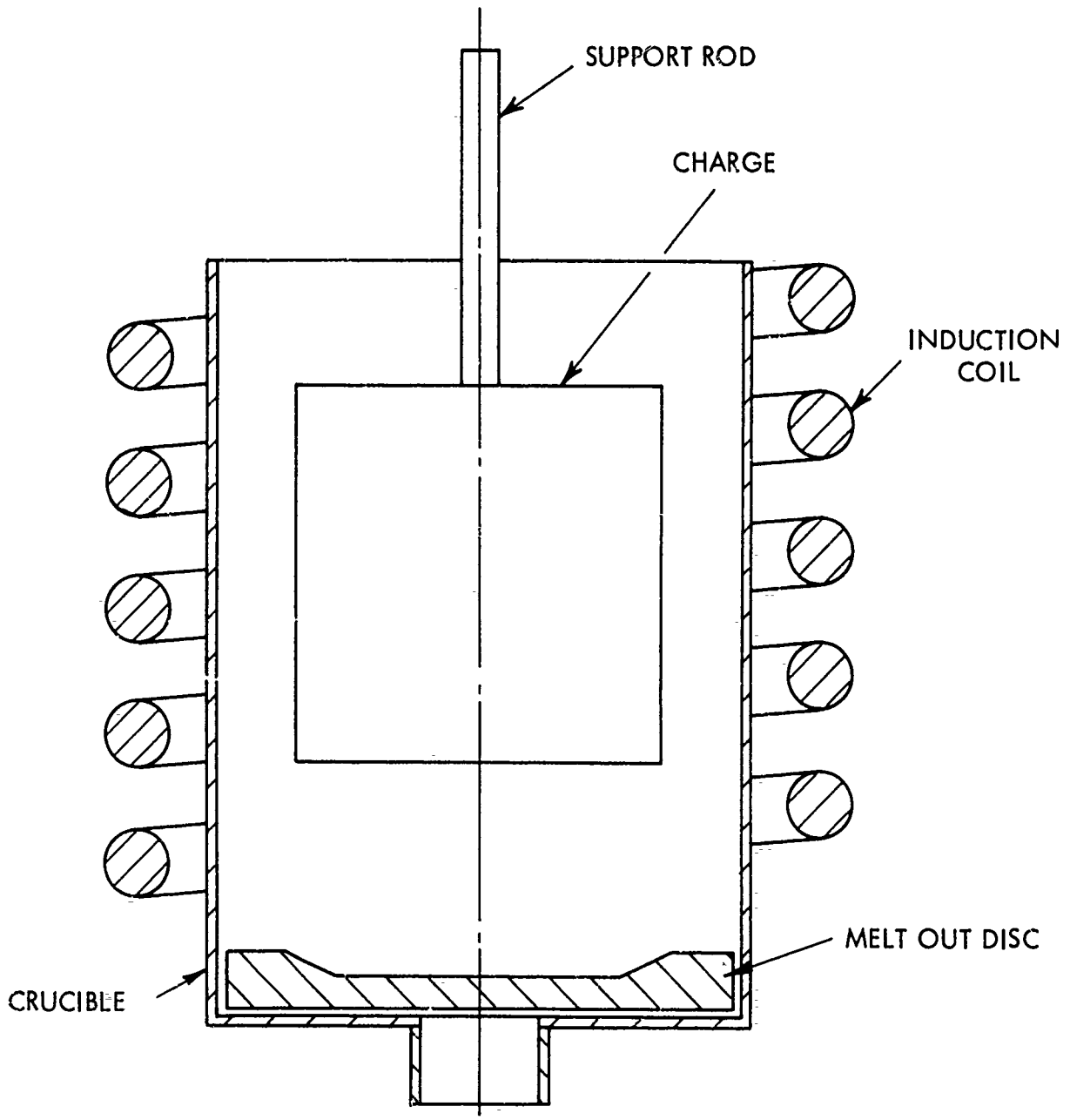

Figure 3. Diagram of Induction Melting Furnace for Titanium Alloys.

Because the heat is induction melted, it is at a uniform temperature, which remains constant during pouring. This may be demonstrated by referring to Figure 4, which is the output trace from an infrared pyrometer. Notice that the temperature of the melt remains constant from the time that it first registers on the pyrometer until it is discharged from the crucible, a period of a little more than a minute. This behavior is a feature of the process, and was verified in repeated runs. This means that melting through the disc in less than a minute (as might be the case if a thinner disc was used) or keeping the metal in the crucible for longer periods of time (by using a thicker disc) will have no effect on the final melt temperature. This finding is consistent with present theories of levitation melting (10), which show that the molten metal reaches a steady-state configuration which is a function of energy input (frequency, power) and coil design, radiation losses, and surface tension. Once this steady state is reached, longer times at constant power inputs have no effect on bath temperature Furthermore, increased power inputs will also have no effect, as they will be balanced by radiation heat loss and energy losses required to maintain the stability of the surface. Thus the TRW induction melting method does not permit superheat control, except by varying coil designs and melting frequencies, a process which does not lend itself to economical production of a product mix of many different parts.

b. Temperature Measurement of Molten Titanium

Because of the high melting point of titanium alloys, few bi-metallic thermocouple systems are candidates for immersion pyrometers. Of these, W-W/Re couples have been used successfully for measuring casting cooling (11,12) in the mold. These couples are sheathed in tantalum or molybdenum to protect them for the short time the alloy is molten. They are, however, dissolved by the molten titanium, particularly when placed in heavy sections or in pouring basins and sprue wells. This experience has discouraged the use of refractory metal sheaths to protect thermocouples immersed in molten metal baths. Oxide refractory protection tubes cannot be used because of molten metal attack of those oxides possessing adequate thermal shock resistance, and lack of thermal shock resistance of those oxides which resist attack by molten titanium.

Optical methods are,therefore, used to monitor melt temperatures. Two-color pyrometers, operating in the visible portion of the spectrum, have been adequate for temperature measurements in the vicinity of 3000°F. However, problems were encountered when they were used to determine superheat temperatures during induction melting trials. The instruments experienced an output instability in the range 3150-3700°F which made reliable determination of temperatures impossible. The instability was traced to the combination of input signal from the violently agitated melt, and the optics and logic curcuit, which were not designed to accommodate the rapidly occurring temperature fluctuations experienced in this temperature range. As few metals are melted in the range 3150-3700°F (steels have lower melting temperatures, columbium alloys and the refractory metals higher temperatures), the problems encountered in melting titanium alloys do not affect the general usefulness of these instruments, which, properly used, are valuable metallurgical tools. For titanium it has been necessary to find another way of measuring the bath temperature.

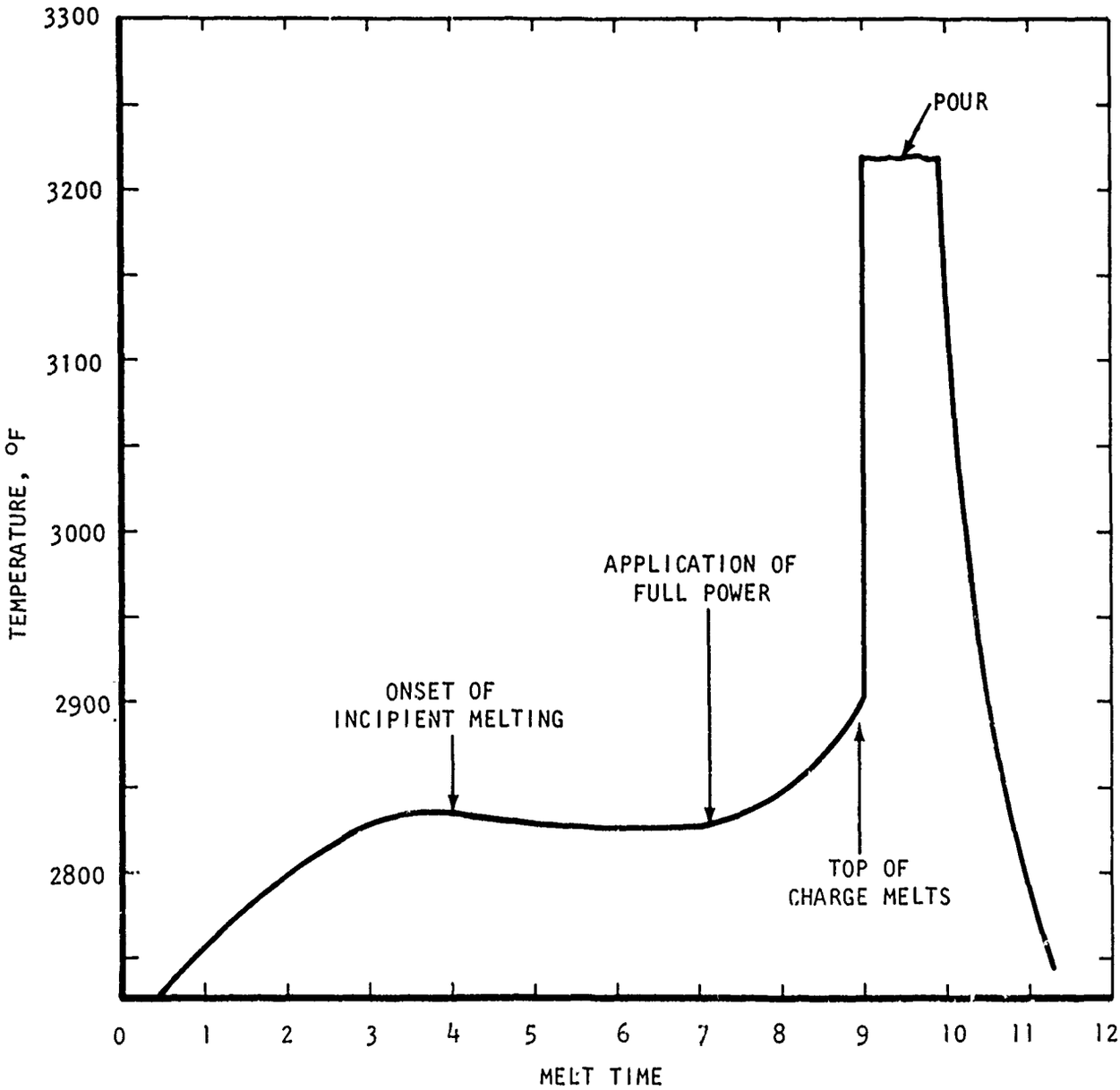

Figure 4. Output Trace from Infrared Pyrometer During Melt.

Infrared pyrometry was suggested as these pyrometers are similar to optical pyrometers, except that they operate by using the infrared spectrum instead of the visible spectrum. In optical pyrometers, the input signal is the radiation from the heated body. This is a function of both the temperature of the body and its emissivity. Unfortunately, the emissivity is also a function of the temperature (10). In the infrared range of the spectrum emissivity varies less with temperature than it does in the visible range. This means that, in the case of measuring a rapidly fluctuating temperature, as in a rapidly stirred melt approaching thermal equilibrium, the infrared pyrometer will read the temperature without being affected by the emissivity changes that would be a cause of errors in the optical pyrometer.

In order to evaluate the capability of infrared pyrometry to record the melting of titanium, a Temptron Model IT 7-A infrared pyrometer, made by Barnes Engineering Co., of Stamford, Conn., was obtained. The unit is shown in Figure 5. Four melts were made using this unit, and the melting arrangement shown in Figure 6. The sensing unit was focused on the shallow hole drilled in the top of the charge. Results of four heats are given below:

Heat	Alloy	Pour Temperature
G 6927	Ti 6Al-2Sn-4Zr-2Mo	3128°F
G 6928	Ti 6Al-4V	3200°F
G 6929	Ti 6Al-2Sn-4Zr-2Mo	3146°F
G 6930	Ti 6Al-4V	3110°F

(values are $\pm$ 1.5%)

These values check well with those obtained from a tungsten-tungsten rhenium couple protected by a molybdenum sheath and placed in pour cups to record the temperature of the falling stream. Thermocouple temperatures were as follows:

Heat	Alloy	Pour Temperature
G 6027	Ti 6Al-4V	3241°F
G 6047	"	3122°F
G 6028	"	3053°F
G 6055	"	3077°F
G 6048	Ti 6Al-2Sn-4Zr-2Mo	3056°F
G 6052	"	3065°F
G 6054	"	3155°F
G 6053	"	3095°F

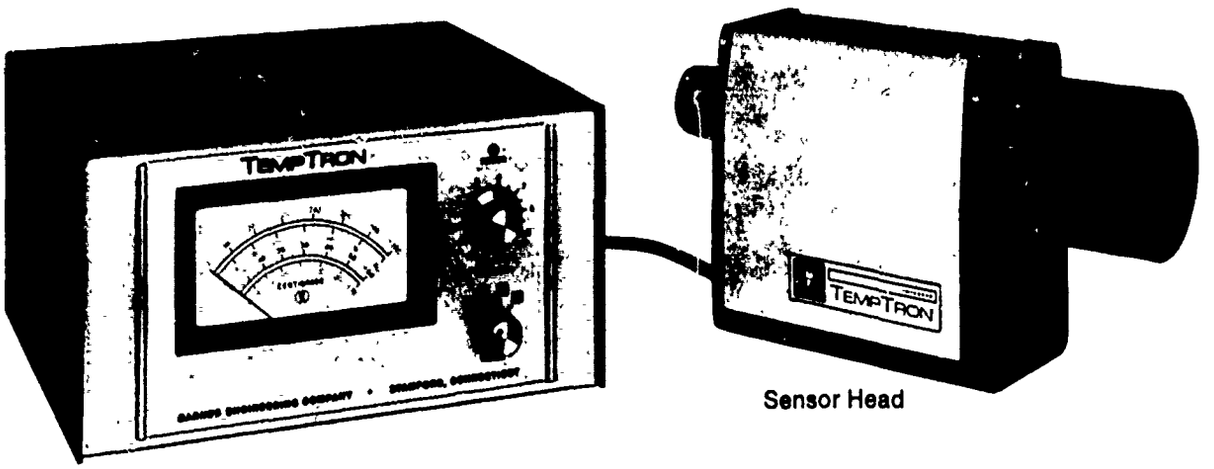

Figure 5. Barnes Engineering Co., Temptron Model IT 7-A Infrared Pyrometer.

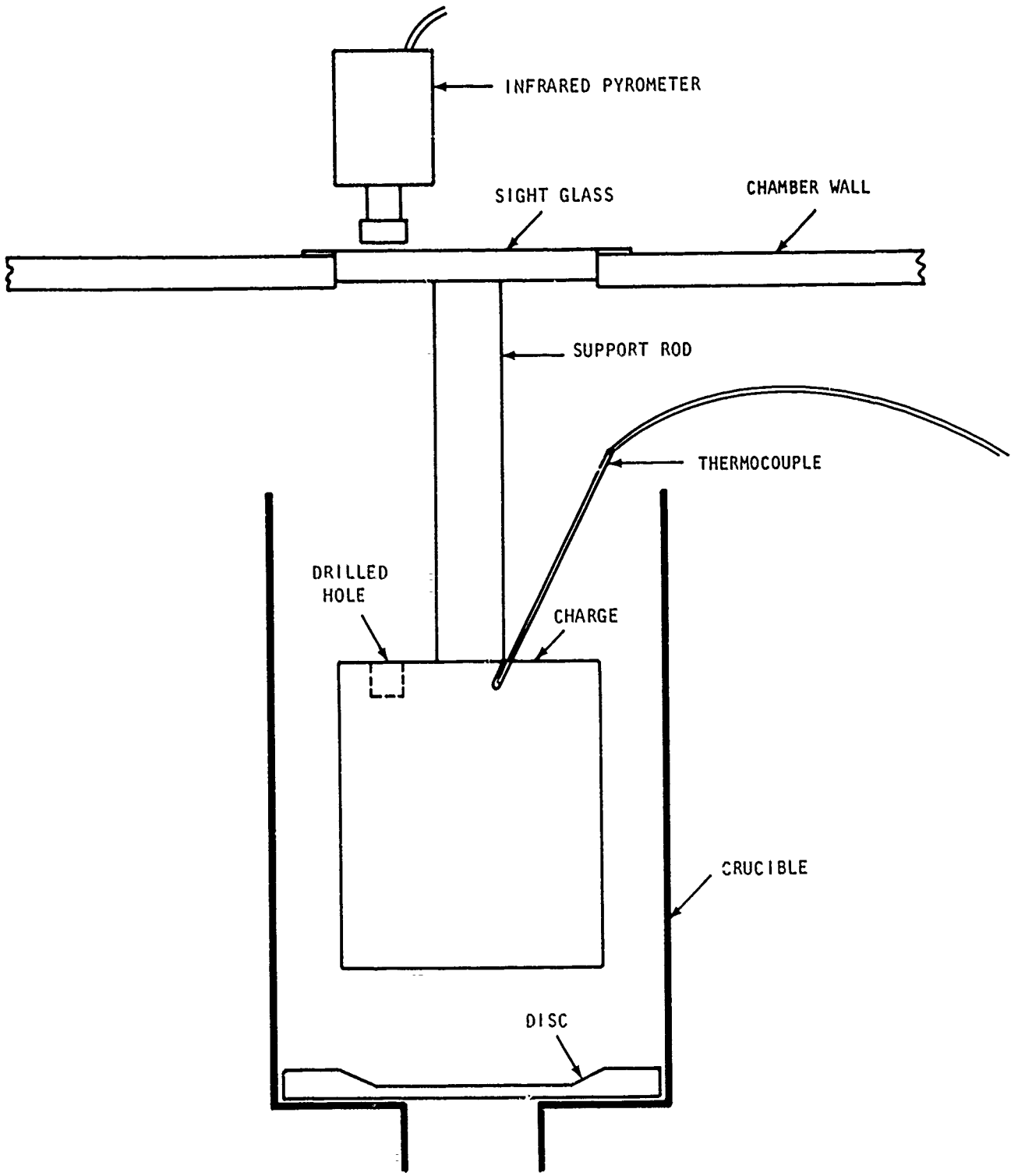

Figure 6. Melting Arrangement for Evaluation of Infrared Pyrometer.

Heat	Alloy	Pour Temperature
G 6065	Ti 3Al-8V-6Cr-4Zr-4Mo	2938°F
G 6064	"	2960°F
G 6081	"	2817°F
G 6080	"	2839°F
G 6095	"	2877°F
F 6094	"	2857°F

A particular advantage of the Barnes pyrometer is that emissivity corrections can be made on the instrument during the measurement. These corrections were made by adjusting the emissivity correction control on the pyrometer until the indicated temperature on the unit corresponded with the reading of the Pt - Pt 13% Rh thermocouple in the ingot. Emissivity corrections were made at 2500°F after the system had reached thermal equilibrium. Emissivity values obtained were:

Alloy	Emissivity
Ti 6Al-4V	0.68
Ti 6Al-2Sn-4Zr-2Mo	0.74

Temperature measurement in the TRW melting system is complicated by the fact that melting is obscured from view by the charge for much of the melt cycle. After the charge has been heated for a period of time incipient melting occurs on the side and bottom of the ingot. The top surface of the charge does not reach temperature as fast as the sides, as it is losing heat to the furnace by radiation. The pyrometer, focused just below the top of the charge, sees a slight drop in temperature when melting begins, because the hottest part of the ingot melts off, lowering the average temperature of the metal that is left. Upon application of full power, the temperature rises quickly, melting the top of the charge, and revealing the melt to the pyrometer which indicates the molten metal temperature. Thus an instrument having a fast response is required.

The infrared pyrometer performed satisfactorily through the evaluation trials, and its use is recommended to monitor titanium melting.

c. Carbon Pickup During Melting

Although the liquid metal charge is in contact with a graphite crucible for only a brief time, this time is sufficient to allow some crucible dissolution and resultant carbon pickup by the melt. One of the objectives of this program was to determine the extent of this pickup and whether it affected castability or casting properties.

Carbon content was determined before and after melting. Carbon levels are consistently held below 0.16% C, and more frequently fall below 0.14% C. Results of analyses of a series of castings are given in Table III and displayed in Figure 7.

It is of interest to note that although carbon pickup increases on remelting, the increase is less than that experienced on the initial melt. This was demonstrated by melting two heats each of Ti 6Al-4V and Ti 6Al-2Sn-4Zr-2Mo into a steel ingot mold, machining the ingots obtained into charges, remelting and pouring into castability molds. The increase after each melting sequence is shown in Figure 8. Carbon levels increased to 0.20% C. This indicates that reclamation of sprues, gates, etc., and scrap castings by remelting is limited to the preparation of alloys containing a higher carbon limit than now permitted. As the use of carbon-containing alloys for castings has not been extensively investigated, despite information that such alloys may have desirable properties (11,12), there is no present-day application for the remelt material generated by the TRW process, although such material may be used in the chemical industry.

Semi-levitation induction melting has no effect on oxygen and nitrogen levels, as shown in Table III. Hydrogen levels appear to be lowered in alpha-beta alloys, and increased in beta alloys.

2. General Electric Pyrolytic Graphite Mold

Molds used in this program were pyrolytic graphite faced ethyl silicate bonded zircon based molds supplied by the General Electric Co.

a. Mold Manufacture

Molds were made by a patented process (16) in which conventional lost wax techniques were used to prepare a shell mold, which was dewaxed and fired to assure complete removal of all wax. The ceramic molds were then subjected to the pyrolytic graphite coating process.

The coating cycle was begun by heating the mold under a vacuum of approximately 200 microns. Shortly before the mold reached coating temperature, nitrogen gas was introduced as a purge system and the vacuum exhaust line properly adjusted to maintain a slight pressure in the furnace.

TABLE III

Interstitial Element Analyses of Titanium Alloy Castings and Alloy Melt Stock

Alloy	Casting No.	Mold Temp. (°F)	Interstitial Element, w/o			
			C	O	N	H
Ti-6Al-4V	As-received[a]		.022	.16	.009	.0090
"	"					.0045[b]
"	G 6010	1000	.104	.14	.007	.0028
"	G 6011	1000	.110	.14	.007	.0017
"	G 6027	1500	.130	.16	.011	.0032
Ti-6Al-2Sn-4Zr-2Mo	As-received[a]		.02	.124	.008	.0052
"	"					.0033[b]
"	G 6049	1000	.104	.145	.006	.0023
"	G 6048	1000	.103	.12	.008	.0018
Ti-3Al-8V-6Cr-4Mo-4Zr	As-received[a]		.022	.094	.009	.0090
"	G 6065	1000	.131	.17	.009	.0134
"	G 6064	1000	.124	.13	.008	.0236
Ti-11.5Mo-4.5Sn-6.0Zr	As-received[a]		.02	.15	.01	.0041
"						.0016[b]
"	G 6325	1000	.14	.14	.002	.0122
"	G 6329	1000	.11	.12	.002	.0076
"	G 6331	2000	.14	.16	.002	.0117

(a) Certified Analysis

(b) TRW recheck of hydrogen content of as-received melt bar stock

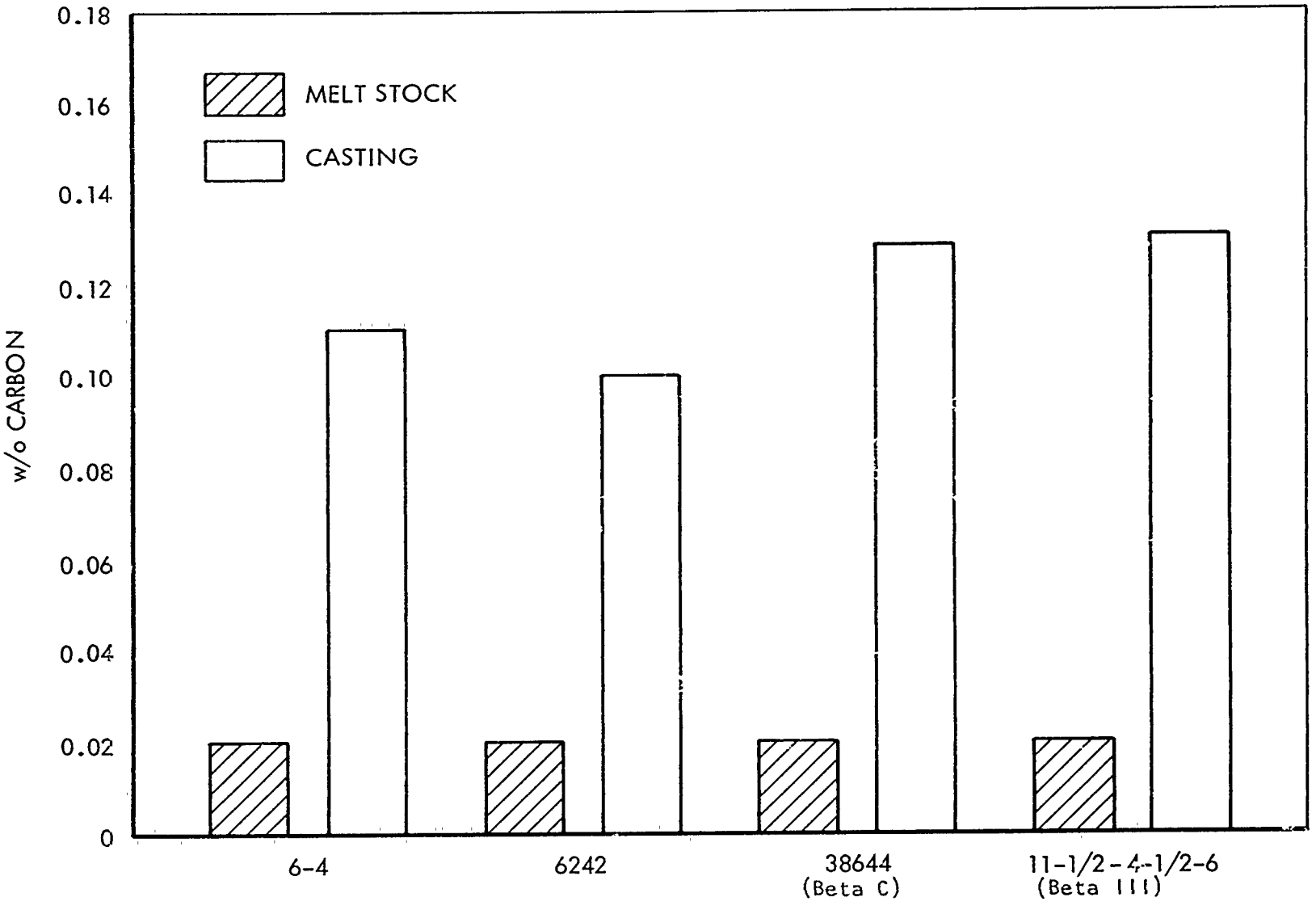

Figure 7. Carbon-pickup during melting for four titanium alloys.

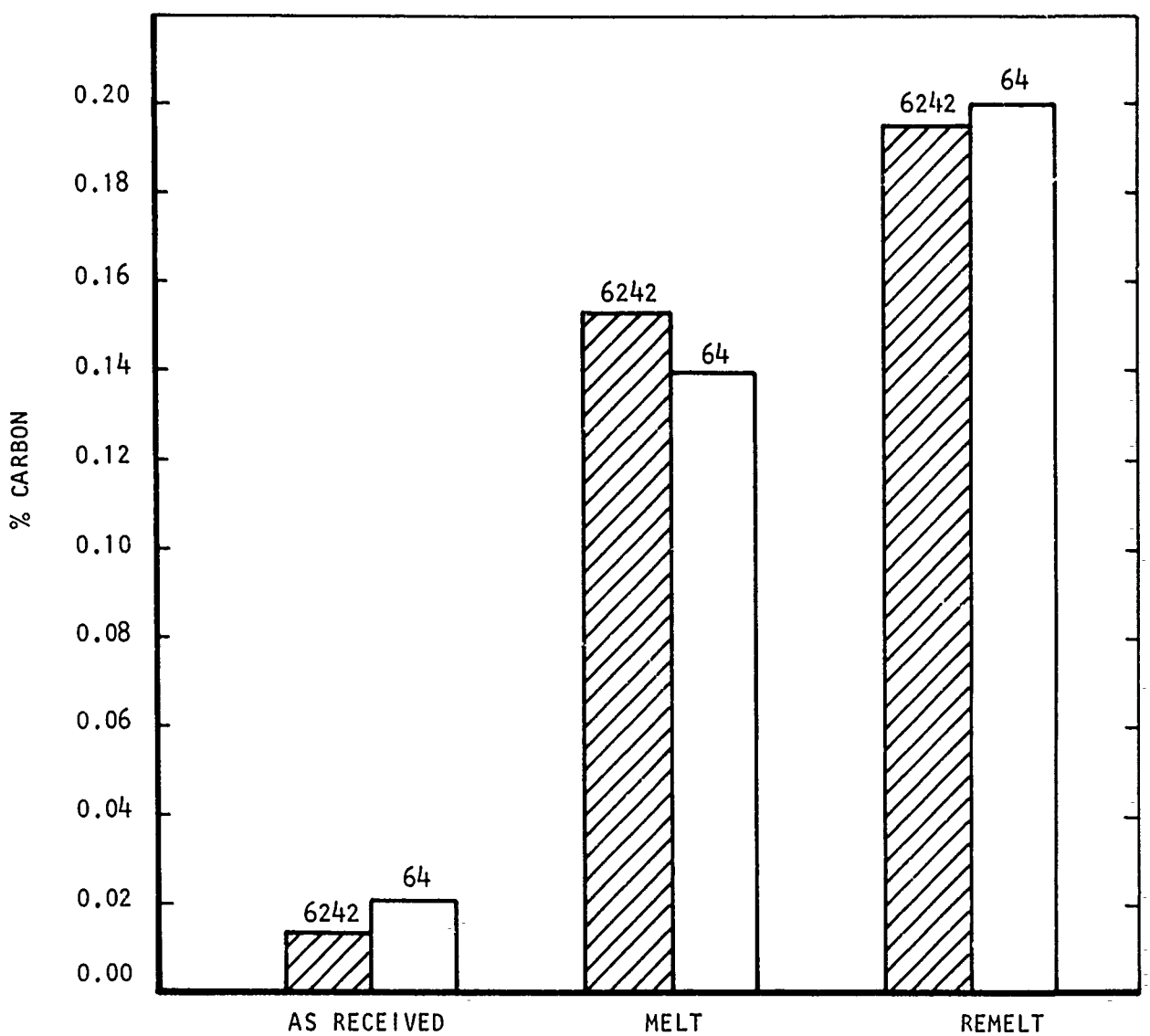

Figure 8. Effect of Remelting on Carbon Content.

Positive pressure in the furnace surrounding the susceptor was under 50 mm Hg. The coating gas (any suitable hydrocarbon gas capable of dissociating to carbon and hydrogen atoms) was introduced in place of the nitrogen gas. The chamber may be operated on acetylene, methane, ethane or other hydrocarbon gas, depending on the operating temperature of the coating furnace. Some gases require higher temperatures for dissociation and yield less carbon atoms per cubic foot of gas consumed; therefore, it becomes a matter of economics as to the gas used and cycle time to accomplish a suitable coating.

Successful operation of the coating furnace requires that the gas flow through the mold be maintained at a rate which did not cause stagnation, which could form soot on the mold. This varied with each different mold configuration and the venting system was designed into the mold. The gas velocity was maintained by control of the incoming gas at a selected positive pressure and flow rate per hour discharging into the mold and furnace chamber which were maintained at a lower pressure such that the gas was accelerated through the mold by its expansion. Inlet gas pressure varied from 15 to 20 psig and furnace chamber pressure varied from 3 mm Hg to 12 mm Hg, depending upon the mold configuration. When the mold configuration was changed, the most successful means of achieving good coating distribution and thickness was by proper selection of the position, number, and size of vents from the chambers being coated to insure even flow and distribution of gas.

After the cycle was established on the castability molds, the surface area being coated was calculated and the relationship between the flow of gas and the area of the vents was used as a basis for establishing flow rates for new mold configurations.

An initial problem was encountered on the pour cup and sprue where the coating thickness was found to be thin compared to the pattern area on some earlier work. When titanium was poured into the cup, the thin pyrolytic coating eroded causing contamination of the casting. This condition was traced to cold gas entering the mold at the pour cup and not dissociating until it had flowed through the mold some distance. This condition was alleviated by preheating the gas before it reached the mold, staying well below the dissociation temperature. For low gas flows, a temperature of 550°F was sufficient, but for larger gas flows such as were used on the bearing housing a preheat temperature of 800°F was used.

b. Characterization of Pyrolytic Graphite Molds

A coated mold is shown in Figure 9. Note the bright shiny surface characteristic of pyrolytic graphite on the interior surface. A mold is shown in cross sections in Figure 10. Note that the carbon penetrates through the entire mold structure. The pyrolytic layer is clearly shown in the scanning electron microscope picture of Figure 11. The coating varied in thickness from 0.0014" to 0.0024". It was dense, continuous and impermeable. The scanning electron microscope picture of Figure 12 shows the cellular nature of the surface. Scattered loose particles appear on the surface of the mold.

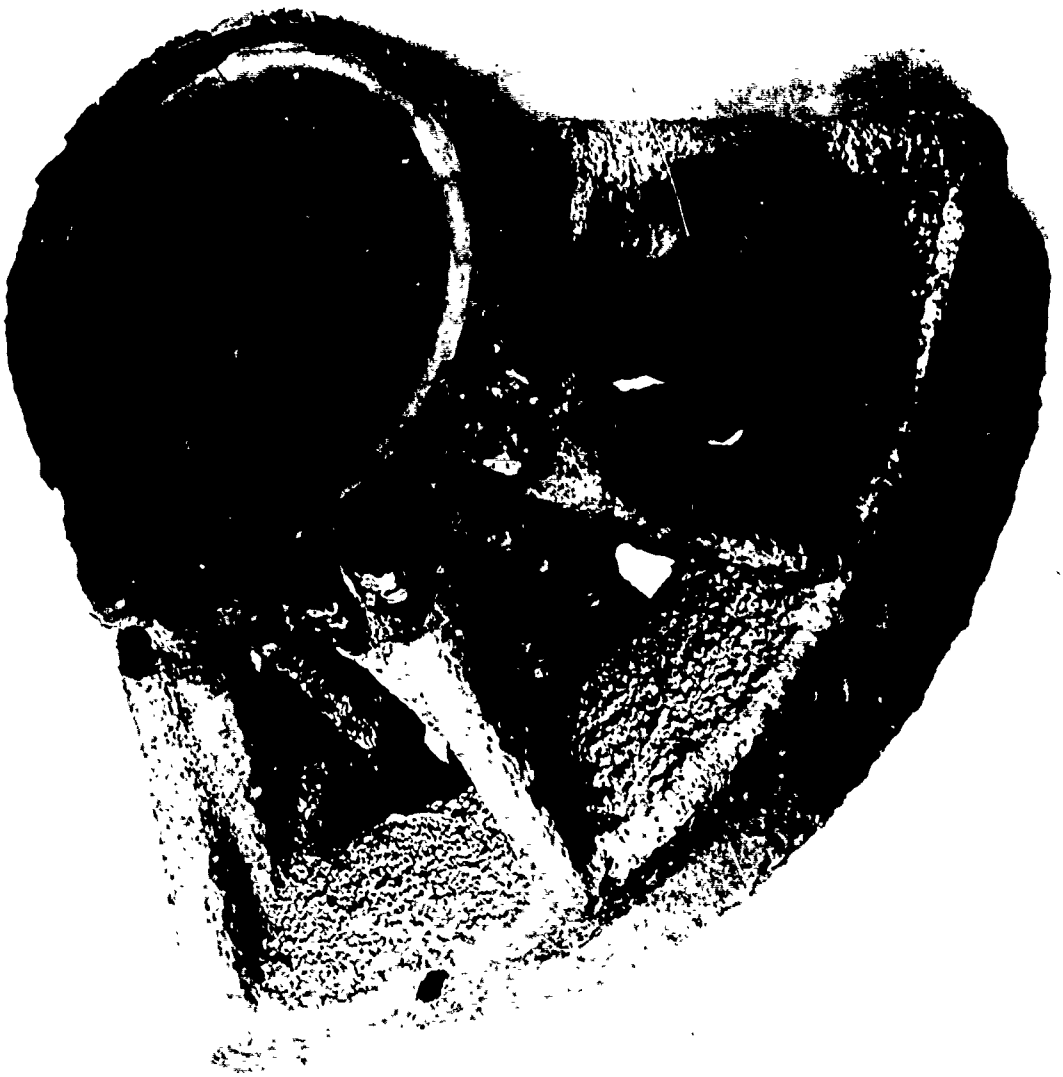

Figure 9. Pyrolytic Graphite Coated Mold.

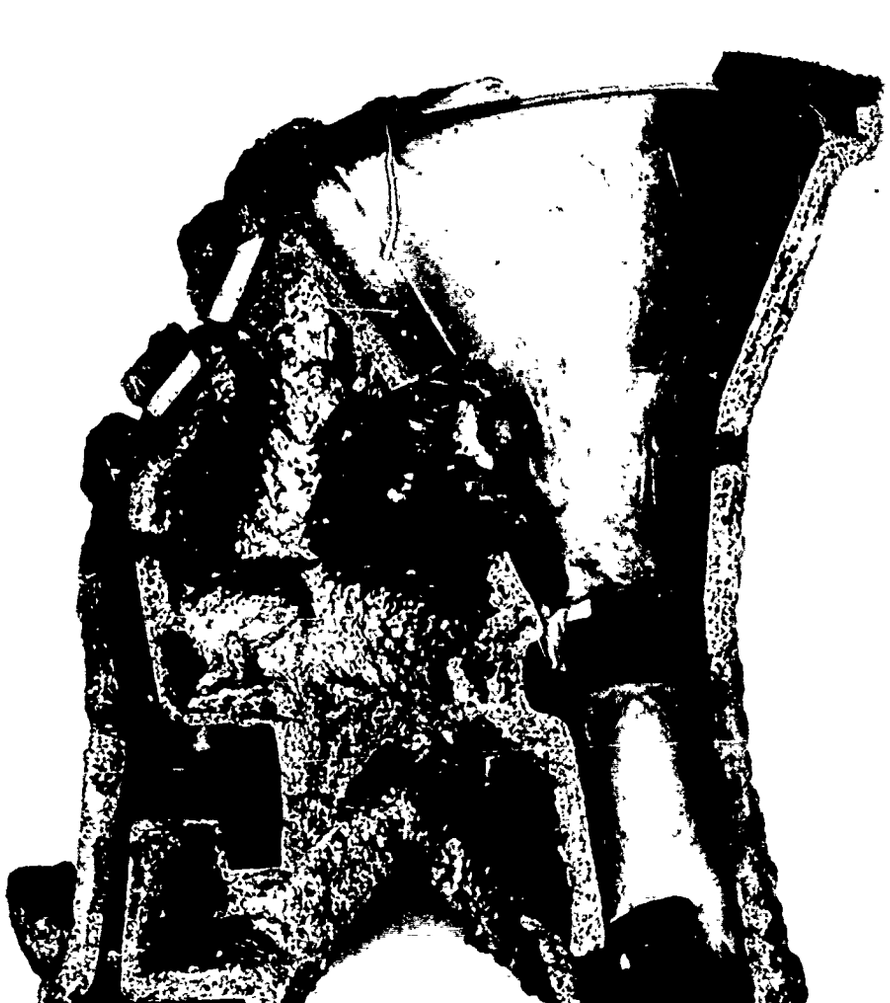

Figure 10. Cross Section of Pyrolytic Graphite Coated Mold.

Figure 11. Scanning Electron Microscope Picture of Pyrolytic Layer Cross Section. 1000X

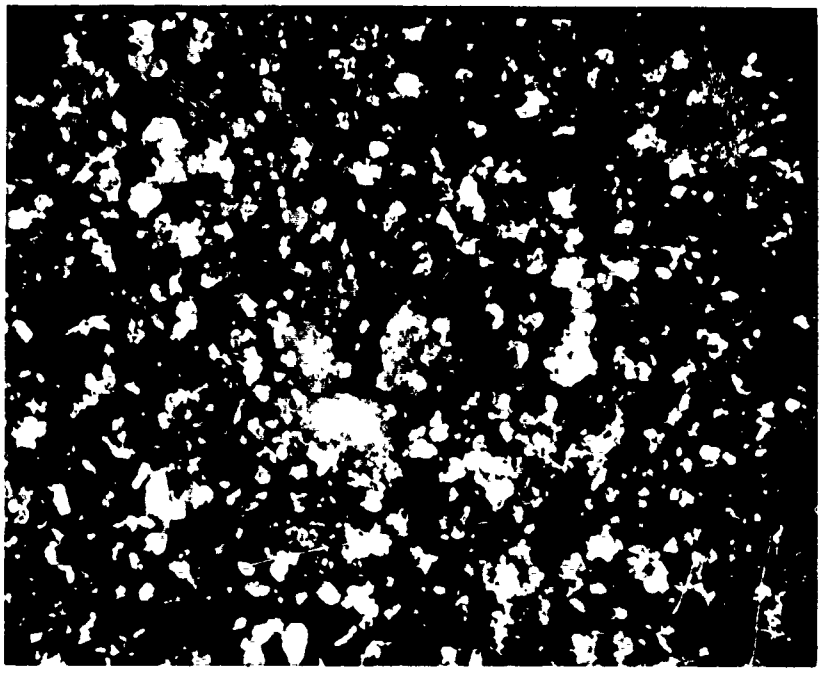

Figure 12. Surface of Pyrolytic Graphite Mold. 1000X

These particles have the electrical characteristics and scanning response of amorphous carbon, which would be expected to form during the transient flow conditions experienced at the termination of coating. They are believed to be the cause of the slight surface reaction found in castings. An interesting artifact of the coating process is shown in Figure 13, taken on the pyrolytic surface. No effect on that casting surface was traced to coating artifacts such as this.

The thermal conductivity of the mold was determined experimentally with a hollow cylinder specimen. An electrical heating element was placed in the center of the cylinder and the power input measured to determine the heat flux through the mold. Thermocouples were placed at the inner and outer surfaces of the mold to measure the gradient through the wall. The conductivity was calculated from the relation

$$k = \frac{q}{\Delta T} \frac{l}{2\pi l} \ln \frac{r_o}{r_i}$$

where

k = thermal conductivity
q = measured heat flux
ΔT = measured temperature gradient
l = cylinder length
r_o = outside radius of cylinder
r_i = inside radius of cylinder

The conductivity was found to be 1.66 $\frac{BTU}{hr.ft^2(°F/ft)}$ This value is between the 0.8 to 1.0 $\frac{BTU}{hr.ft^2(°F/ft)}$ found for ceramic shell molds and the 3.5 $\frac{BTU}{hr.ft^2(°F/ft)}$ value found for carbon.

Mold strength was measured in a three-point bending test and found to be 2360 psi. This is higher than the value of 1200-1400 psi usually found as a mean value for ceramic shell molds. This high mold strength made the mold resistant to handling damage.

Venting, required to coat the mold, is also essential to the production of sound castings, as gas, given off during solidification, must have a place to escape. Positions of these vents should be selected so as to facilitate both the coating and the casting processes. For instance, all risers should be vented, as should all runner systems.

The pyrolytic graphite coating faithfully reproduces the surface of the mold. This means that the mold must be free of defects and loose particles prior to coating. Loose ceramic particles are covered over by the adherent graphite layer, and cannot be removed subsequently. Such areas will become pits on the casting surface and will require weld repair.

Figure 13. Pyrolytic Graphite Artifact on Surface of Pyrolytic Mold. 200X

C. Castability Experiments

1. Mold Design and Experimental Procedure

One objective of this program was to determine the castability of the four subject alloys. Because of the nature of cold crucible melting, accurate fluidity tests are difficult to carry out and evaluate on skull melted material. Induction melting, in which metal is poured at a uniform temperature, is ideal for fluidity determinations. Since the fluidity of a reactive metal will, to a large extent, depend upon the degree of reaction with the mold, it is appropriate that surface area to volume ratios be varied if an accurate measure of the alloy's ability to fill thin sections is to be obtained. For this reason, a fluidity or "castability" mold was designed which contained two clusters of four bars as shown in Figure 14. Each mold had two clusters of four plates 0.75" wide by 4" long. Plate thicknesses were 0.030", 0.060", 0.090", and 0.250". One cluster was gated at both top and bottom of the mold, and the other at the bottom of the mold only.

Fluidity is normally found to be a function of mold preheat, increasing as preheat is increased. However, in the case of alloys which react extensively with molds, the reverse is found. Therefore, one test of the reactivity of the mold-metal system, and hence the suitability of the mold for use with the alloy, is the dependence of fluidity on mold preheat temperature. Three preheat temperatures were used, 1000°F, 1500°F, and 2000°F. It is expected that a non-reactive mold metal system will show the normal increase in fluidity as mold preheat temperature increases.

Molds were supported on firebricks within an Inconel can, which protected the vacuum furnace in the event of mold runout (no runouts were actually experienced in the program). The mold can was placed within an induction heated graphite susceptor below the melting crucible. A Pt/Pt-13% Rh thermocouple, protected by a silica sheath, was positioned between the downsprue and the castability specimen cavities to monitor mold temperature. Molds were dried overnight at 400°F prior to being placed in the vacuum chamber for preheating and pouring. Molds were preheated 30 minutes minimum (see Appendix A) at pressures below 10 microns. Castability molds took six pound charges. All molds were statically poured.

2. Results of Castability Experiments

The results of the castability experiments are tabulated in Table IV. There is wide scatter for sections less than 0.250". This is due to normal variations in pour stream configuration (the ability to fill a thin section is a function of the stream velocity; in a free-falling bottom-pour stream, the configuration of which is not controlled, stream velocity will vary within the stream cross section from pour to pour), and to the presence of gas entrapped in the mold during solidification. This gas exerts a back pressure on the entering metal stream and limits its flow.

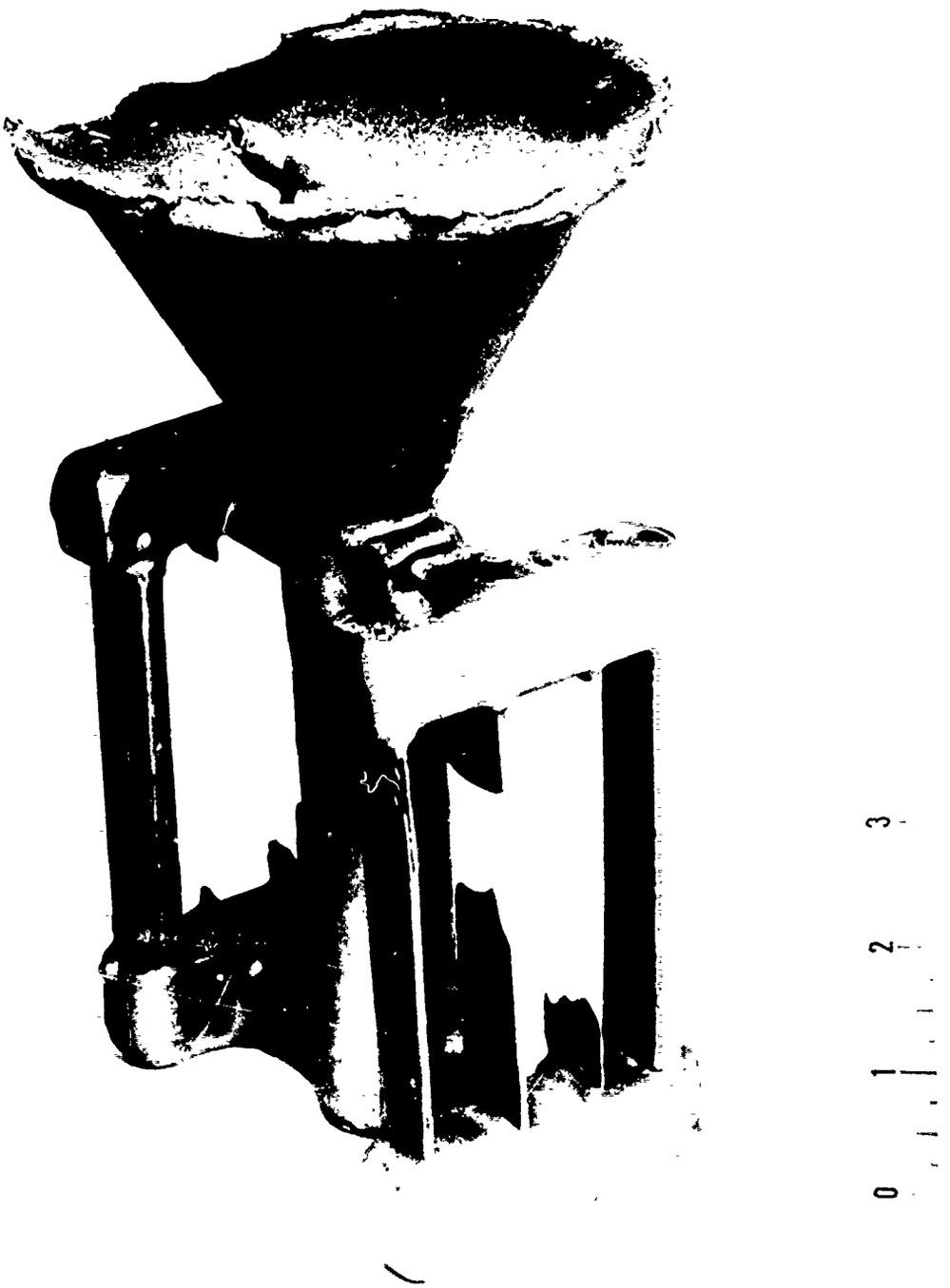

Figure 14. Castability Mold Design.

TABLE IV

Effect of Alloy Composition and Mold Preheat Temperature on Mold Fill

Alloy	Casting No.	Mold Temp (°F)	% Mold Fill[1]							
			Bottom Gated Section Thickness (Inch)				Top & Bottom Gated Section Thickness (Inch)			
			0.250	0.090	0.060	0.030	0.250	0.090	0.060	0.030
6Al-4V	G 6010	1000	100	100	33.1	19.7	100	100	87.4	32.0
	G 6011	1000	100	100	36.9	28.8	100	100	76.2	23.1
	G 6012	1500	100	100	64.2	40.8	100	100	78.3	10.1
	G 6027	1500	100	100	61.2	39.1	100	98.5	94.0	28.5
	G 6047	2000	100	100	100	25.1	100	100	76.8	6.4
	G 6028	2000	100	100	100	71.3	100	100	91.2	11.4
6Al-2Sn-4Zr-2Mo	G 6049	1000	100	100	20.7	22.4	00	100	100	9.0
	G 6048	1000	100	100	50.7	18.6	100	100	96.0	43.2
	G 6052	1500	100	100	58.4	41.5	100	100	76.2	22.8
	G 6050	1500	100	100	70.3	32.4	100	100	100	22.8
	G 6054	2000	100	100	100	14.5	100	100	100	20.4
	G 6053	2000	100	100	67.1	23.4	100	100	100	18.2
3Al-8V-6Cr-4Mo-4Zr (Beta C)	G 6065	1000	100	57.2	30.4	6.4	100	36.1	49.0	15.6
	G 6064	1000	100	40.3	27.4	6.2	100	59.1	28.8	14.3
	G 6081	1500	100	98.6	40.4	18.9	100	56.5	29.8	19.3
	G 6080	1500	100	100	51.8	22.5	100	100	98.5	39.0
	G 6095	2000	100	100	50.8	27.4	100	100	47.0	12.8
	G 6094	2000	100	100	39.9	19.6	100	100	97.6	8.1
11.5Mo-4.5Sn-6.0Zr (Beta III)	G 6325	1000	100	7.2	4.0	2.0	100	23.9	12.8	2.1
	G 6329	1000	100	58.3	32.6	7.9	100	100	49.3	15.2
	G 6328	1500	100	99.3	74.8	19.8	100	43.0	19.4	7.4
	G 6326	1500	100	16.4	4.0	2.0	100	66.9	30.3	6.4
	G 6330	2000	100	99.0	34.3	4.9	100	97.7	42.0	14.5
	G 6331	2000	100	100	95.6	25.5	100	100	78.8	5.7

[1] Determined as a percentage of the total 0.75" x 4" section.

Interpretation of the castability data may be facilitated by the graphical presentation, Figures 15-18. In Figure 15 are plotted the relationship between percent fill and section thickness for each of the four alloys at each mold preheat temperature in the bottom gated clusters. Similar information is shown in Figure 16 for clusters gated at both top and bottom of the plates. The data is replotted in Figure 17 as the relationship between percent fill and mold preheat temperature for each of the four alloys at each section thickness for bottom gated clusters. Figure 18 shows these relationships for top and bottom gated clusters.

In spite of the experimental scatter of data, the data show a number of important facts:

1. Castability of the alpha-beta alloys, Ti-6Al-4V and Ti-6Al-2Sn-4Zr-2Mo is better than that of the beta alloys, Ti-3Al-8V-6Cr-4Mo-4Zr and Ti-11.5Mo-4.5Sn-6Zr (Beta III). Beta III had the least fluidity of any of the alloys. It was observed during melting and pouring of the alloy that Beta III melted in a sluggish manner and did not respond to levitation forces as well as did the other alloys. Its melt behavior and fluidity may be related.

2. Castability generally tended to increase with increasing mold preheat temperature, indicating that the mold system is non-reactive. The one major exception to this was the 0.030" sections of the top and bottom gated clusters (Figure 18), which showed no general trend. As these sections freeze very quickly because of their high surface area to volume ratio, scatter due to the above-mentioned causes would be expected to be more severe than in thicker sections.

3. There is a slight tendency for bottom gated plates to fill more completely than top and bottom gated plates. This may be explained by noting that metal entering the vertical plate from the top will prevent evolved gas from escaping through the riser vents, whereas in bottom gated plates, the liquid metal will push the gas ahead of it to the vents.

4. In alpha-beta alloys no difficulty should be expected in filling 3/4"x4" sections down to 0.090". Thinner cross sections, however, may be filled only in less extensive areas, or must be more generously gated for static pouring.

3. Effect of Carbon Content on Castability

In order to assess the effect of carbon content of the alpha-beta alloys on their castability, two molds each were cast in Ti-6Al-4V and Ti-6Al-2Sn-4Zr-2Mo from double induction melted stock. These charges were prepared from ingots induction melted in a graphite crucible and solidified in a stainless steel ingot mold. The castability clusters were bottom gated only.

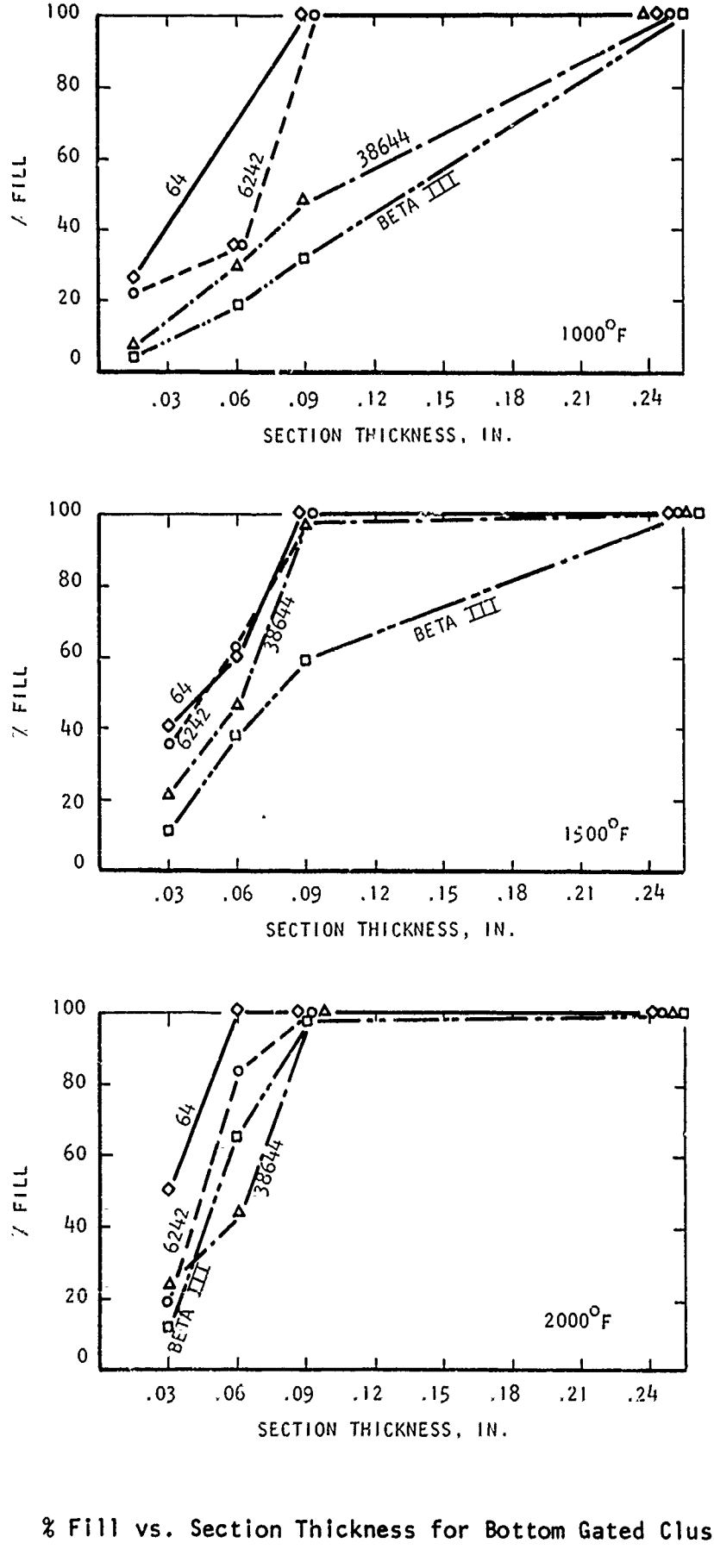

Figure 15. % Fill vs. Section Thickness for Bottom Gated Clusters.

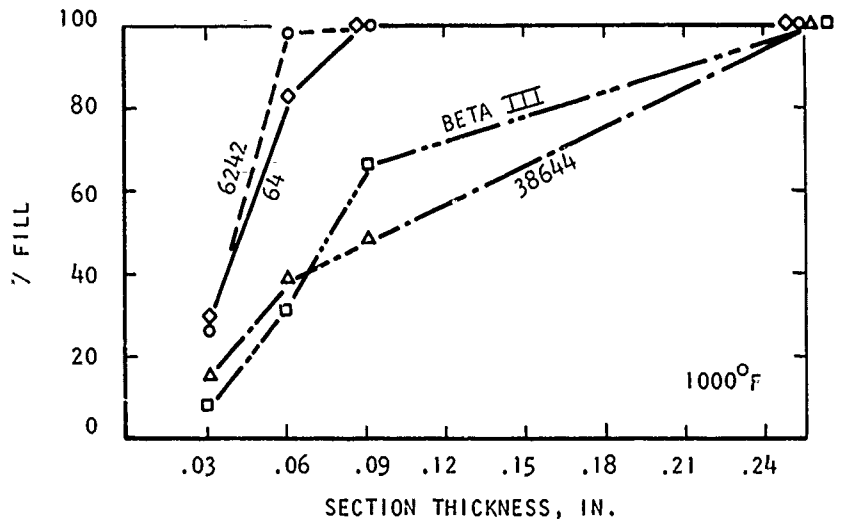

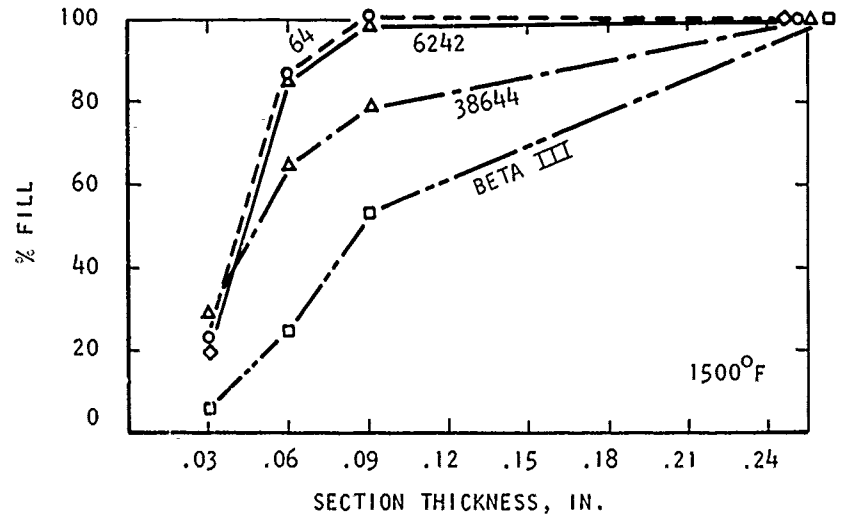

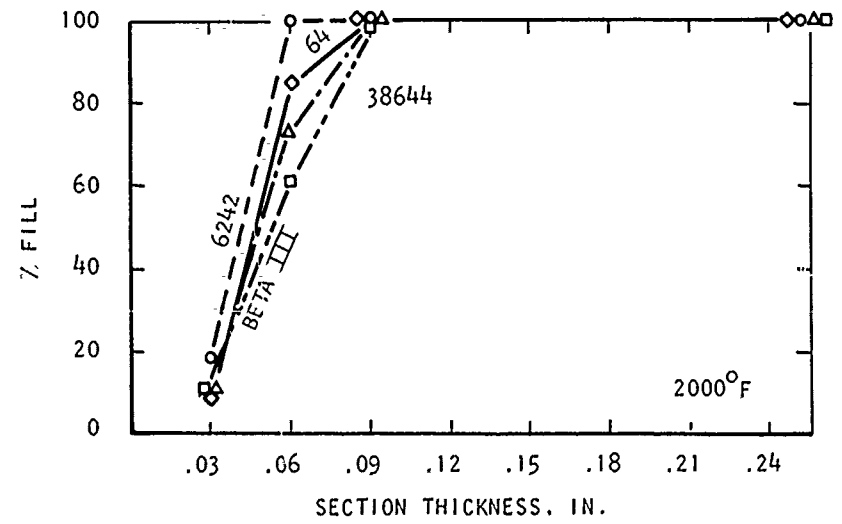

Figure 16. % Fill vs. Section Thickness for Top and Bottom Gated Clusters.

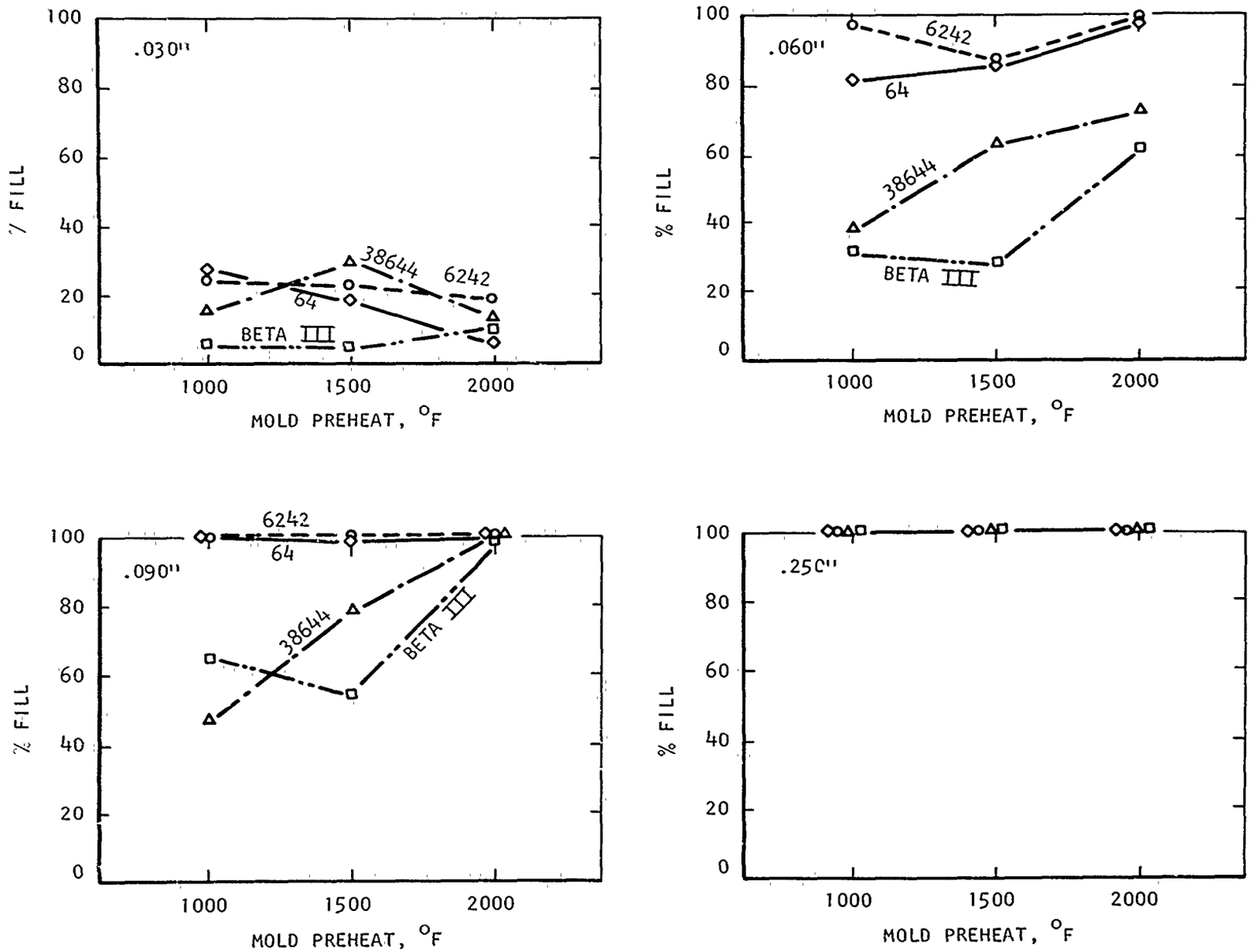

Figure 17. % Fill vs. Mold Preheat Temperature for Bottom Gated Clusters.

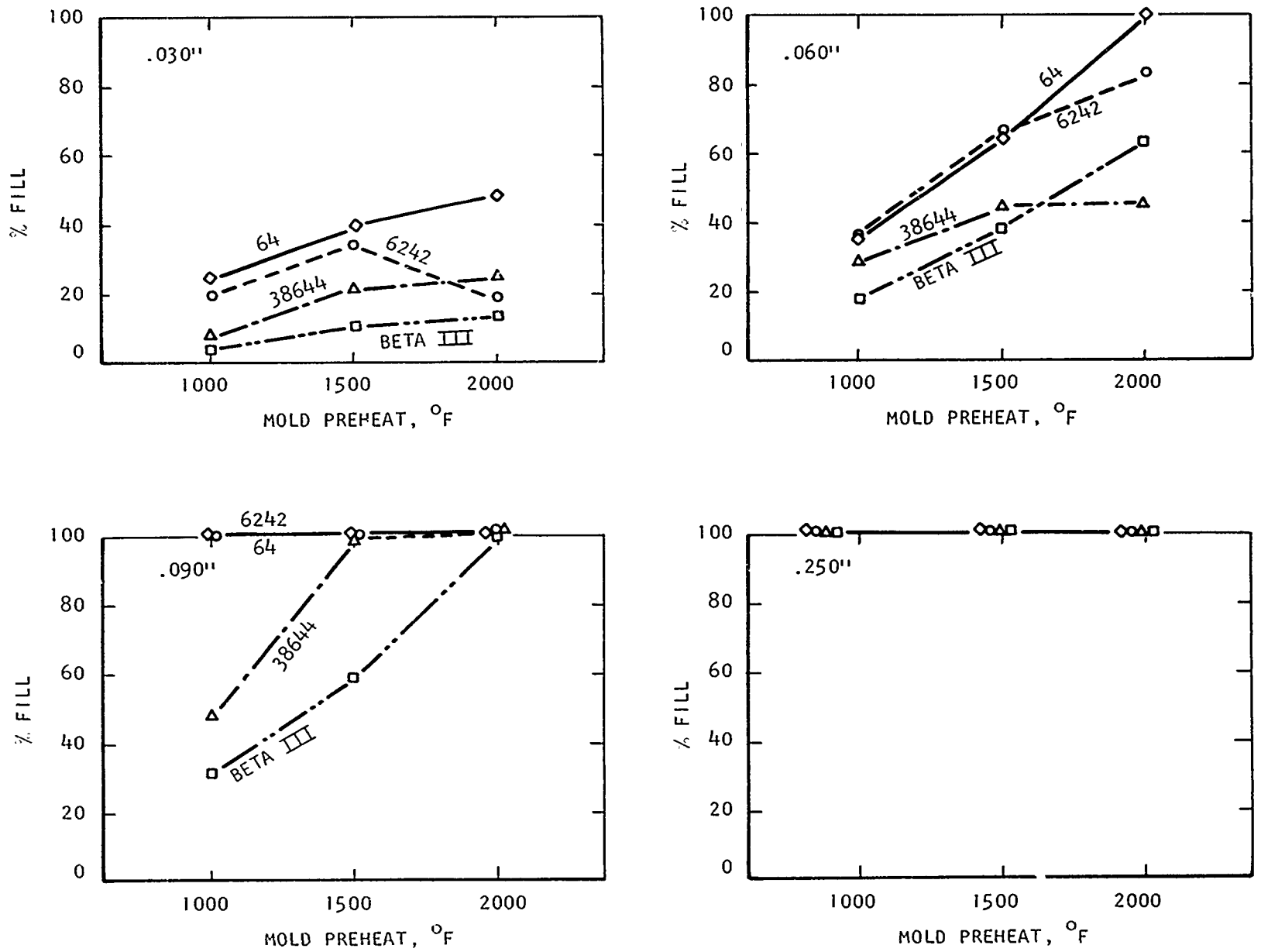

Figure 18. % Fill vs. Mold Preheat Temperature for Top and Bottom Gated Clusters.

Results are shown in Figure 19. Within the range of experimental error, fluidity decreases with increasing carbon content. This may be expected as increasing the carbon content increases the liquidus-solidus zone (17) thus promoting mushy freezing, which decreases fluidity.

D. Tensile Property Characterization

1. Test Bar Preparation

Tensile properties of the four induction melted titanium alloys were determined from cast-to-size test specimens. Six standard 0.250" diameter test bars were poured per cluster, three gated from both top and bottom, and three gated from the bottom only, as shown in Figure 20. Pouring procedure was the same as that used for castability molds.

Initially, one cluster was poured in Ti-6Al-4V alloy at a 2000°F mold preheat. Grips were machined on all bars, but the gage length surface was not finished. Two bars were tested in this condition, two were etched in a nitric acid-hydrofluoric acid solution prior to testing, and two were sandblasted prior to testing. The etching treatment removed a 0.002" surface layer, while sandblasting removed a layer approximately 0.001" thick. Test results are given in Table V and shown in Figure 21.

The test results showed an effect of surface condition on tensile properties. Metallographic examination of the test bar gage section revealed a 0.0001" thick surface reaction layer. The smoothest surface was produced by sandblasting. The reaction layer was removed by both etching and sandblasting. The reaction layer was identified by microprobe analysis as titanium carbide. The formation of titanium carbide may be traced to the presence of amorphous carbon on the mold surface.

As a result of these findings, tensile bar mold preheat temperatures were reduced to 1750°F and 1500°F, and bars were sandblasted prior to test. Bars were tested at a strain rate of 0.005 in/in/min. to yield and thereafter at a crosshead rate of 0.05 in/min. to fracture. All bars were heat treated prior to testing as follows:

Alloy	Treatment
64	1300°F - 2 hrs. - rapid furnace cool
6242	1100°F - 8 hrs. - rapid furnace cool
38644	1350°F - 15 min. - rapid cool, 1100°F - 8 hrs. - rapid cool
Beta III	1500°F - 15 min. - rapid cool, 1100°F - 12 hrs. - rapid cool

Beta alloy bars were coated with a proprietary ceramic during heat treating to prevent oxidation. Tensile tests were run at room temperature and at 600°F.

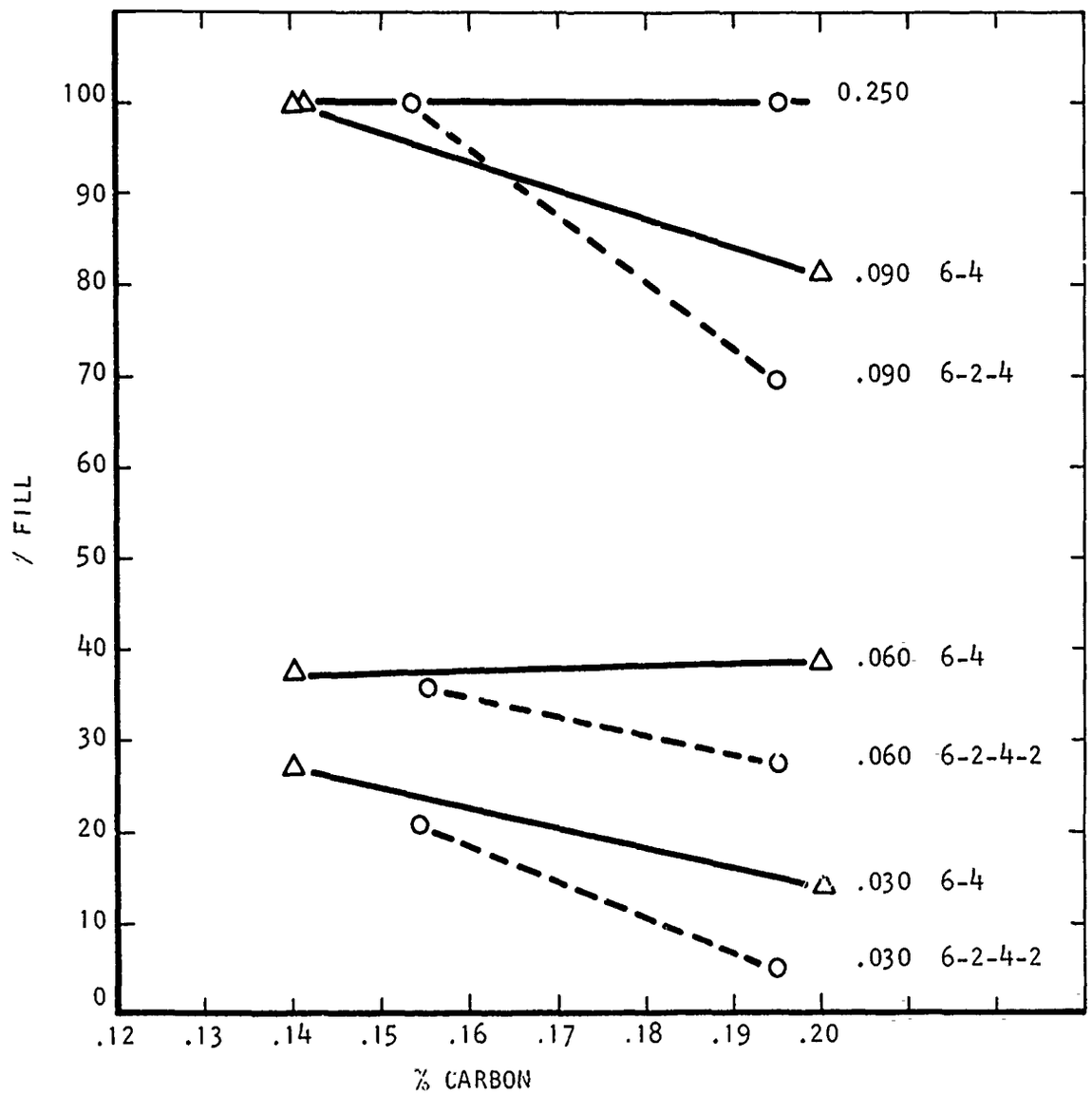

Figure 19. Effect of Carbon on % Fill.

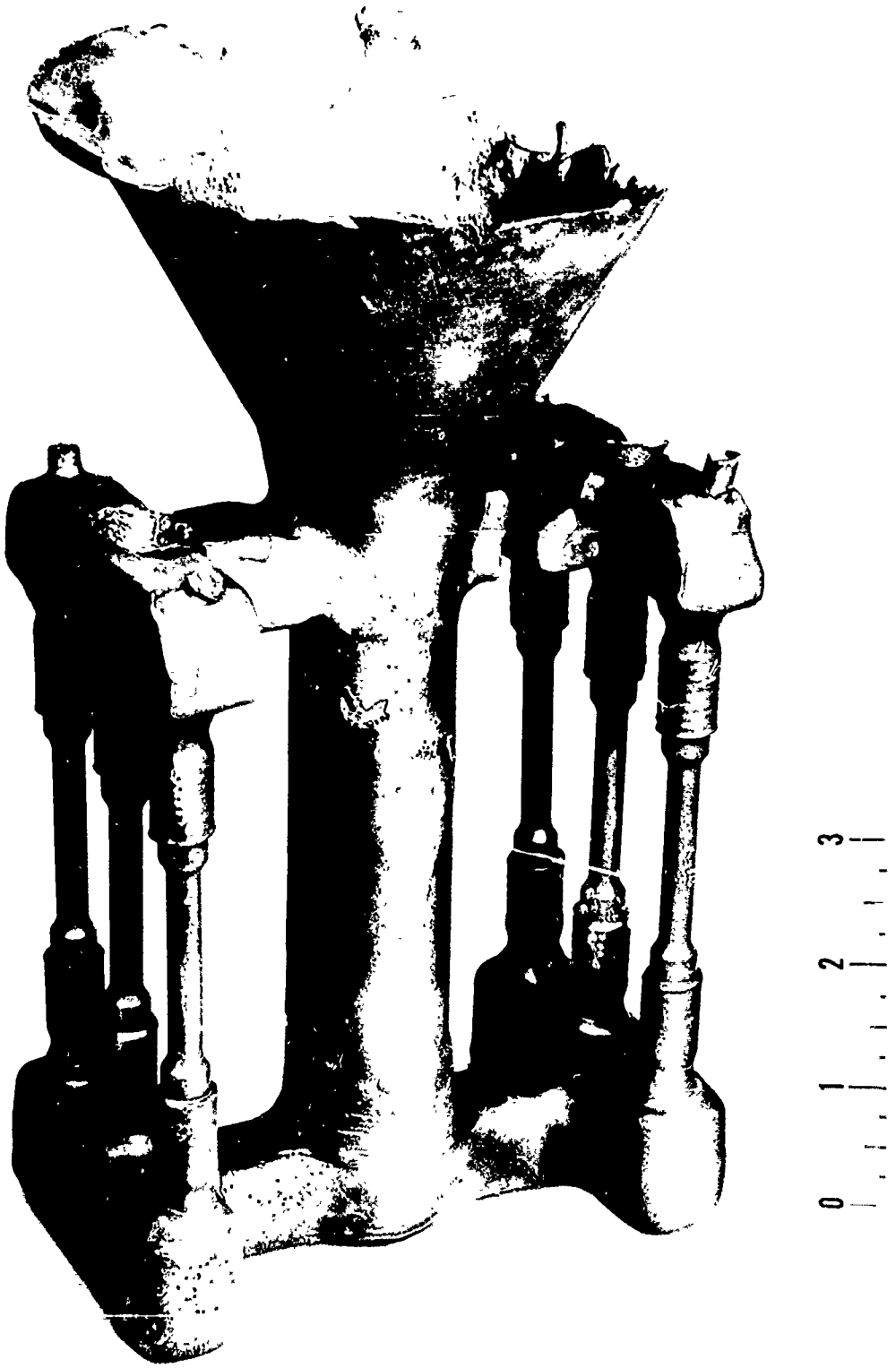

Figure 20. Design of Tensile Test Specimen Mold.

TABLE V

Effect of Surface Treatment
on Properties of Ti-6Al-4V
Mold Preheat 2000°F

Surface Condition	Ultimate Strength (Ksi)	Yield Strength (Ksi)	Elongation (% in 4 d)	R.A. (%)
As-Cast	128.5	121.5	1.1	0.8
As-Cast	136.7	121.6	2.9	5.5
Etched	139.6	124.4	7.1	10.2
Etched	133.5	122.5	4.3	2.4
Sandblast	141.0	125.7	8.0	8.6
Sandblast	139.5	120.0	8.8	4.7

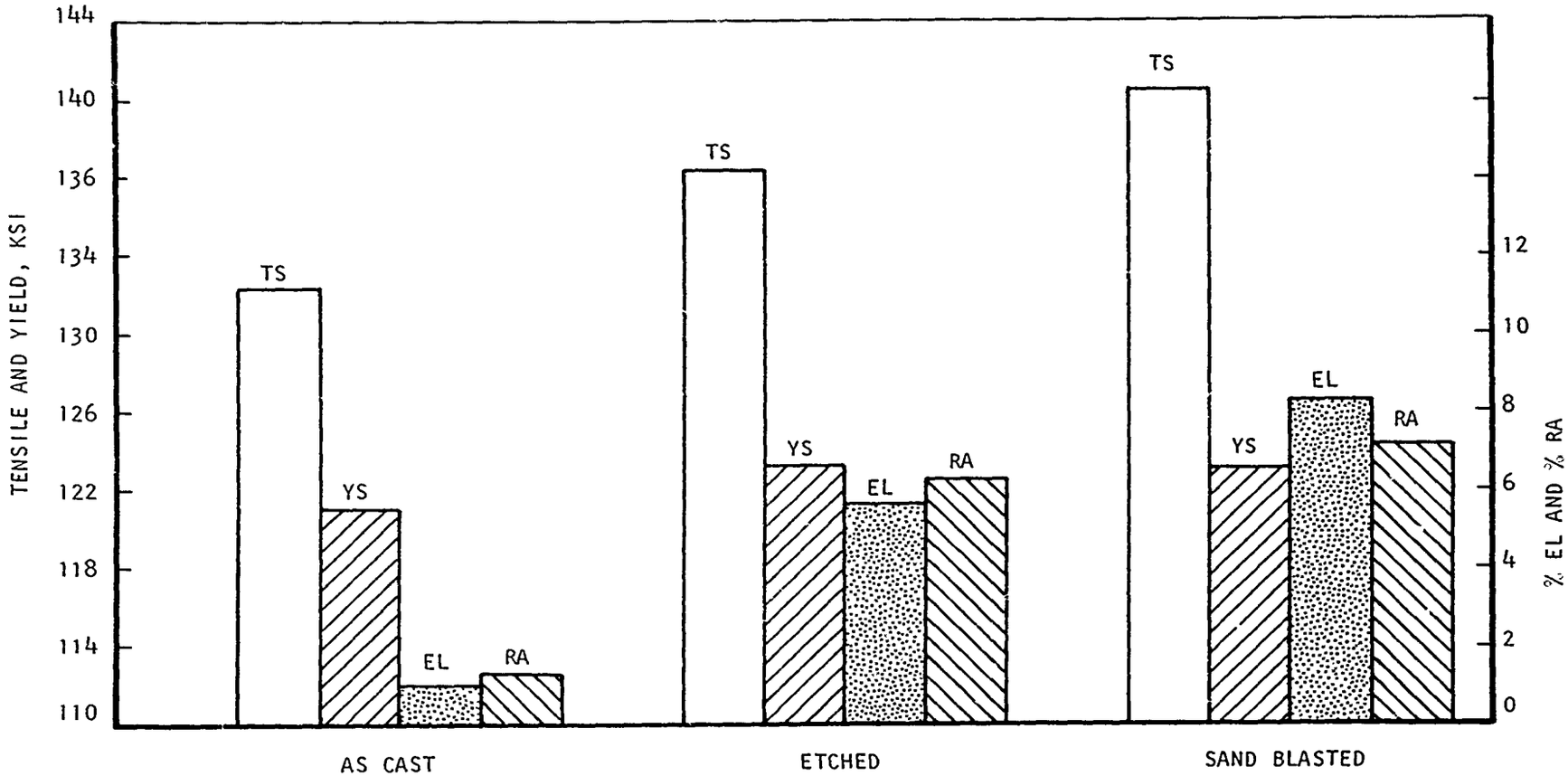

Figure 21. Effect of Surface Condition on Tensile Properties Ti-6Al-4V Alloy.

2. Test Results

Results of tests are given in Table VI and Figures 22 and 23. In the alpha-beta alloys, Ti-6Al-2Sn-4Zr-2Mo alloy has higher tensile properties than Ti-6Al-4V alloy at both room temperature and 600°F. The largest differences were in room temperature tensile ductility, which was in the range 9.5 to 18.0% elongation for the Ti-6Al-2Sn-4Zr-2Mo alloy, compared to 3.5 to 6.5% elongation for the Ti-6Al-4V alloy, and in the 600°F strength levels the Ti-6Al-2Sn-4Zr-2Mo yield strength averaged 73,100 psi compared to 68,200 psi for the Ti-6Al-4V alloy. Ductility levels were also more uniform for the Ti-6Al-2Sn-4Zr-2Mo alloy at 600°F compared to the Ti-6Al-4V alloy.

For beta alloys, Ti-3Al-8V-6Cr-4Zr-4Mo alloy has appreciably higher strength values at both room temperature and 600°F than Ti-11.5Mo-4.5Sn-6.0Zr alloy. The ductility or elongation values for both alloys range from 0 to 2.0% at room remperature to values of 1.0 to 4.0% at 600°F. These values are very low compared to the tensile elongation values obtained for both alpha-beta alloys Ti-6Al-4V and Ti-6Al-2Sn-4Zr-2Mo. The low tensile ductility levels in both beta alloys has been traced to intergranular carbide particles present in the cast structure. These two highly alloyed beta alloys cannot retain in solid solution the 0.11 to 0.14% carbon picked up from melting in a graphite crucible. The carbon content results in grain boundary precipitation of the carbide phase during cooling.

This may be confirmed by examining the microstructure of a 0.250" thick castability specimen of Ti-3Al-8V-6Cr-4Zr-4Mo alloy in Figure 24. Note the carbide particles present in the center of the section as well as at the surface. Alpha-beta alloys did not show comparable structures.

The test results show that the alpha-beta alloys have superior properties at room temperature, while the beta alloys have better strengths at 600°F. Because of the deleterious effect of the carbon picked up (and the lower solubility of carbon in the beta phase) on properties, melting in graphite crucibles is not recommended for the beta alloys. However, the process appears to be quite satisfactory for alpha-beta alloys, and is probably equally applicable to alpha alloys.

3. Quality of Test Bar Castings

Test results must be viewed in light of the quality of the test bar castings. These castings were not completely sound, showing evidence of center line shrink. Examples are shown in Figure 25. As the strength levels obtained are generally quite acceptable, it may be concluded that cast titanium tensile properties are insensitive to reasonable amounts of porosity.

TABLE VI

Room and 600°F Tensile Properties

Alloy	Specimen No.	Test Temp. (°F)	Ultimate Strength ($\times 10^3$psi)	Yield Strength ($\times 10^3$psi)	Elong. 1" G.L. (%)	R.A. (%)
Ti-64	2	Room	134.6	118.0	6.5	9.2
"	3	"	135.3	120.5	5.0	7.7
"	4	"	133.5	120.4	3.5	4.7
"	7	"	135.6	123.5	3.5	3.9
"	1	600	85.8	65.9	22.0	34.5
"	6	"	85.6	66.8	18.0	25.9
"	9	"	88.5	69.1	12.0	17.7
"	11	"	86.0	71.0	5.0	7.0
Ti-6242	16	Room	141.5	123.7	15.0	19.6
"	19	"	138.9	125.3	11.0	6.2
"	20	"	139.7	122.3	18.0	13.3
"	22	"	139.0	123.1	9.5	13.8
"	13	600	96.0	74.3	18.5	27.0
"	17	"	90.8	71.7	10.0	17.0
"	21	"	94.2	75.1	10.5	16.6
"	24	"	92.1	71.3	13.0	23.9
Ti-38644	33	Room	143.1	137.9	2.0	-
"	43	"	141.7	141.5	2.0	-
"	44	"	140.5	-	0.0	-
"	45	"	141.1	139.7	1.0	0.8
"	31	600	124.4	114.1	2.0	2.7
"	32	"	128.4	115.7	3.0	3.1
"	47	"	126.6	114.2	3.5	2.8
"	48	"	126.2	114.1	1.0	5.2
Ti-11.5-4.5-6.0	27	Room	120.0	-	0.5	1.2
"	68	"	120.8	-	0.0	0.0
"	61	"	124.8	116.6	0.0	-
"	62	"	122.5	118.2	0.5	2.0
"	63	600	99.0	83.1	5.0	3.9
"	64	"	98.2	72.3	5.0	3.9
"	65	"	95.9	84.5	2.0	3.2
"	66	"	99.8	82.5	4.5	3.2

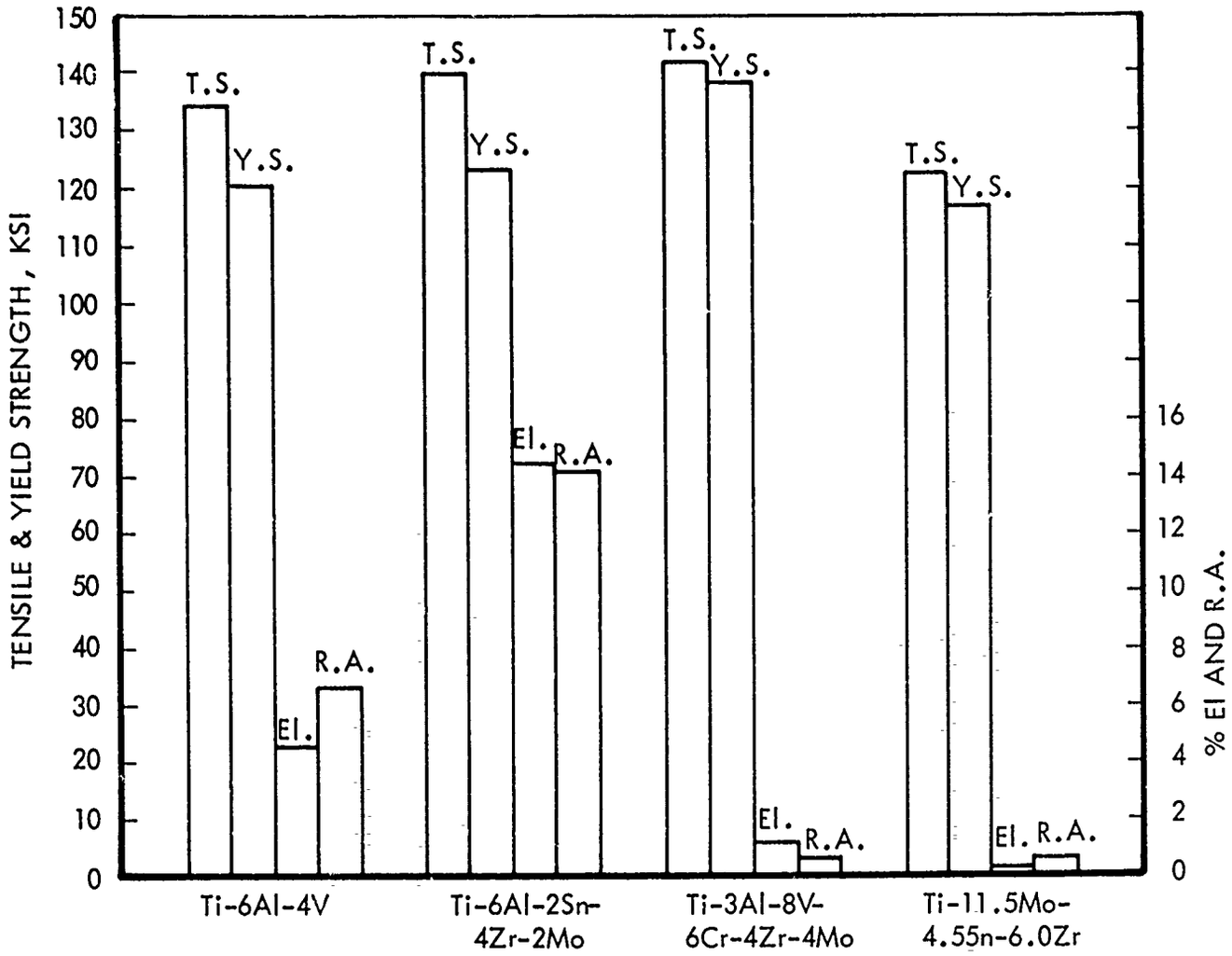

Figure 22. Room Temperature Tensile Properties of Induction Melted and Cast Titanium Alloys.

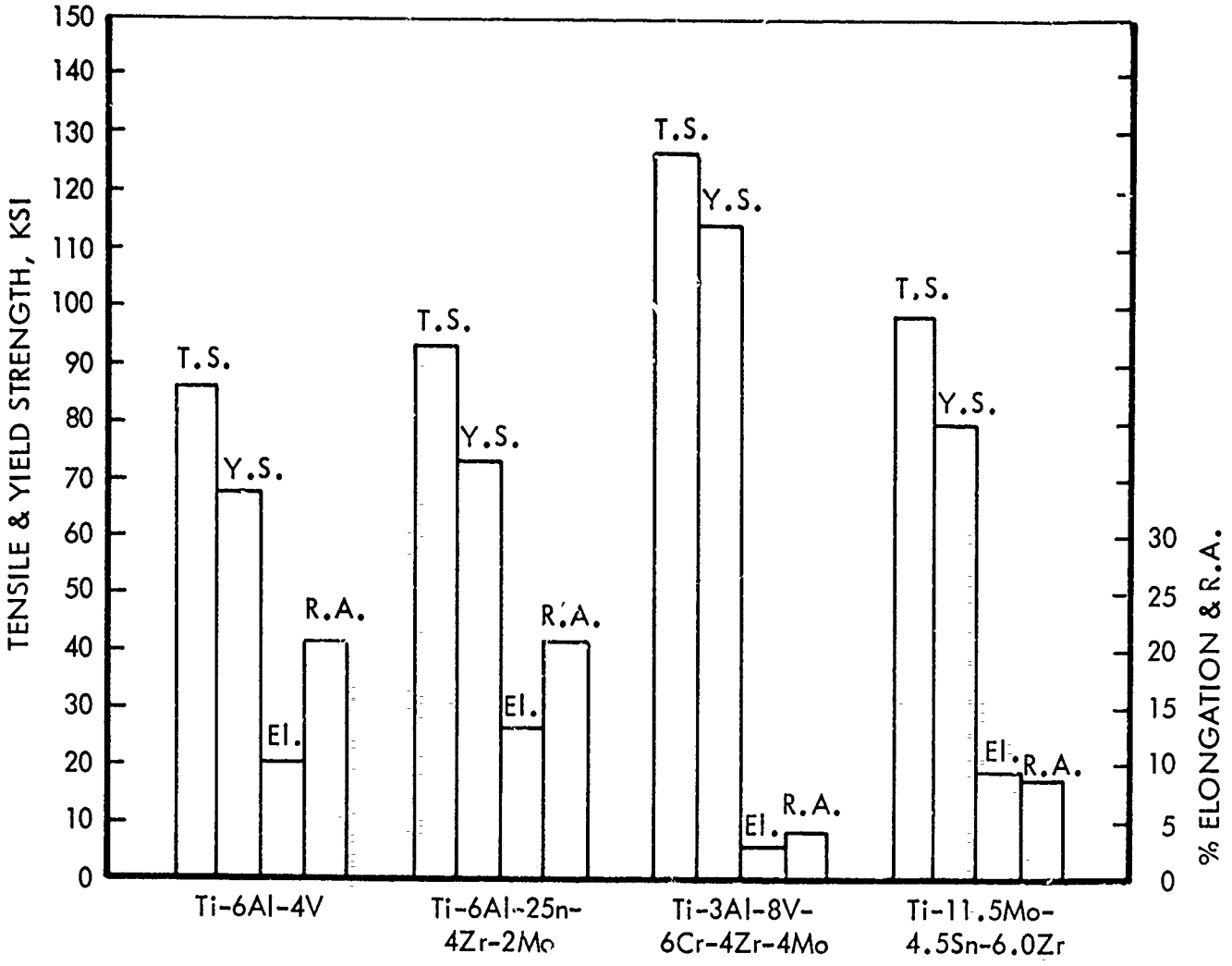

Figure 23. 600°F Tensile Properties of Induction Melted and Cast Titanium Alloys.

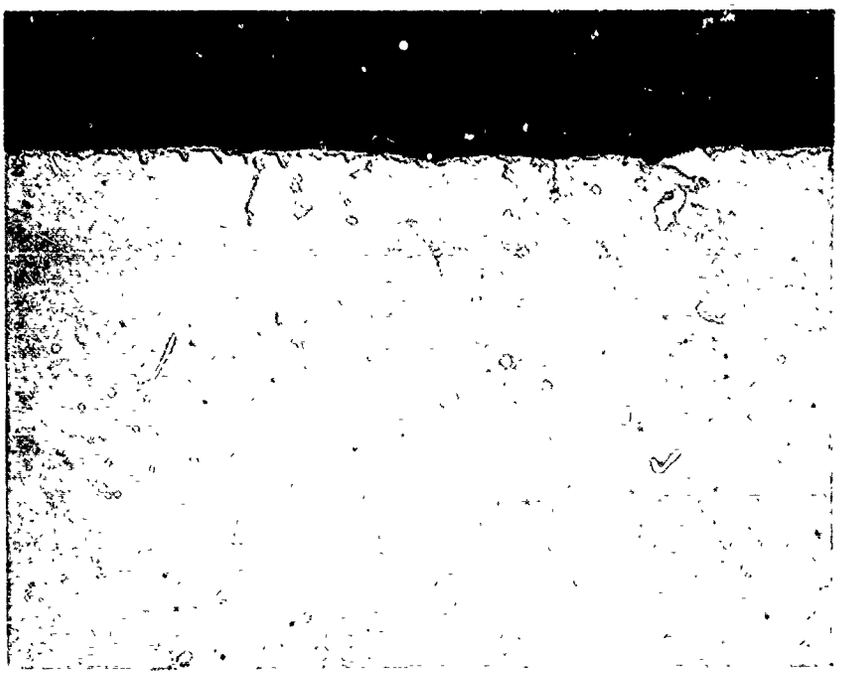

(a) Surface of casting

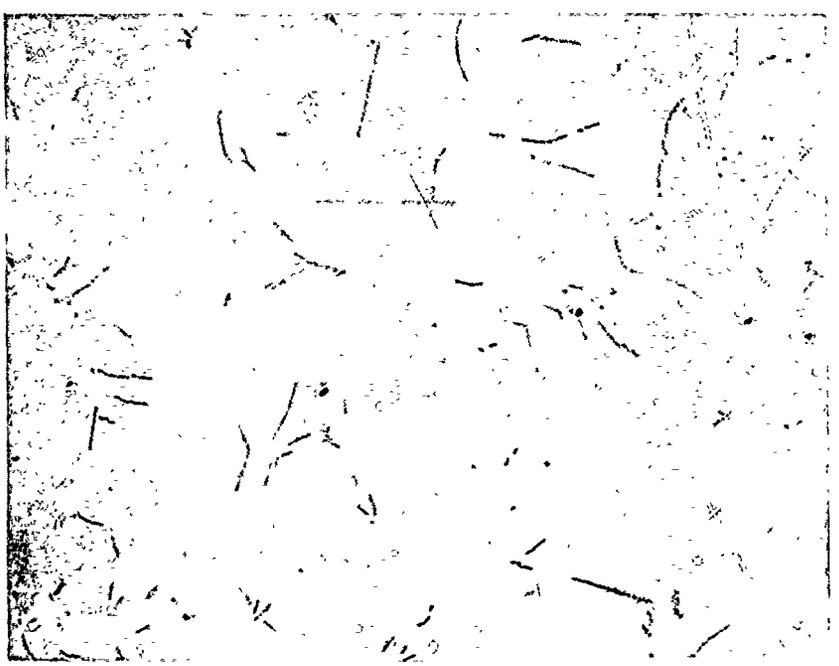

(b) Center of casting

Figure 24. Carbide Network in Ti-3Al-8V-6Cr-4Zr-4Mo Alloy Bars - Unetched. 250X

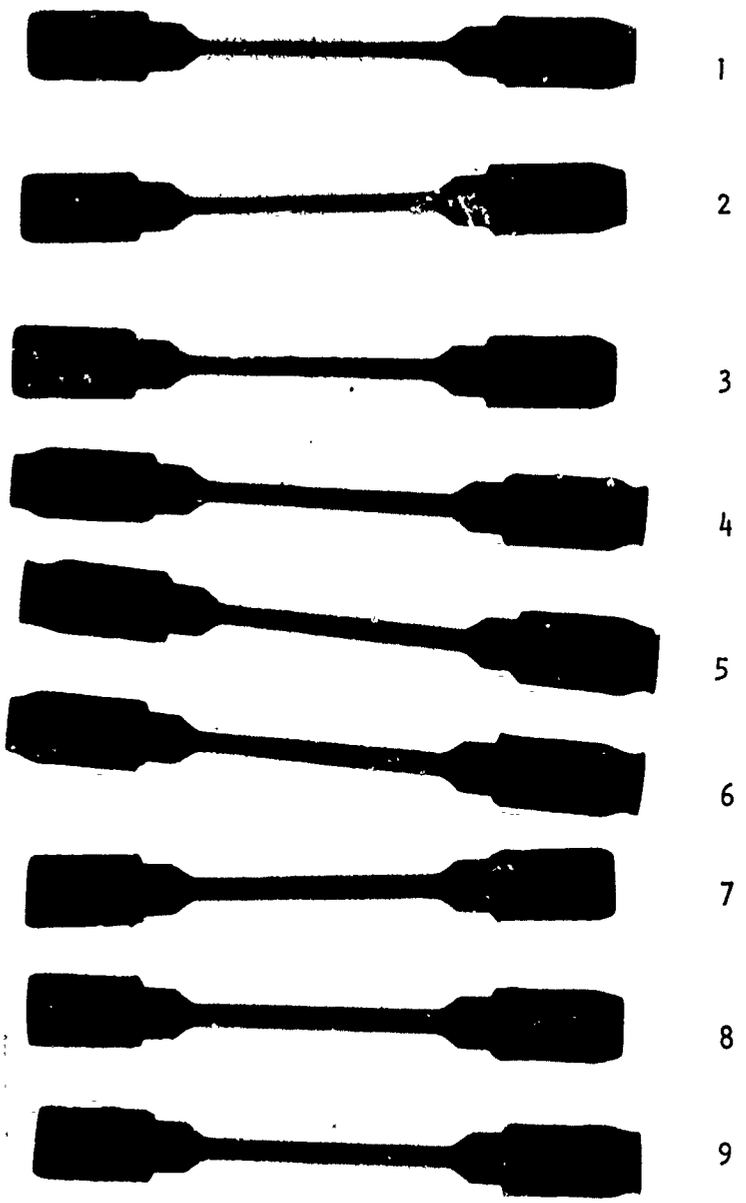

Figure 25. Soundness Typical of Test Bars Evaluated in Program. See Table VI for Properties.

E. Quarter Bearing Housing Castings

1. Alloy and Part Selection

The evaluation of the castability and mechanical properties of induction melted alloys indicated that Ti-6Al-2Sn-4Zr-2Mo possessed the best combination of tensile properties and fluidity. For this reason it was selected as the alloy to be used in making shaped castings.

The casting selected was the bearing housing shown in Figure 26. It has an outside diameter of 16.91" and is 4.41" high, with a minimum wall thickness of 0.125". Because of melting equipment limitations which limited the charge weight to 10 pounds, only a one-quarter section of the bearing housing was poured. Plans to scale the casting up to one-half sections were abandoned when a TRW-funded program showed that it was not feasible to increase the melt weight above 10.5 pounds on available equipment.

2. Casting Trials

Three gating schemes, with minor modifications, were used in an attempt to produce sound castings. All castings were poured statically. The gatings used were designed to be compatible with both the feeding needs of the alloy and the gas flow requirements of the mold coating system. Some compromise between the optimum system of both was inevitable.

The first gating system is shown in Figure 27. The casting was positioned horizontally with the large flange at the bottom, and fed from three 3/4" square gates into the bottom flange and four 1/2" square gates into risers above the heavy inner race. This gating permitted metal to enter the lower casting wall from two directions, effectively trapping evolved gas, much as would be expected from the results of castability experiments. The gating was therefore revised so that the castings filled from the bottom, as shown in Figure 28. Gates were removed from the inner race and castings poured from these molds showed a major area of porosity opposite the center runner. This runner was choked down to 3/8", to provide a balanced feeding system.

Modification of the third mold design by decreasing the thickness of the center feeder by 50% eliminated shrink in the base of the cast quarter bearing housing by providing more balanced feeding. However, the large void areas present in the center portions of the base in previous castings moved over a considerable distance to one of the ends of the base in subsequent castings. Because a balanced feeding system was used in this casting, it was expected that the shrink would be symmetrically distributed, and, should have occurred at both ends. The large movement of the void area to one of the ends suggested that it was related primarily to gas and could not be eliminated through changes in feeder design alone. The gating was thus modified to permit maximum opportunity for evolved gas to escape during solidification by inverting the casting as shown in Figure 29. Four gates were located on the flat flange (top of casting), and four on the inner circular race. Four 3/8" vents, shown in Figure 30, were required between the sprue and the casting skirt to permit coating of the mold. They remained on the final gating system as auxiliary runners. Note also the extensive venting on upper surfaces of the casting, required both for coating and casting purposes.

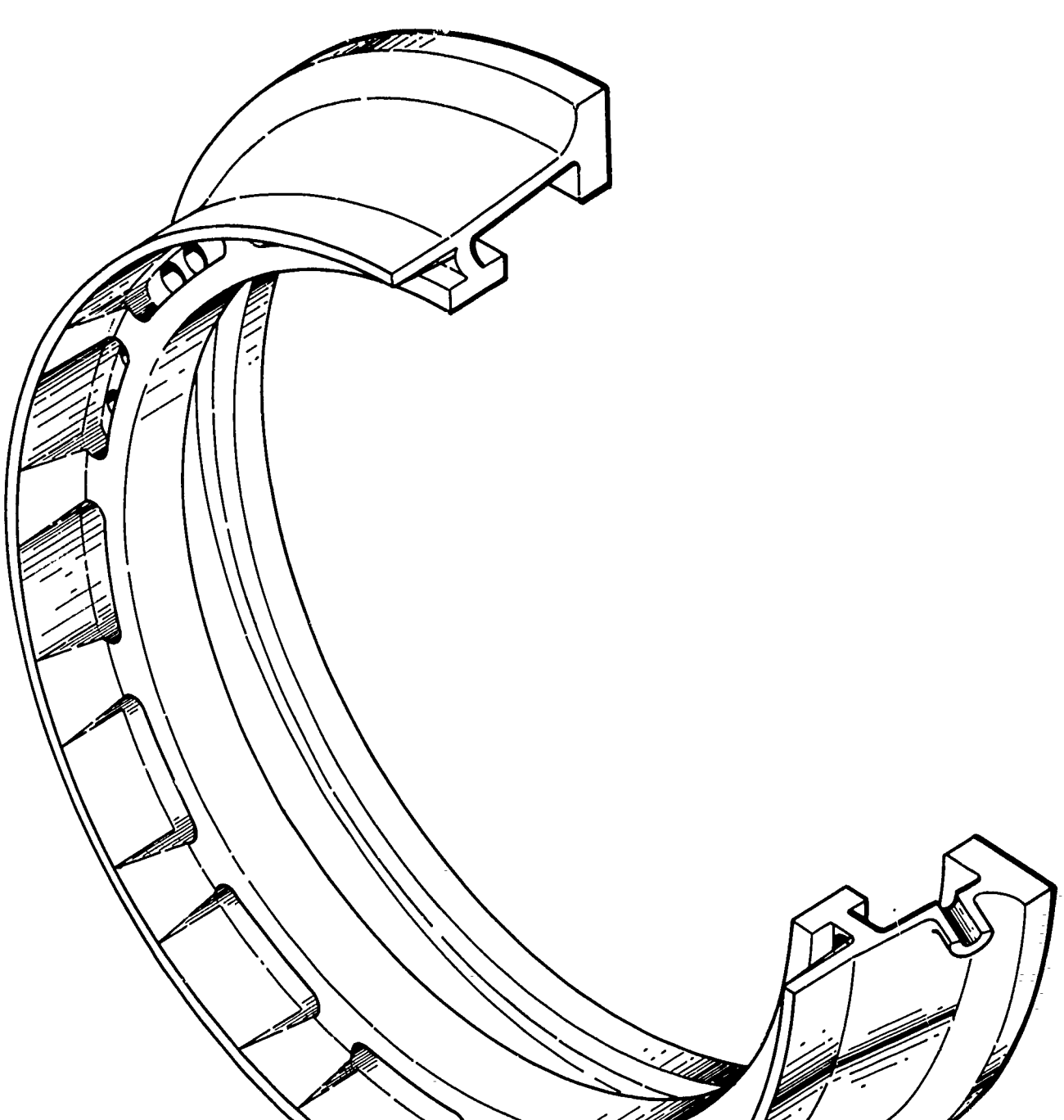

Figure 26. Bearing Housing for TF 39 Engine.

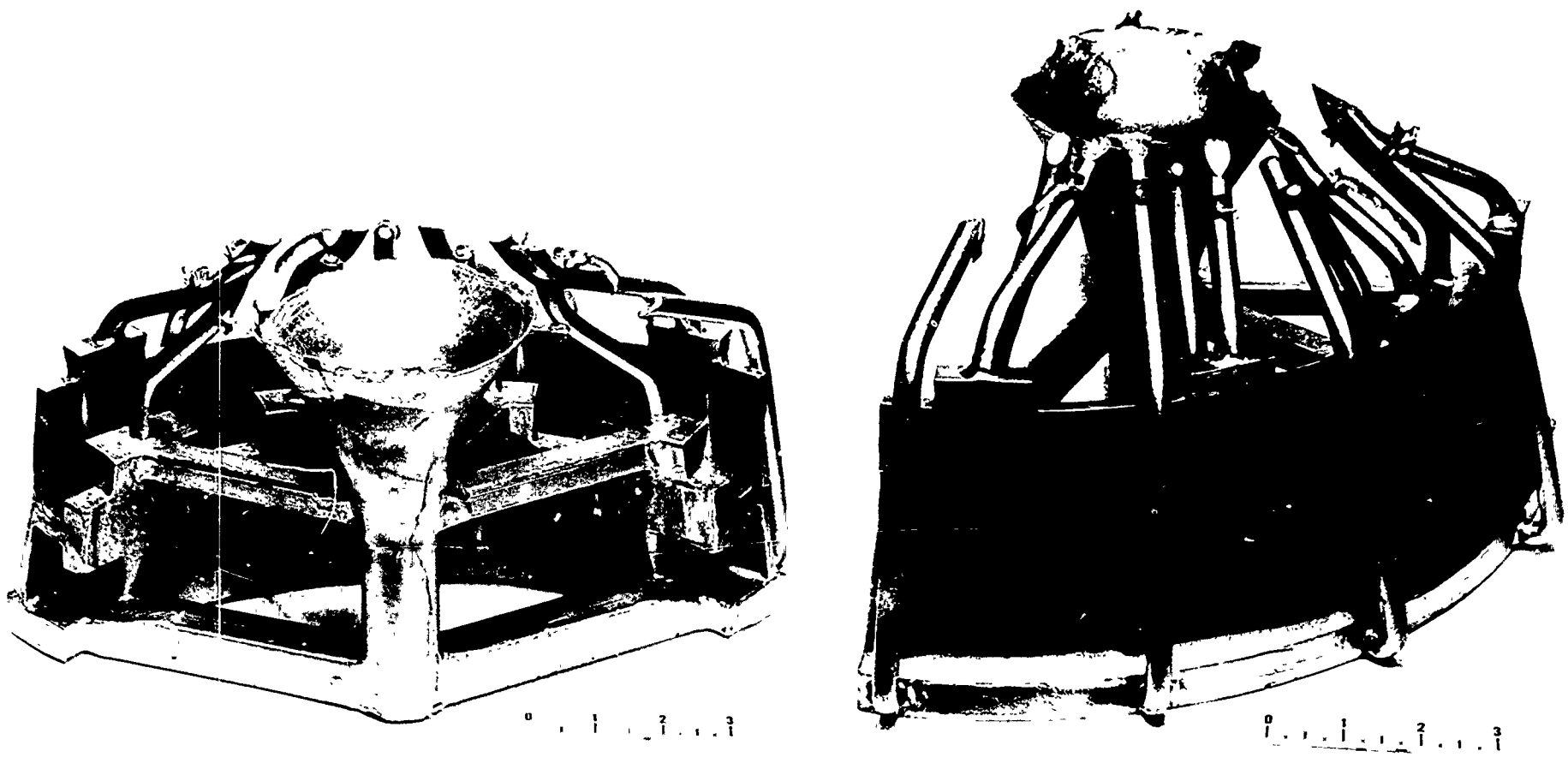

Figure 27. Initial Gating Design.
Casting F 7642.

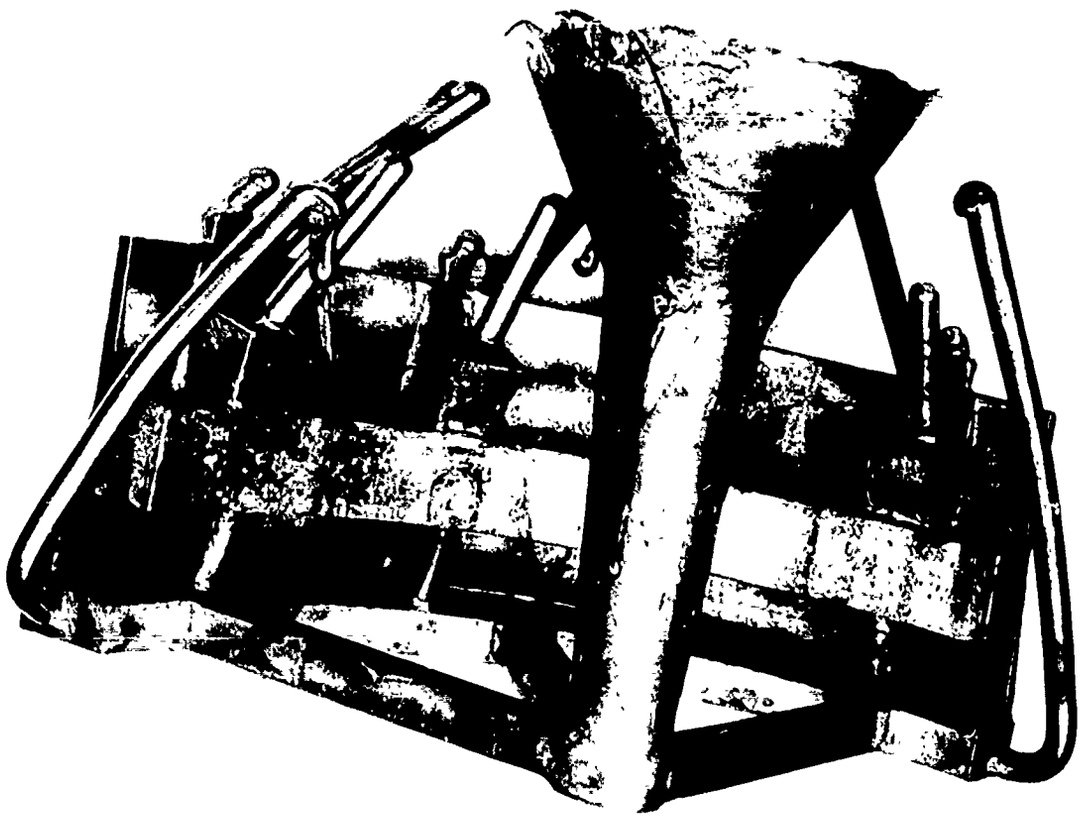

Figure 28. Revised Gating System Using Bottom Filling. Casting G 6509.

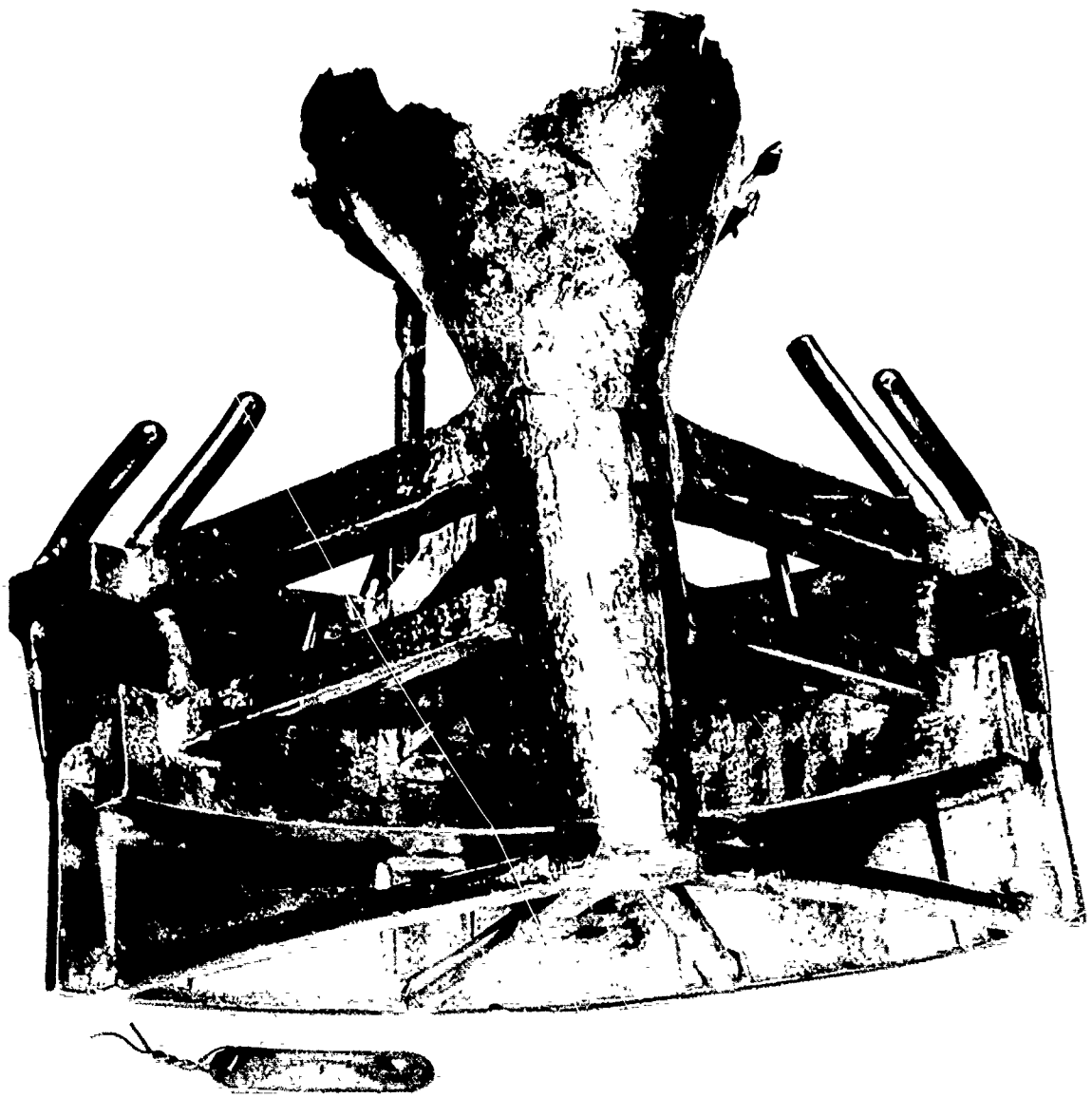

Figure 29. Final Gating System Developed in Casting Trials. Casting G 6607.

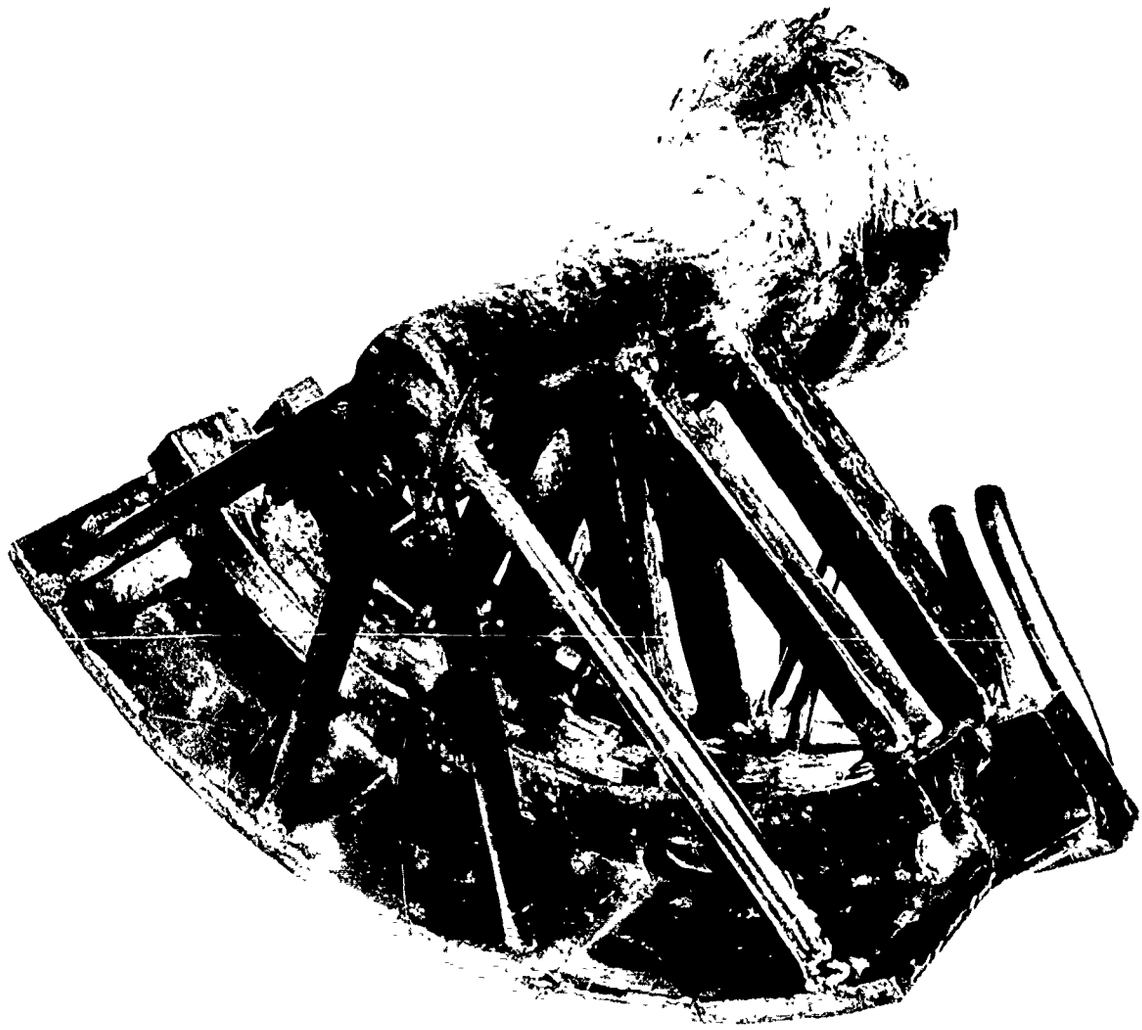

Figure 30. Vents Attached to Bottom of Sprue for Gas Flow During Coating. Casting G 6608.

This gating was most nearly successful in producing sound castings, although problem areas remained, as discussed below.

3. Pouring Procedure

Quarter bearing housing castings were poured using the same furnace setup and procedure as used for castability and tensile bar castings, except that mold preheat times under vacuum were extended and the crucible was preheated prior to melting. These steps were taken to degas the crucible and mold, thereby minimizing their contribution to gas porosity in castings.

Although the first casting was poured at a mold preheat of 2000°F, a subsequent investigation of the microstructure at the surface of a 0.250" castability sample of Ti-6Al-2Sn-4Zr-2Mo alloy showed that a carbide layer was formed at this temperature, as shown in Figure 31. The preheat temperature was thus lowered, first to 1750°F, and then to 1500°F. Two castings were poured each at preheat temperatures of 1250°F and 1000°F to determine the effect of lower preheat temperatures on mold fill and casting surface quality.

4. Quarter Bearing Housing Quality

The quality of castings produced was generally disappointing. Particular problem areas were in casting surface condition and porosity.

a. Casting Surface Defects

Surface defects, similar to those encountered in conventional casting processes were prevalent. Four types of surface defects were encountered and have been categorized as follows:

1. Hot tears
2. Misruns and cold shuts
3. Inclusions
4. Rattails

A hot tear is shown in Figure 32. It was caused by mold cracking during solidification as shown in Figure 33, leaving tears in the casting. Similar cracks were found in which the casting wall is locally displaced, but there is no tearing of the metal. The defect indicates that during cooling, and while the casting is still mushy, thermal stresses cause the mold to crack. Because of the rigidity of the mold, it deforms the casting as it cracks.

A cold shut defect is shown in Figure 34a at 2.5X magnification. The appearance of this defect is similar to oxide fold type defects in aluminum and magnesium castings. Metallographic examination revealed the presence of a 0.00015 inch thick carbide layer on the cast surfaces adjacent to the fold area, but no carbide layer was observed in the fold (Figure 34b). A titanium X-ray photograph (Figure 34c) reveals

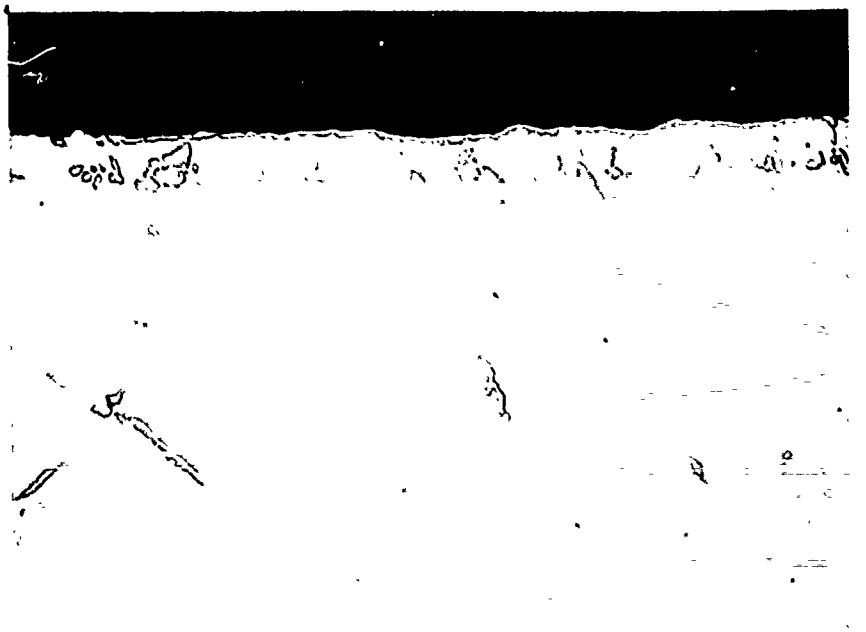

(a) Mold Preheat Temperature 1500°F, Casting G 6052

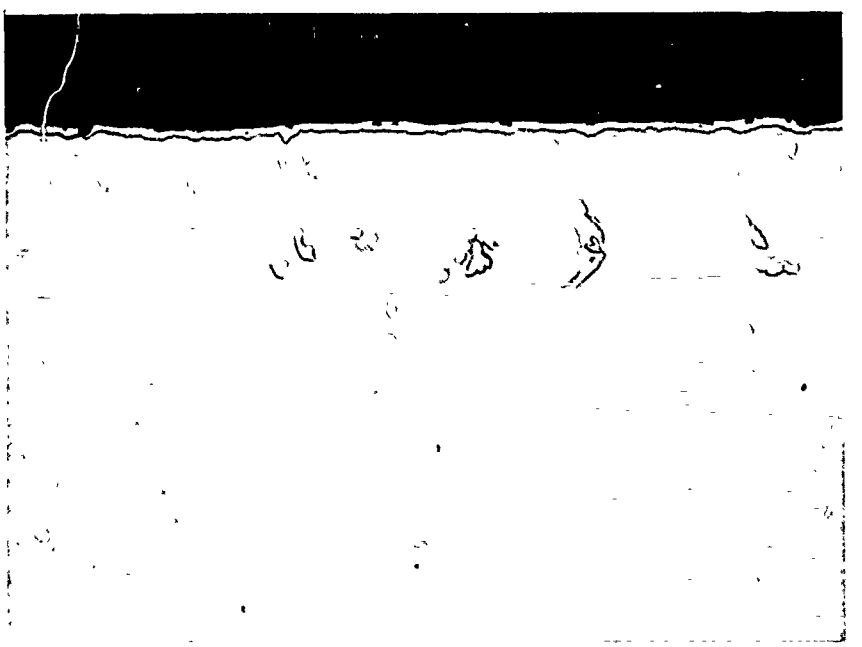

(b) Mold Preheat Temperature 2000°F, Casting G 6054.

Figure 31. Carbide Network Present in As-Cast Surfaces of 0.250 Inch Thick Castability Section, Ti-6Al-4Zr-2Mo Alloy, Showing Effect of 2000°F Preheat - Unetched. 250X

Casting #6108

Figure 32. Hot Tear in Casting.

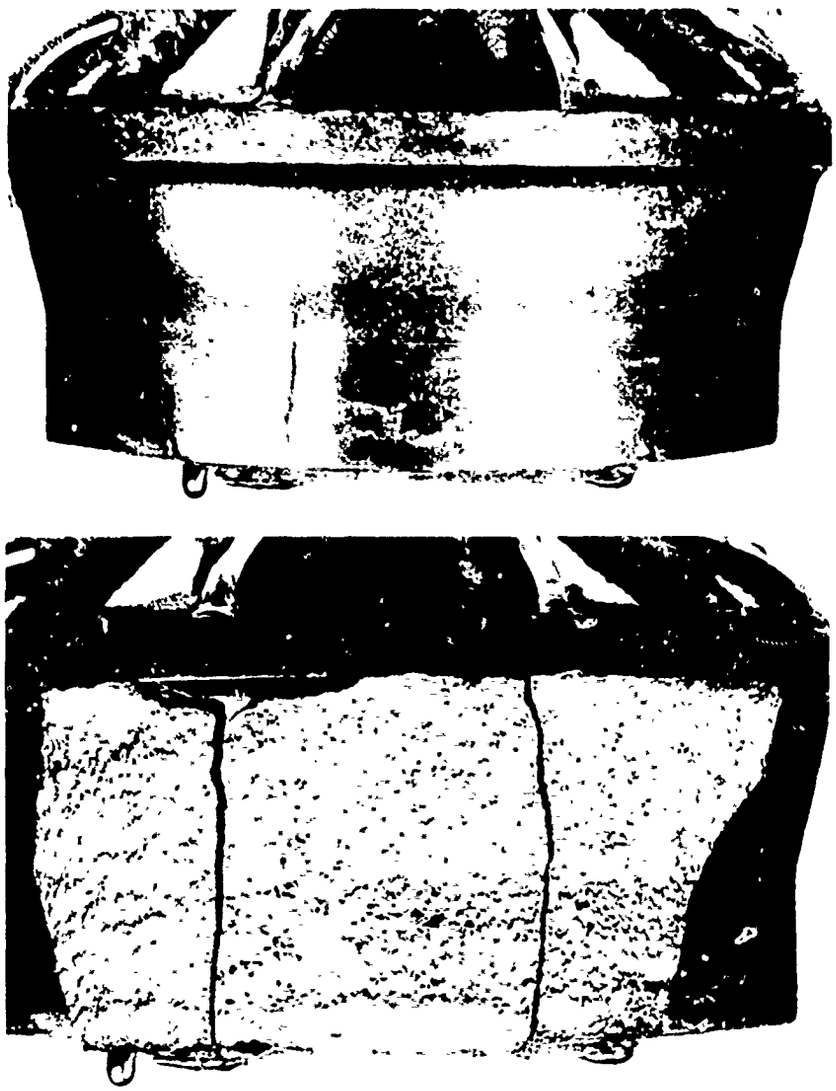

Figure 33. Correlation of Position of Hot Tears with Mold Cracks.

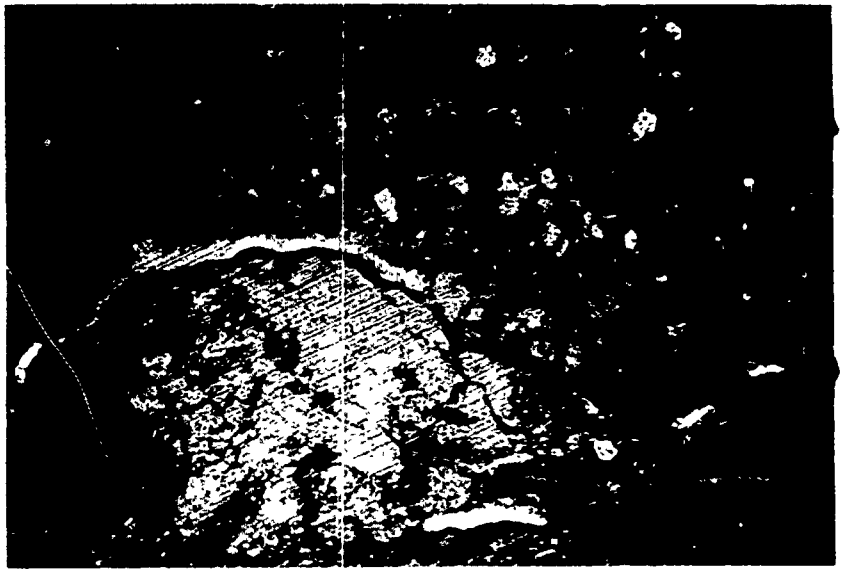

(a)

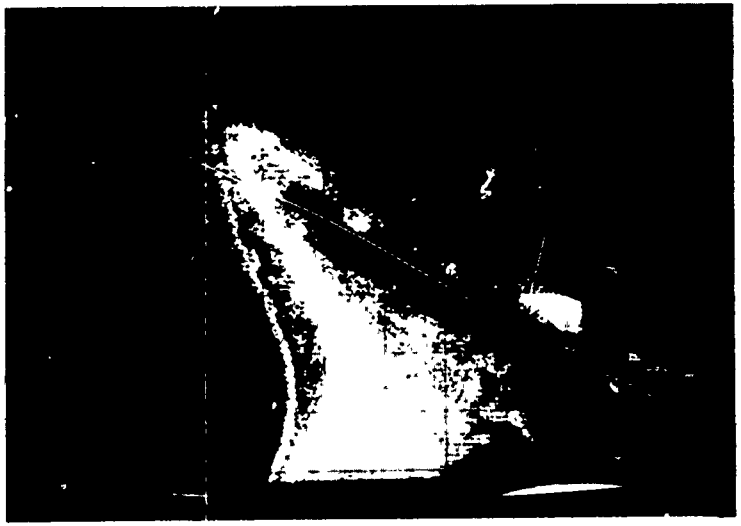

(b)

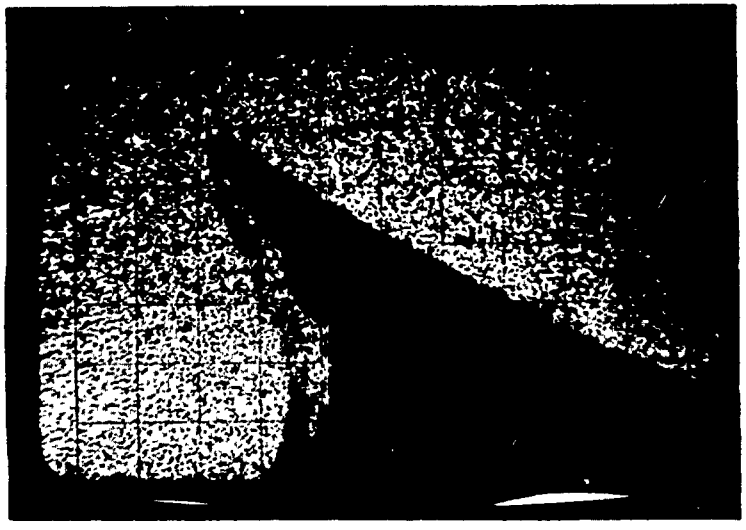

(c)

Figure 34. (a) Cold Shut Defect in Titanium Casting Surface. 2.5X
(b) Carbon X-Ray Photograph of Cross Section. 400X
(c) Titanium X-Ray Photograph of Cross Section. 400X

some discontinuity of titanium metal deposited in the defect area. This defect is formed by reaction between titanium and particles lying on the pyrolytic surface, to form titanium carbide on the surface of the liquid as it enters the mold. Because of stream turbulence this layer is folded at the casting surface.

The cold shut defect results from improper gating and the use of too cold a mold. No cold shuts were present on the surface of casting G 6232, poured at a 2000°F mold preheat; however, all other quarter bearing housings, poured at lower mold preheats, showed cold shuts. A typical example is heat G 6544, poured at 1000°F preheat, shown in Figure 35. This casting was made with the second gating system. Note the surface indications found in the casting wall opposite the gates; indicating that the stream initially entered at these points, and flowed upward to fill the casting while the stream edges began to freeze, forming cold shuts.

An inclusion type defect, typical of those found in castings, is shown in Figure 36a at a 2.5X magnification. Metallographic analysis, Figures 36b and c, revealed the defect area to contain a pyrolytic graphite layer on the titanium alloy cast surface. Another graphite inclusion is shown at 10X in Figure 37. It appears to have broken off of a section of mold, or to have spalled during pouring.

Figure 38 is an example of a mold defect which produces a pit in the casting surface. Such defects are similar to those found in conventional precision casting processes. Typically, they are caused by mold spalling or improper dipping and drying of the mold. No inclusions were found which were directly related to the pyrolytic process of coating the mold. It is essential, however, that molds be thoroughly cleaned prior to coating, as loose particles will be coated over in situ, forming an integral part of the mold and causing pits of this type.

The fourth defect encountered is one usually associated with sand molds. "Rattails", such as the one shown in Figure 39 appear on several of the earlier castings. Microprobe examination of this defect, Figure 40, showed it to contain mold material. Rattails are caused by expansion and spalling of the surface of the mold due to radiant heat transfer from the first metal to enter the mold. Revising the gating to provide a faster fill system eliminated the defect.

b. Casting Porosity

Radiographs of all quarter bearing housing castings showed extensive occurrence of porosity in amounts greater than normally accepted by aircraft engine manufacturers. Figure 41 shows the best casting produced, G 6608, poured at the end of the initial part of the program. Mold making and pouring followed the process specification, Appendix B. Porosity is evident, in spite of re-gating, and an extensive effort to remove sources of gas by degassing the charge for 4 hours at 1800°F at a pressure of 10^{-4} torr, preheating the mold at 1000°F for 2.7 hours at 10^{-2} torr, and preheating the crucible at 2400°F for 2 hours at 10^{-2} torr. Vacuum conditions were maintained in the mold and crucible between degassing and pouring. The persistence of substantial porosity despite these procedures made it necessary to re-direct program efforts to determine the causes of the porosity.

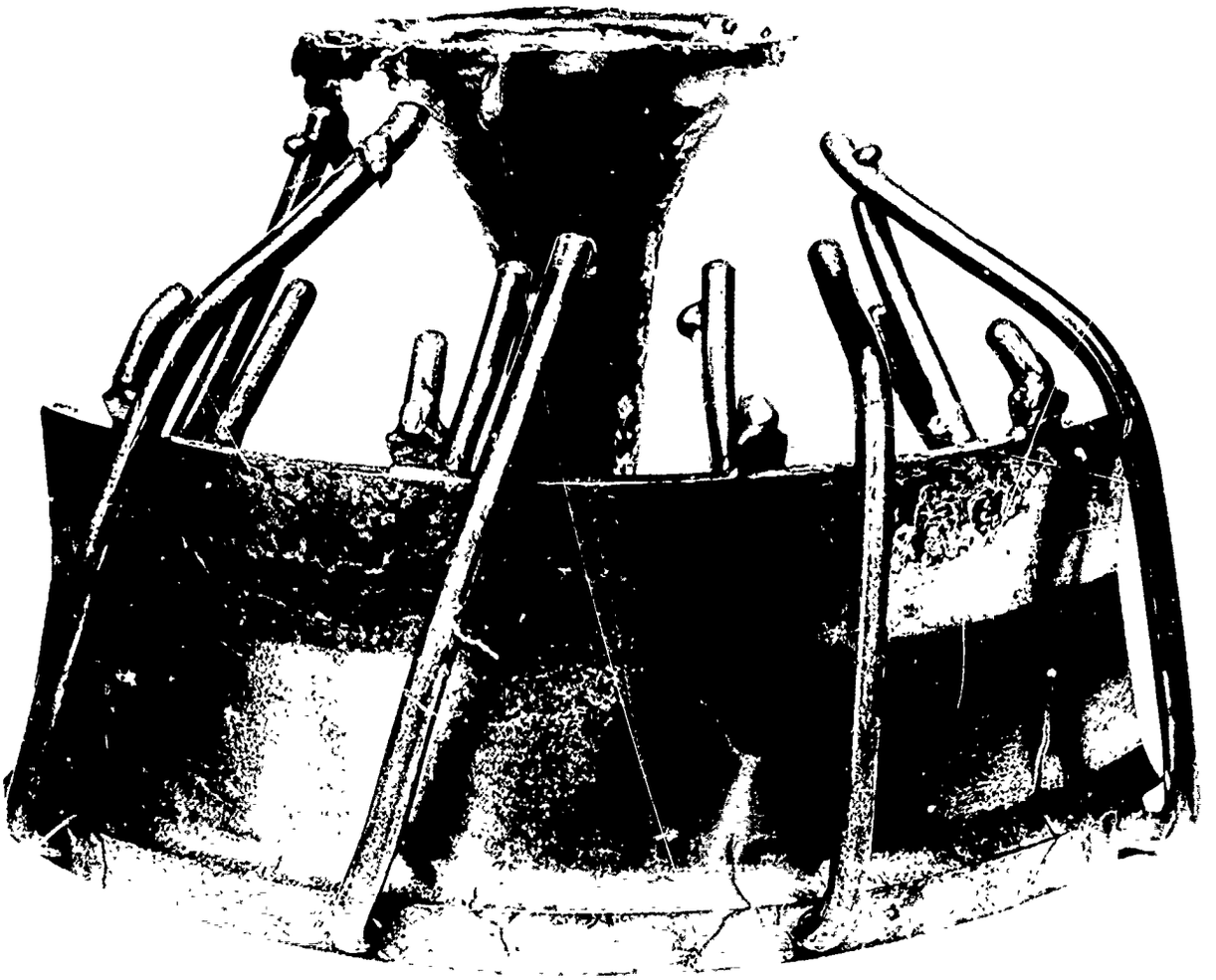

Figure 35. Casting G 6544, Poured at 1000°F Preheat. Note Cold Shuts Opposite Gates.

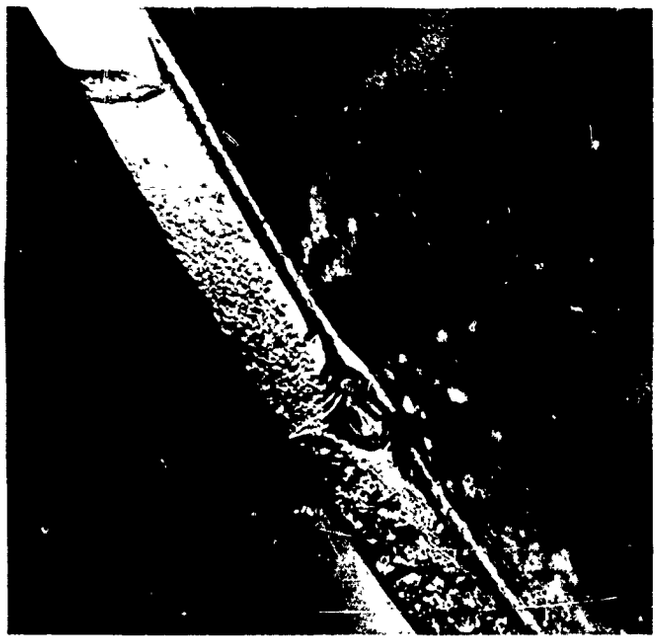

a. As-cast surface, 2.5X

b. Defect area etched after microprobe analysis. Square represents unetched scanned microprobe area. HNO_3-HF Etch, 250X

c. Polarized light photomicrograph of the area shown in (b) above, revealing pyrolytic graphite layer, 250X

Figure 36. Inclusion Type Defect in Cast Surface of Ti-6Al-2Sn-4Zr-2Mo Alloy Quarter Bearing Housing Casting, No. G 6509.

Figure 37. Large Graphite Mold Inclusion in Casting.

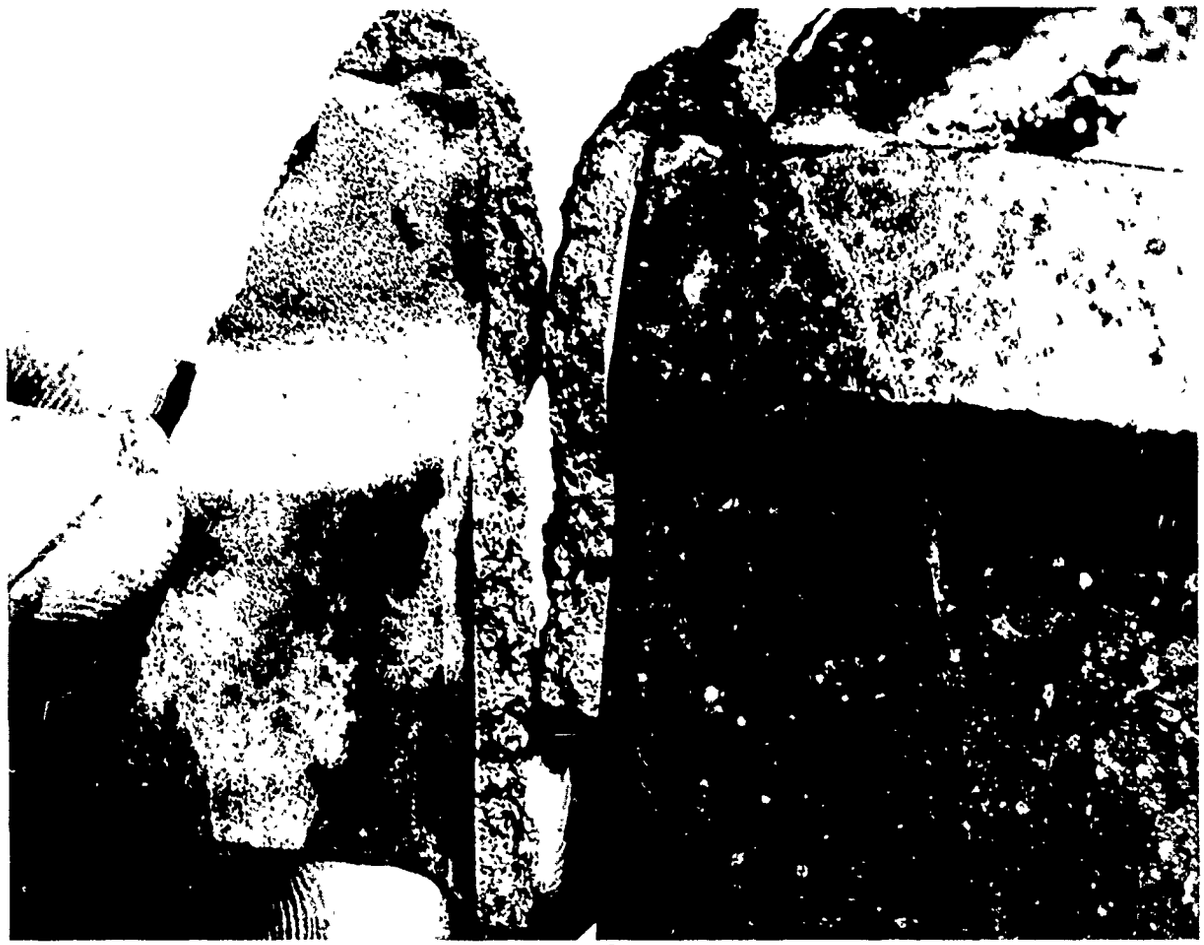

Figure 38. Pit in Casting Surface Caused by Ceramic Inclusion Attached to Mold Face.

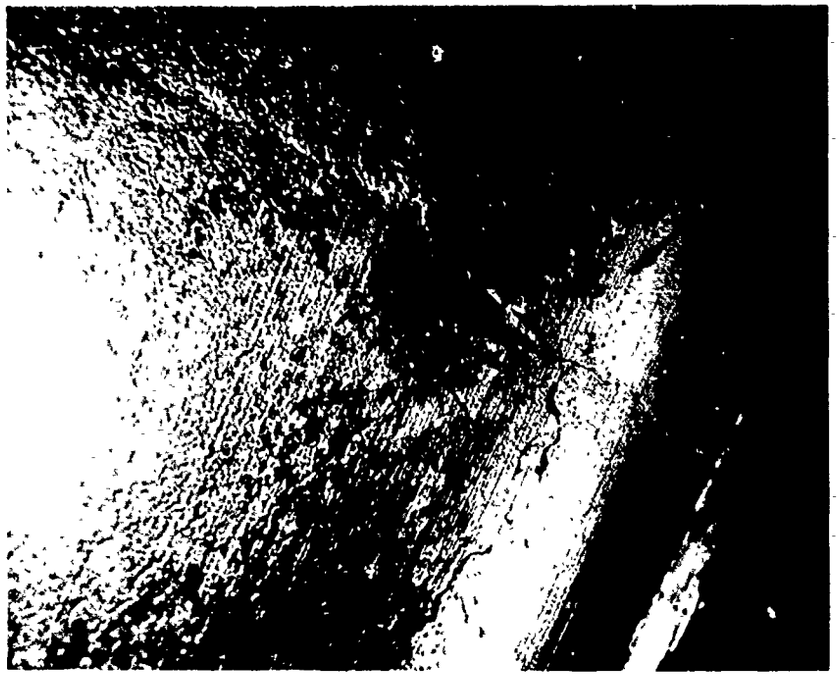

a) As-cast surface, 2.5X

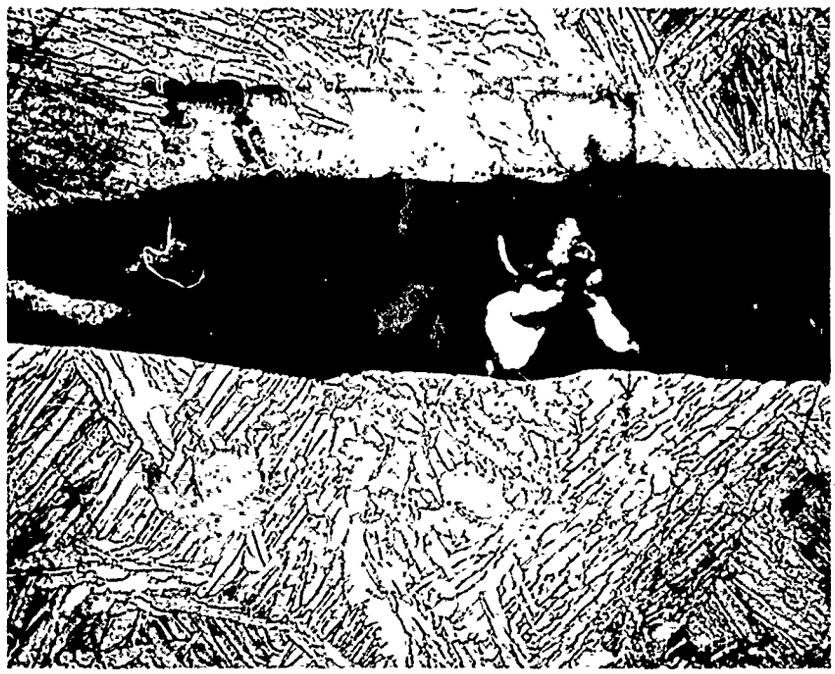

b) Defect area etched after microprobe analysis. Square represents unetched scanned microprobe area. HNO_3-HF Etch, 250X.

Figure 39. Rattail Type Defect in Cast Surface of Ti-6Al-2Sn-4Zr-2Mo Alloy Quarter Bearing Housing. Casting No. G 6509.

a) Zirconium X-ray photograph

b) Silicon X-ray photograph

c) Oxygen X-ray photograph

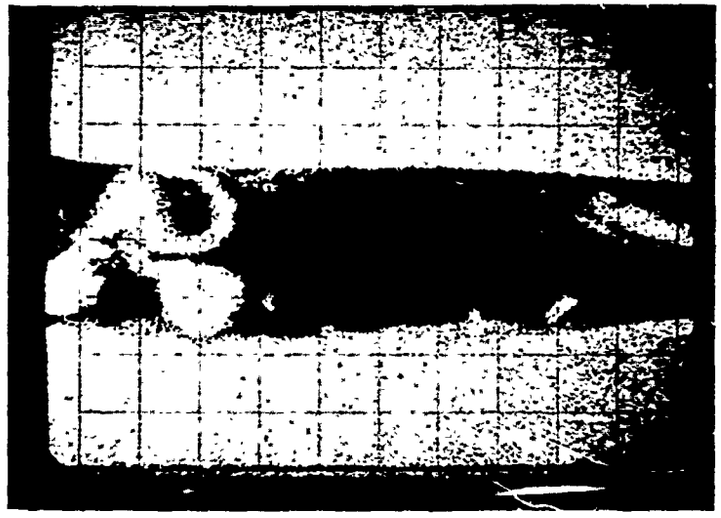

d) Titanium X-ray photograph

Figure 40. X-Ray Photographs of Material in Rattail Defect, 10-Minute Exposure. 400X

Figure 41. Radiographs of Bearing Housing Showing Porosity Distribution.

C. Mechanical Properties

Bearing housing casting G 6608 was sectioned to determine the mechanical properties. Tensile specimens and notched tensile specimens were prepared from the bearing housing sidewalls where the casting was about 1/4" thick. The specimens had a diameter of 0.235" and a gage length of 0.75". The notched specimens were of the same size with 60° V notches reducing the diameter to 0.167" with a .007" radius at the base of the notch. All specimens were vacuum stress relieved at 1100°F for 8 hours.

The tensile tests were made at a .005"/"/min strain rate to the yield point and at .05"/min cross head speed thereafter. Notched specimens were tested at .05"/min to fracture. The data are shown in Table VII.

Two specimens were tested for stability by exposure at 400°F and at 600°F at 50,000 psi stress for 300 hours prior to tensile testing at room temperature.

The results indicate that the strength is acceptable while the ductility at room temperature is marginal. At elevated temperatures the properties appear acceptable. The notched to unnotched strength ratios of about 1.5 represented by this data indicate that the induction melted and cast Ti 6Al-2Sn-4Zr-2Mo alloy is not notch sensitive. The stress stability tests indicate that the material was not embrittled by exposure under these conditions.

F. Casting Analysis

1. Porosity

The extensive occurrence of porosity was the major obstacle to the production of acceptable castings. There is evidence (12) that porosity is a general problem in titanium casting. The program thus concentrated on studying the causes of porosity.

a. Porosity in Titanium Castings

Porosity in titanium castings is frequently present as a smooth walled cavity within the casting. This has led to an arbitrary qualification that when the cavity is large and non-spherical, it is due to solidification shrinkage, whereas when it occurs as dispersed spheres, it is due to gas (18). Such a classification is not entirely accurate, because pores are caused by both shrinkage and gas, acting in combination, as shown by fundamental studies of porosity (19,20). An example of both types of shrinkage is shown in Figure 42.

TABLE VII

Mechanical Properties - Ti-6Al-2Sn-4Zr-2Mo Bearing Housing Casting

Test Temp. (°F)	Ult. Tens. Str. (KSi)	Yield Str. (0.2%) KSi	Elong. % in 3 d	Red. of Area, %	Remarks
R.T.	143.9	134.1	13.0	17.1	
R.T.	132.9	132.0	3.1	5.5	Porosity in fracture
R.T.	140.2	132.1	5.2	13.1	
R.T. (1)	140.0	128.1	7.1	11.5	
R.T. (2)	138.5	127.9	8.1	9.9	
550	101.5	83.9	13.9	24.6	
600	98.2	79.3	18.9	26.8	
600	97.3	79.9	10.9	21.7	
R.T.	205.9	-	-	-	Notched spec.
R.T.	207.1	-	-	-	" "
R.T.	198.9	-	-	-	" "

Casting G 6608

(1) Specimen exposed at 400°F for 300 hours at 50 KSi stress prior to tensile testing at room temperature - 0.13% creep elong.

(2) Specimen exposed at 600°F for 300 hours at 50 KSi stress prior to tensile testing at room temperature - 0.13% creep elong.

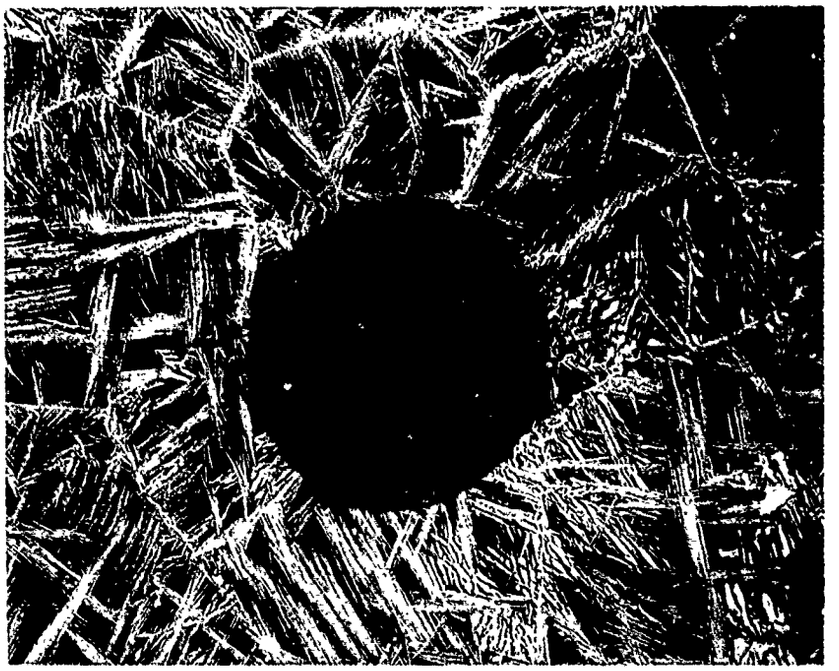

Figure 42. Porosity Formed by Combination of Gas (Circular Area), and Interdendritic Shrinkage. Heat G 6910. 100X

In these studies, it is shown that pores must overcome metallostatic and external applied or atmospheric pressure heads in order to form. Thus pouring under vacuum magnifies the effect of gas, as does the use of a light alloy such as titanium, which lacks the density required to establish a high metallostatic head. Gas is rejected from the solid at the liquid-solid interface. If the gas bubble is large enough to rise at an appreciable rate, and if there is a continuous path of liquid to the atmosphere, the bubble will float out. However, if the surface of the casting freezes quickly, as in titanium alloy castings (because of the high melting point), the bubble will be trapped in the liquid, and will be found located in that part of the casting which is the last to solidify, combined with solidification shrinkage, which also occurs there.

Shrinkage is a function of the density difference between the liquid and the solid, and the mode of solidification, which is governed by the freezing range of the alloy. It has been found (21) that in titanium alloys with small freezing ranges, shrinkage cavities are smooth walled, but that as the freezing range increases the cavities become dendritic. Because of the difficulty in holding liquid titanium in a non-reactive vessel long enough to obtain accurate liquid density readings, there is little information on values of solidification shrinkage for titanium alloys. Magnitskii (22) has shown that shrinkage may increase or decrease with alloying content, depending on the alloy system, and recommends that alloys with wide freezing ranges not be used to produce complex parts because of the difficulty of feeding such alloys adequately. He found, however, that the contribution of gas to total porosity is of greater importance than that of shrinkage. This arises from the great difference in gas solubility between liquid and solid titanium, such that the gas concentration in liquid is frequently greater than the solubility limit in the solid. Gas is present in the liquid because it is picked up from the crucible, the mold, or was present in the original charge material.

Molds can contribute gas to the casting, either from reaction with molten titanium alloys (23), or by solution of adsorbed gases on the mold surface (24). While the reaction contribution can be minimized by eliminating silicate binders from the system, the adsorption problem remains, particularly if adsorbent materials, such as carbon, are used as mold materials. One calculation (23) predicts that 300 cc of gas can be evolved from a 10 cm x 10 cm plate mold made of MgO if the solidification chamber pressure is 1 torr. While MgO has not been used in this program the magnitude of gas volume which can be evolved in such systems is relevant.

The charge may also contribute to gas porosity. As the solubility of hydrogen decreases with increasing temperature in the solid, charge ingots used in this program were prepared from vacuum melted billet stock and were further degassed by holding them at elevated temperatures and reduced pressures prior to melting. It is not known whether the charge material was prepared at a pressure lower than the melting pressure as recommended in order to remove residual dissolved gases (15). Obviously, melting temperatures should be kept below the point where alloying constituents are volatilized to eliminate them as a source of gas.

Because the alloy was selected on the basis of its combination of fluidity and mechanical properties the magnitude of its solidification shrinkage is established and cannot be altered. As discussed above, the response of porosity location to gating changes indicated that the primary cause of porosity was due to gas trapped in the solidifying metal. Early experiments adding argon gas to the vacuum chamber after melting but prior to pouring in order to reduce porosity (heats G 6230, G 6231, and G 6232) did not succeed in significantly reducing the amount of porosity found, and attention was turned to the elements of the pouring system, i.e., the charge, the crucible, and the mold.

b. Crucible Investigation

A preliminary experiment, in which an ingot was poured, radiographed, and the gas in the void pocket analyzed, showed the gas to be hydrogen. Based on this finding, all subsequent charges were de-gassed at 1800°F at 10^{-5} torr, to remove interstitial hydrogen in the charge. The pressures measured during this vacuum treatment indicated that we were removing gas. The occurrence of gas in the castings was, however, not significantly reduced by this practice.

Suspicion then fell on the crucible. Machined from high density, high purity graphite, the crucibles could have been a source of gas, either adsorbed on its surface, or entrapped in its pores. It was reasoned that holding at 2400°F in vacuum for four hours prior to pouring should serve to remove any gas present on or in the crucible. It was further reasoned that if the crucible was coated with pyrolytic graphite on its inner surface, the coating, which is impermeable (see Figure 43), would prevent any gas in the pores from entering the melt. In addition, if the gas were being evolved in a reaction between the molten titanium alloy and trace elements in the graphite binder, the pyrolytic layer would serve as a mechanical barrier to this reaction.

In order to eliminate the mold as a source of gas which would confuse the experiment, "bottle" molds were machined from stainless steel (see Figure 44). These molds had an ingot cavity connected to the riser by a thin neck; when the metal was poured, the neck froze first, trapping gas in the ingot cavity. The interior surfaces of the molds were lightly blasted, blown out with air, wiped with a paper towel, and held at 400°F overnight in air, followed by 400°F in vacuum prior to pouring. Three experiments were run as follows:

1. Machined graphite crucible, no preheat, Heat G 6826.
2. Machined graphite crucible, preheated 4 hours at 2500°F at 5 microns, Heat G 6884.
3. Pyrolytic graphite coated machined graphite crucible, preheated 4 hours at 2400°F at 5 microns, Heat G 6885.

Figure 43. Pyrolytic Graphite Coating on Machined Graphite Crucible. Note the Dense Impermeable Layer. Polarized Light. 500X

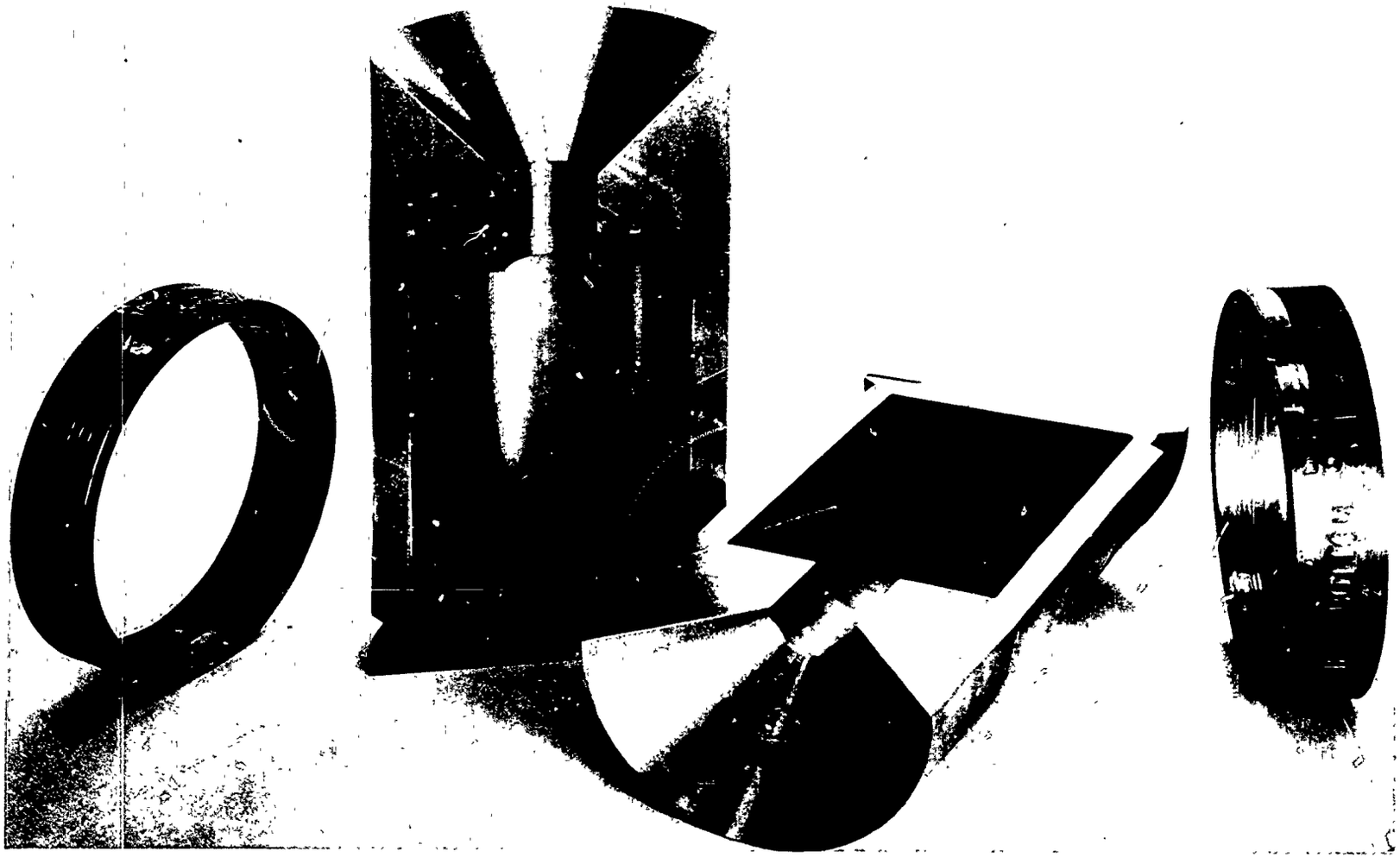

Figure 44. Stainless Steel Bottle Mold Used for Studies of Crucible Gas Evaluation.

After cooling, the ingots were removed from their molds, sectioned, and the gas void measured.

Pressure rise in the furnace chamber was monitored during melting and the results are shown in Figure 45. The heat with the untreated crucible showed a rise to 45 microns during melting. However, the preheated graphite crucible showed a smaller pressure rise (to 7.5 microns), which began at a lower absolute pressure. The pyrolytic coated crucible pressure rise started at a still lower pressure (just above zero microns), and the pressure rose to only 1.5 microns during melting. It is clear that the treatment lowered the gas content of the crucible.

On sectioning the ingots, however, and measuring the actual void volume, it was found that there was little difference in the gas content. The results were as follows:

Heat	Void Volume
G 6826	.6334 in^3
G 6884	.6041 in^3
G 6885	.6455 in^3

Sections from the bottle mold ingots are shown in Figures 46, 47 and 48. Note that the voids are smooth walled, a clear indication of gas.

The above data indicate that there is a contribution to gas porosity which is not due to the crucible (as the de-gassing treatments did not affect it), nor to the mold (as no gas is expected from the permanent mold).

c. Mold Investigation

Although the crucible investigation indicated that no treatment of mold or crucible would be capable of entirely eliminating gas from the casting, there still existed the question of the magnitude of the mold contribution to the total gas content. It was possible that gas might be adsorbed on the mold surface or entrapped in mold pores that did not fill with carbon. A long time hold under vacuum at high temperature prior to pouring was suggested as a way of removing any residual gas that might remain after conventional drying (an overnight bake-out at 400°F). Thus, the following series of experiments was carried out to determine what effect mold de-gassing would have on total gas content.

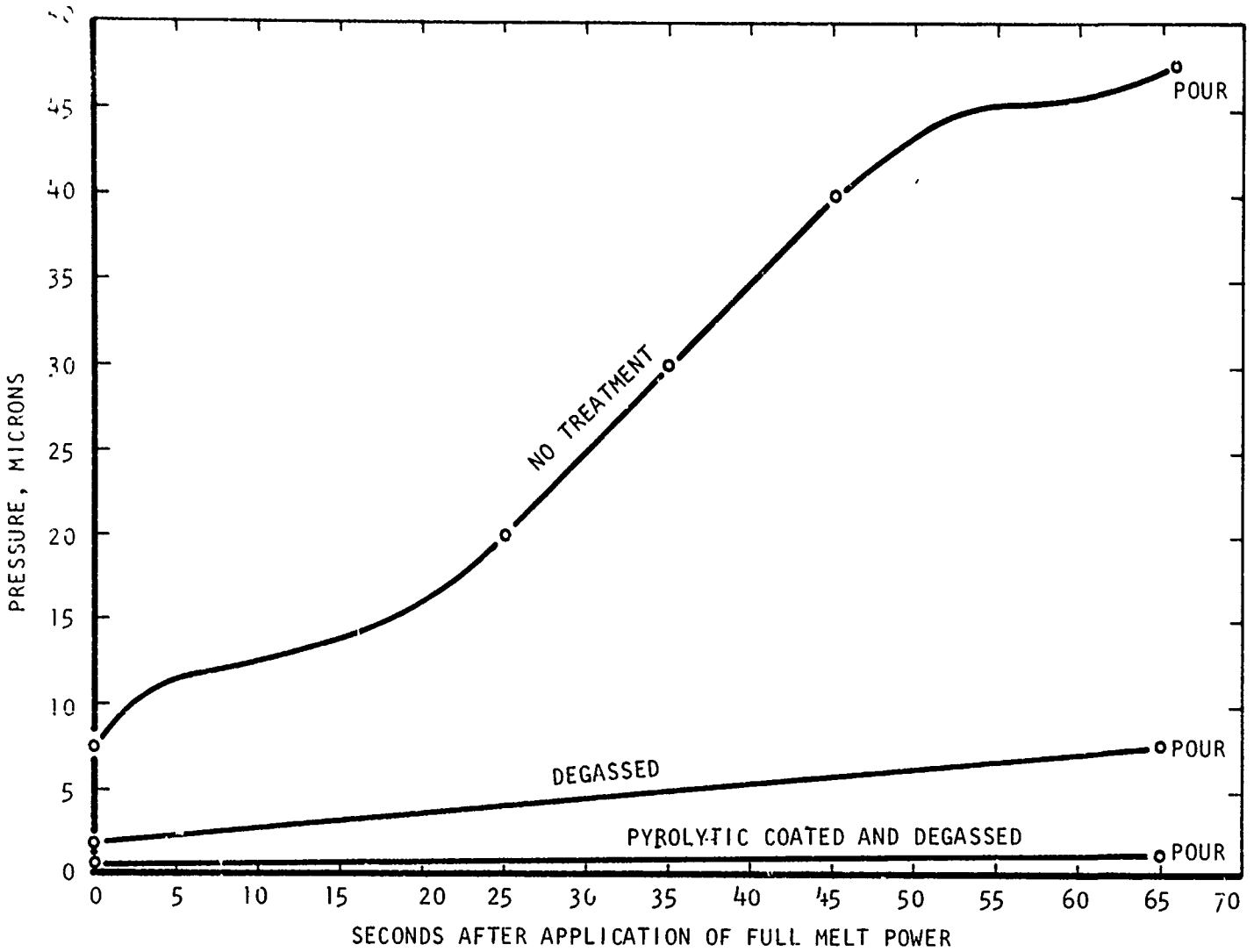

Figure 45. Pressure Rise During Melting for Three Crucible Treatments.

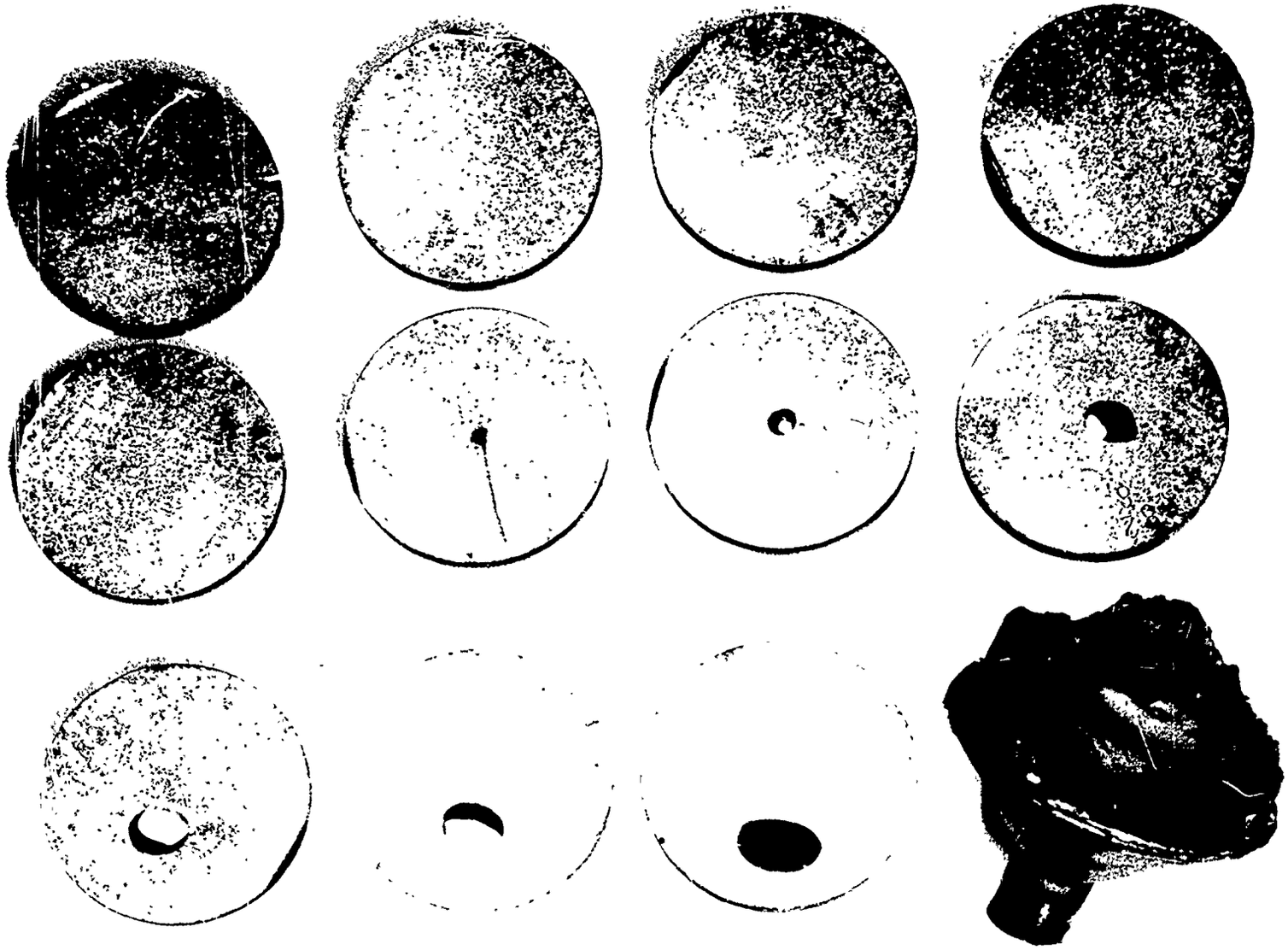

Figure 46.

Sections from Heat G 6826. The Machined Graphite Crucible was not Degassed.

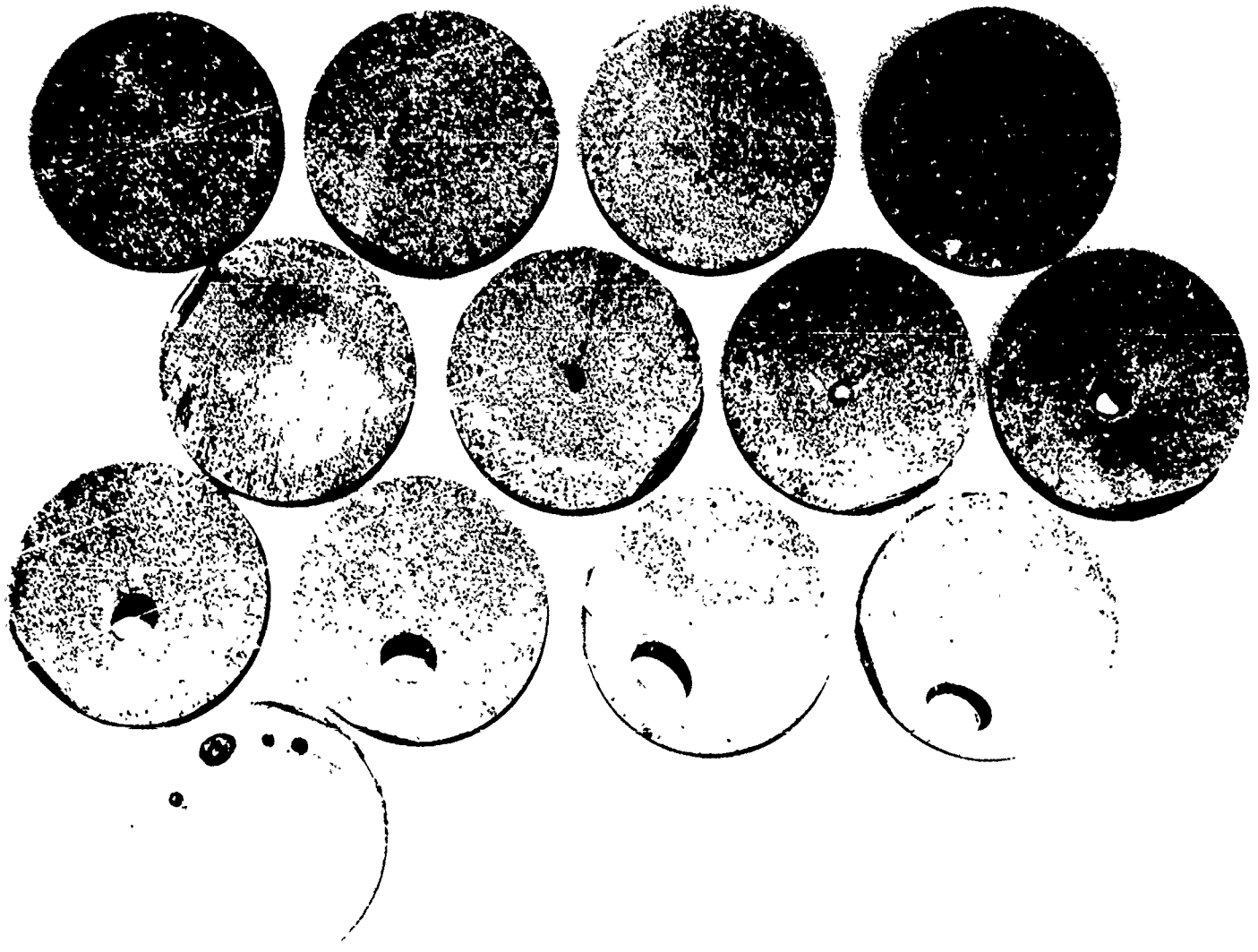

Figure 47. Sections from Heat G 6884. The Machined Graphite Crucible was Degassed 4 Hours at 2400°F under 10 Microns Pressure.

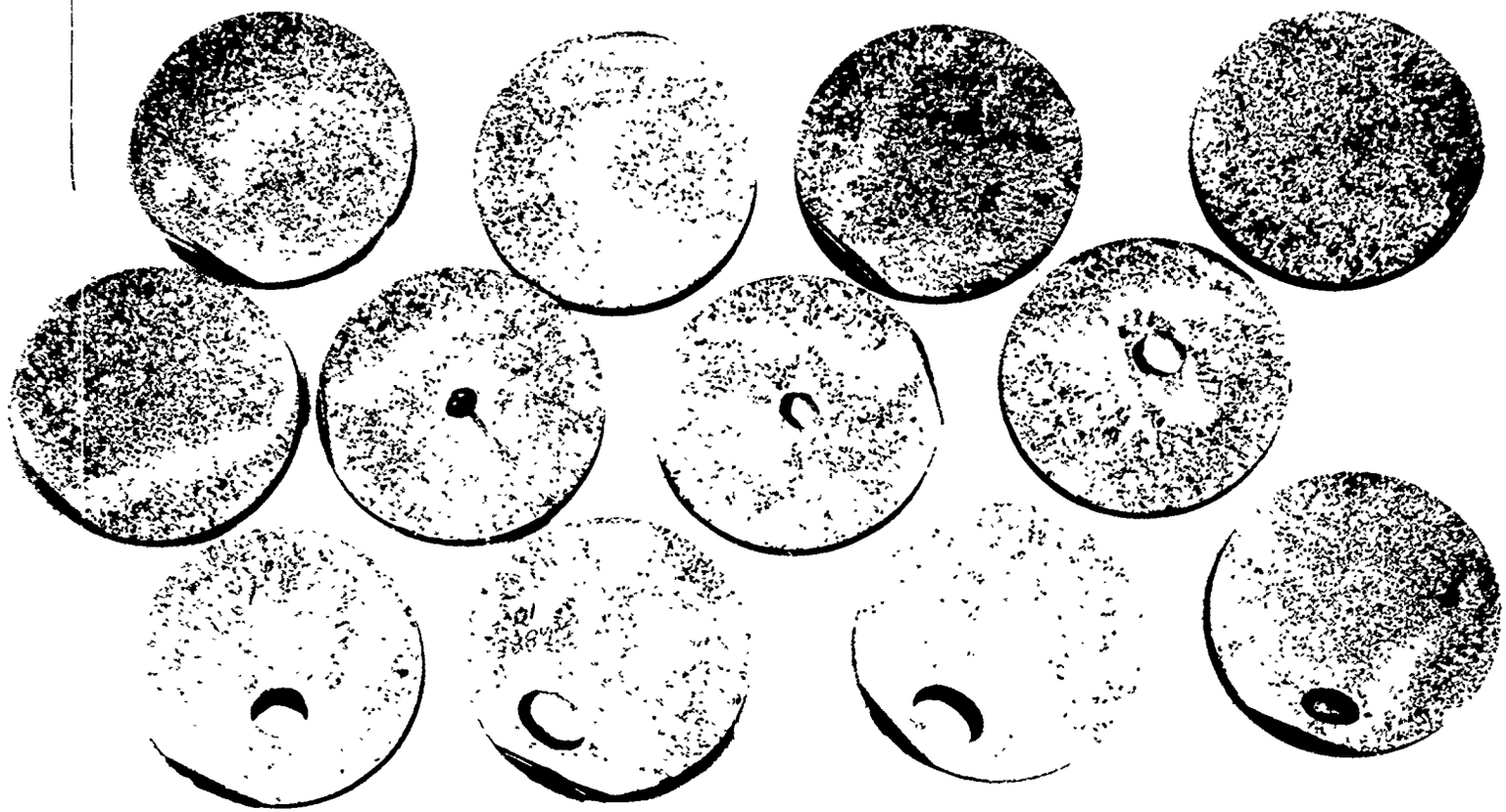

Figure 48. Sections from Heat G 6885. The Machined Graphite Crucible was Coated with Pyrolytic Graphite and Degassed 4 Hours at 2400°F under 10 Microns Pressure.

Heat	Crucible	Mold Treatment
G 6910	Machined Graphite	2 hrs. at 2500°F, cool to 400°F
G 6911	Machined Graphite	1/2 hr. at 400°F
G 6912	P G. Coated Machined Graphite	2 hrs. at 2500°F, cool to 400°F
G 6913	P.G. Coated Machined Graphite	1/2 hr. at 400°F

Vacuum levels were under 5 microns. Approximately four hours were required to cool the mold under vacuum to 400°F; no inert gas was used to accelerate the cooling. All crucibles were de-gassed for 30 minutes at 2425°F. The pyrolytic coated crucibles were included as a recheck of the crucible work.

The molds used were re-designed test-bar molds, shown in Figure 49. All bars are gated from the bottom, vented, and individually risered. This was done to provide a smooth bottom fill condition, which would not entrap gas as a result of flow conditions.

Castings were cooled, the mold material removed, and the test bars cut off, blasted and radiographed. The radiographs are shown in Figures 50 and 51. As expected, gas is present in all bars. The mold de-gassing treatment used had no effect on the gas content of the castings.

d. Charge Material Investigation

It was hypothesized that the gas might be due to volatilization of an alloy element, specifically aluminum, during melting. Microprobe examinations were made of the surface of the cavities from the steel molds, assuming that volatilized aluminum would have plated out on the mold cavity walls. There was, however, no increase in aluminum content at the cavity surfaces.

As a further check of this hypothesis a test bar mold of CP grade (i.e., pure) titanium was poured and radiographed. These radiographs, Figure 52, show that voids are present in the CP material, and clearly do not arise from alloying elements.

These radiographs are of interest as they show the porosity concentrated in the upper portion of the bars and gating system, where it would be expected to be found if gas rather than shrink. The effect of mold preheat temperature on gas porosity is compared in Figure 53, which shows bars from a mold preheated at 2000°F for 1 hour prior to pour (heat G 6935) and Figure 54, which shows bars from a mold preheated at 400°F for 1 hour prior to pour (heat G 6936). There is no significant difference in porosity levels.

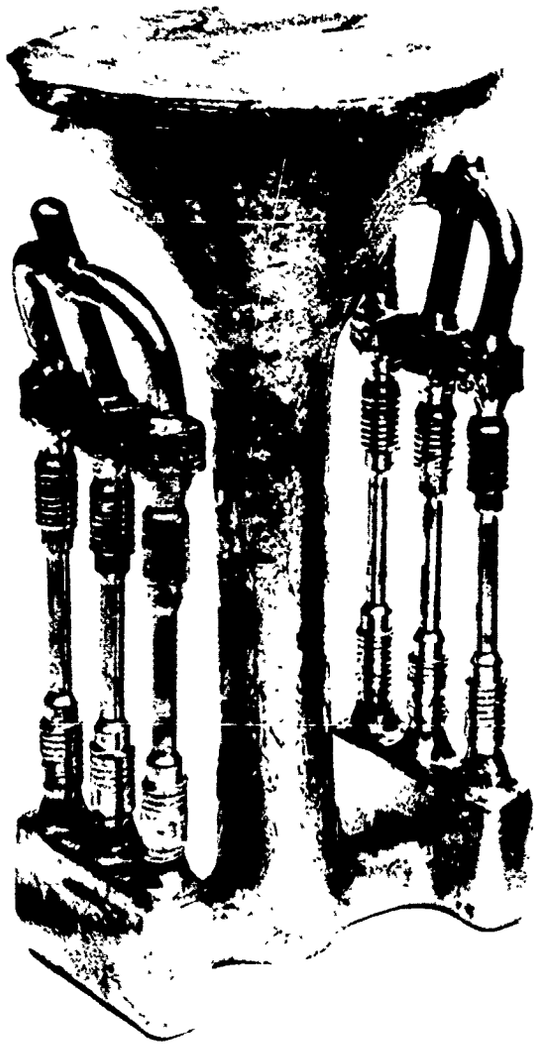

Figure 49. Tensile Cluster.

(a) Heat G 6912

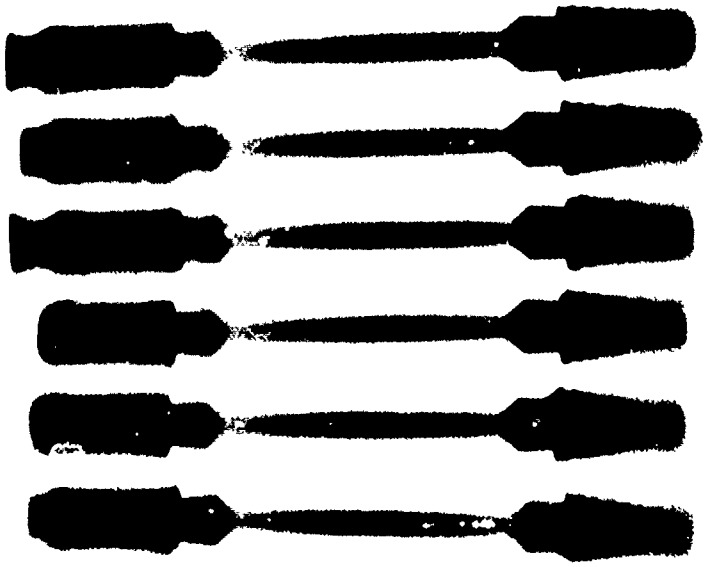

(b) Heat G 6913

Figure 50. Radiographs of Test Bars Poured from Machined Graphite Crucible Coated with Pyrolytic Graphite.

(a) Mold degassed 2 hours at 2500°F, cooled under vacuum to 400°F.

(b) Mold degassed 20 minutes at 400°F.

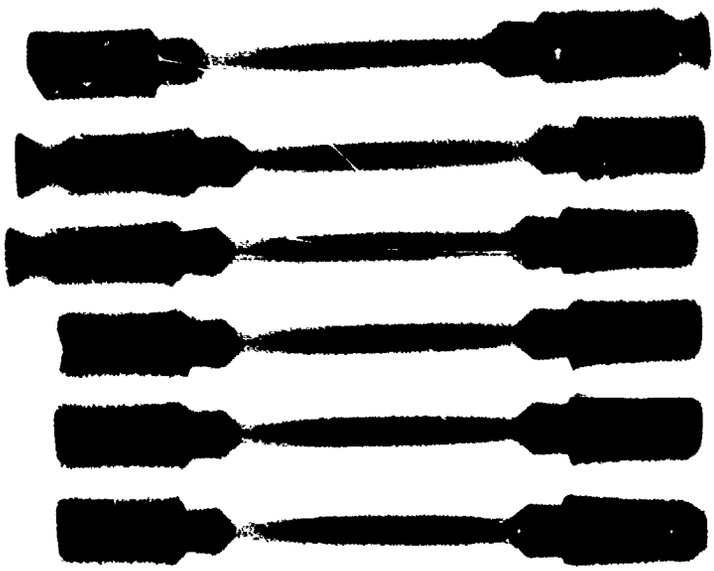

(a) Heat G 6910

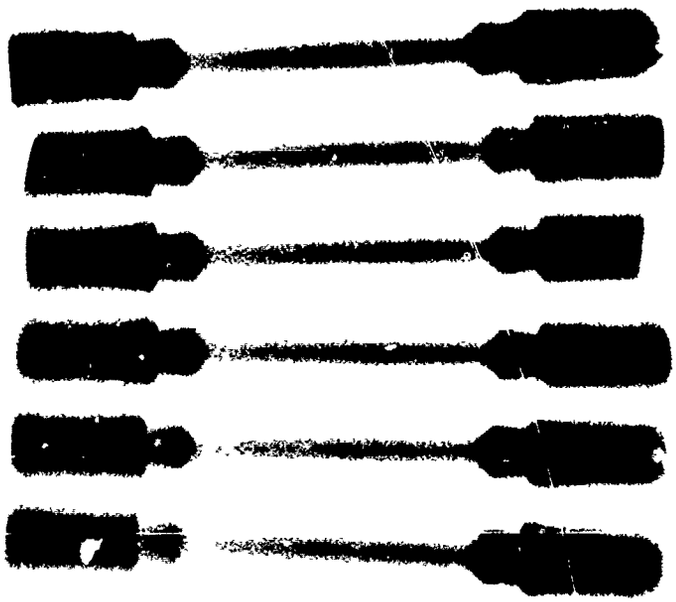

(b) Heat G 6911

Figure 51. Radiographs of Test Bars Poured from Machined Graphite Crucible.
(a) Mold degassed 2 Hours at 2500°F, cooled under vacuum to 400°F.
(b) Mold degassed 30 minutes at 400°F.

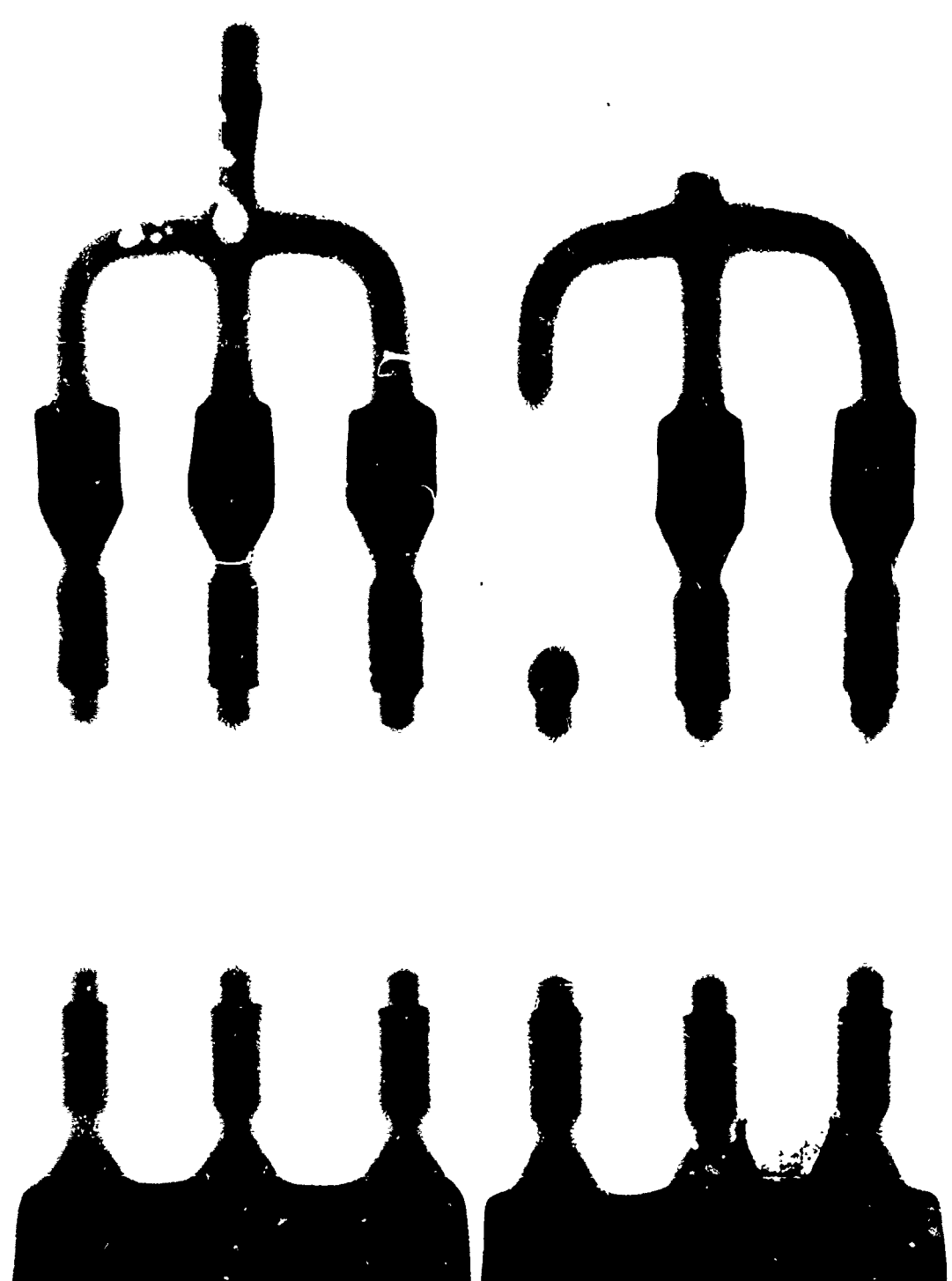

Figure 52. Radiographs of Test Bars Poured in Pure Titanium. Note the Presence of Gas Voids within the Bars, Runners, and Vents. Full Size. G 6937.

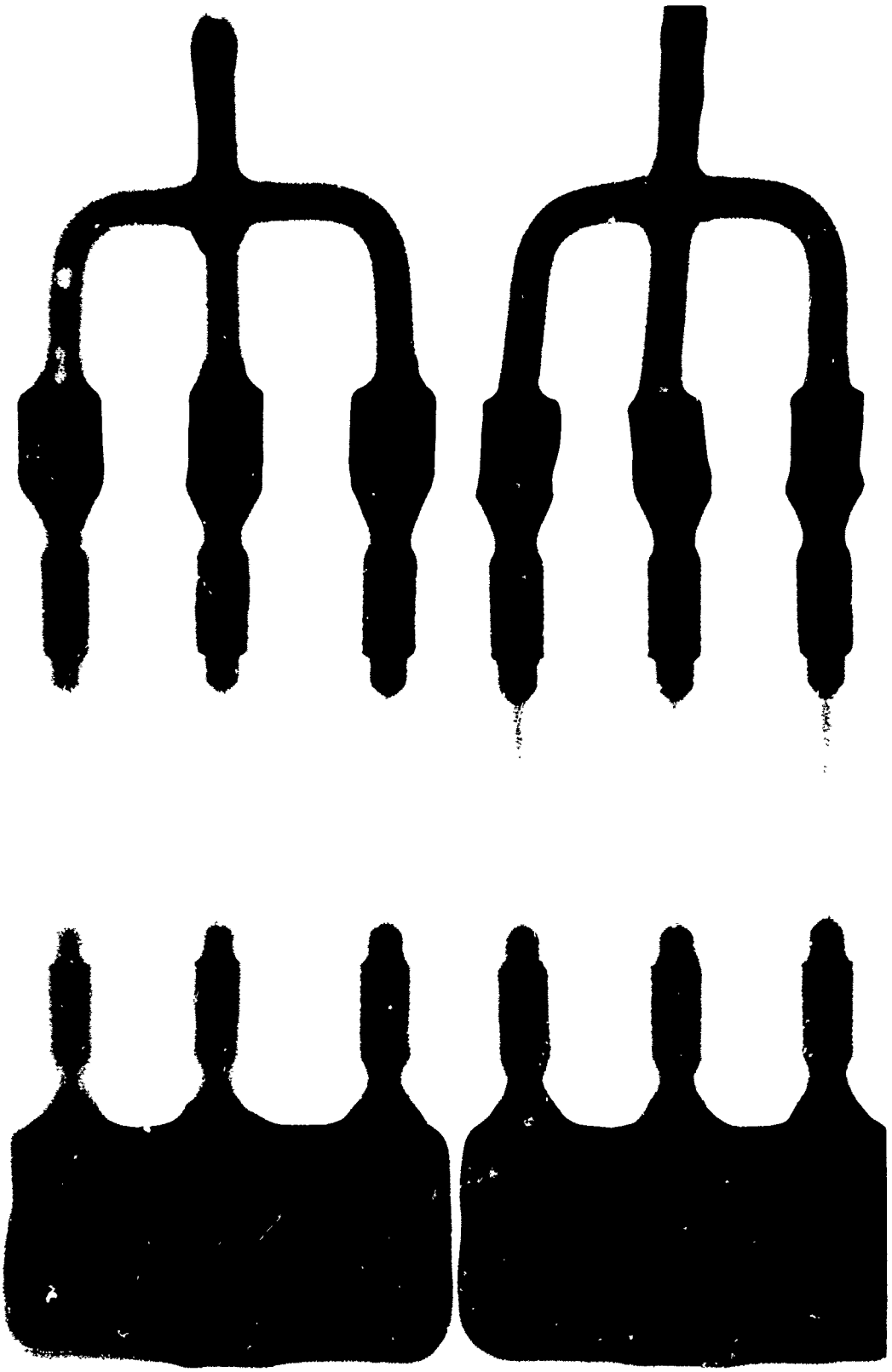

Figure 53. Porosity Occurring in Ti-6Al-2Sn-4Zr-2Mo Test Bars Poured in a Mold Preheated One Hour at 2000°F below 5 Microns Pressure. Full Size. G 6935.

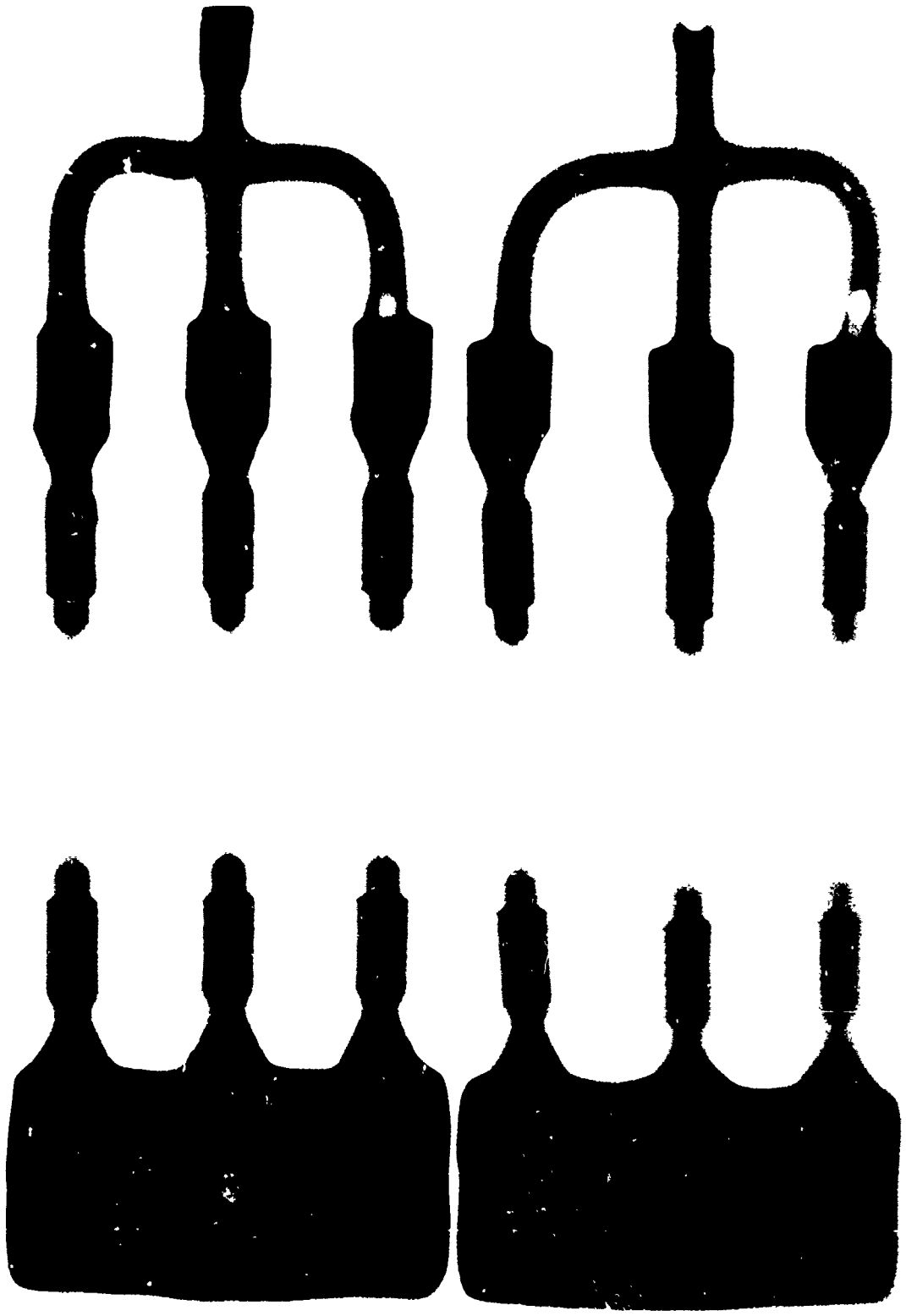

Figure 54. Porosity Occurring in Test Bars Poured in a Mold Preheated One Hour at 400°F below 5 Microns Pressure. Full Size. G 6936.

e. Summary of Porosity Investigation

The results of these experiments indicate that porosity is primarily due to gas, very probably originating in the charge material, and most probably hydrogen. While gas porosity can be minimized by using degassed charge material, and vacuum degassing the molds and crucibles prior to pouring according to the process specification, Appendix B, the only effective method found so far for the elimination of gas pores is centrifugal or some other non-static form of casting, in order to exert sufficient pressure to suppress the formation of pores. The alternative to this method would appear to be the use of massive gating systems.

2. Microstructure

The alloys evaluated in this program have been developed for application as wrought materials. Two of the alloys can be expected to have both alpha and beta phases present at room temperature as a result of their composition, i.e., Ti 6Al-4V and Ti 6Al-2Sn-4Zr-2Mo. The microstructures obtained with these alloys can be varied, however, through variations in the rates of cooling from the high temperature beta phase field, and by heat treatment. The effects of post casting heat treatments were not studied in this program. The cooling rates were varied, as a reuslt of variations in section thickness and mold temperature.

In Figures 55 and 56, the microstructures obtained in .090" thick sections of the two alpha-beta alloys when cast into molds at 1000°F and 2000°F are shown. The microstructures are similar showing the Widmanstatten plates of alpha and small percentages of beta in the interstices. The 1000°F mold temperature permitted a more rapid cooling from the beta field resulting in smaller platelets and smaller grain size. The Ti 6Al-4V microstructure is coarser than that of the Ti 6Al-2Sn-4Zr-2Mo alloy for equivalent mold temperatures indicating that the kinetics of the transformation and growth processes are slower for the latter alloy. The finer structure tends to increase the ductility and strength as noted in the earlier discussions of tensile properties. The solubility limit of the alpha phase for carbon is approximately 0.13% and since none of these castings exceeded that limit there are no carbides apparent.

In Figures 57 and 58, the microstructures obtained in 0.090" thick sections of the two beta alloys when cast into molds at 1000°F and 2000°F are shown. Both of these alloys are metastable beta alloys in which the beta phase can be retained to room temperature. Higher strength properties can be developed by aging at intermediate temperatures which results in a fine alpha transformation product. The effects of post casting heat treatments were not studied in this program. The beta alloys differ from the alpha-beta alloys also in that the solubility limit for carbon in the beta phase is very low. Thus, the carbon contamination from the induction melting process results in titanium carbide in the microstructure. The beta

1000°F Mold - G 6010

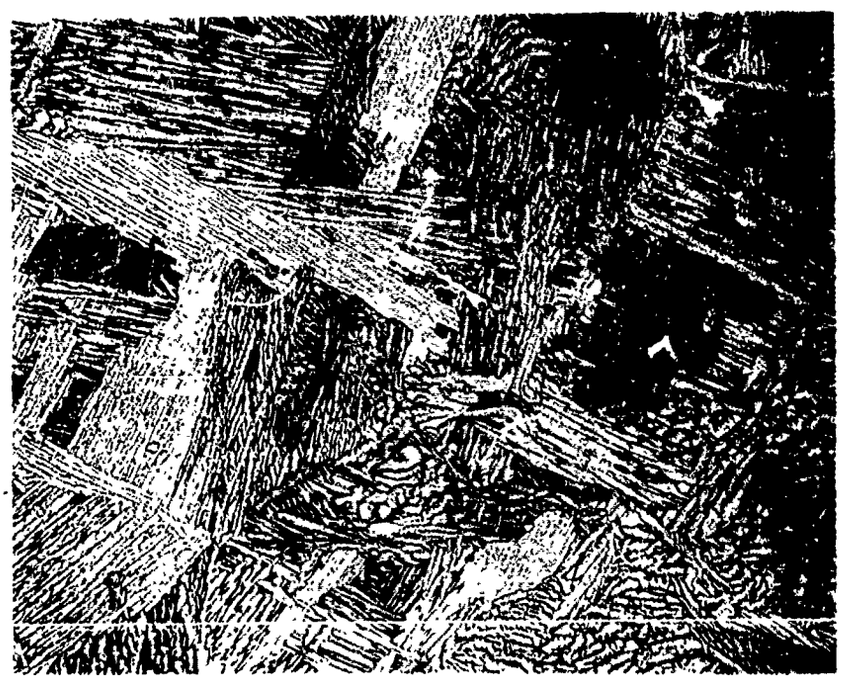

2000°F Mold - G-6028

Figure 55. Ti-6Al-4V Alloy As-Cast .090" Thick Sections from Molds Preheated to Indicated Temperatures. Etchant $2HF:2HNO_3:96H_2O$. 100X

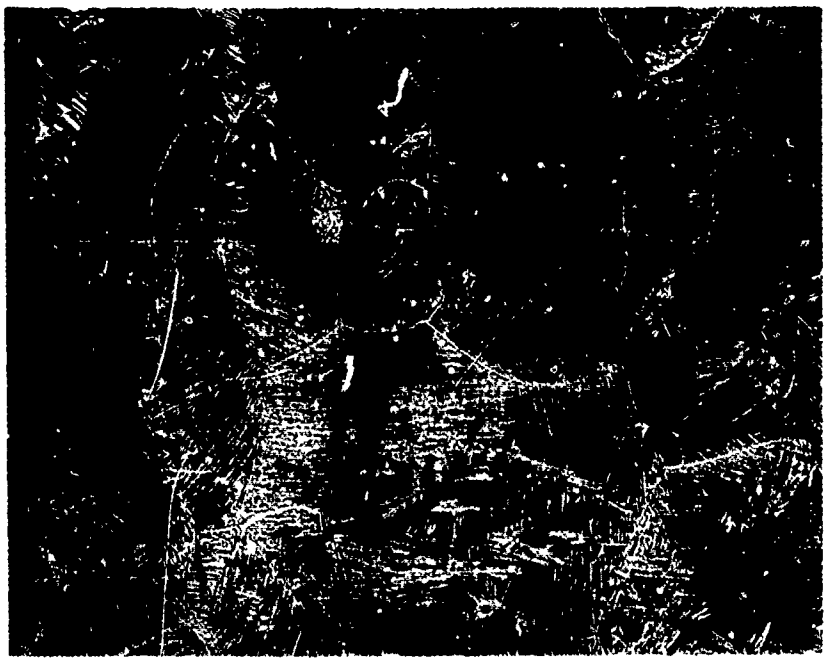

1000°F Mold - G 6049

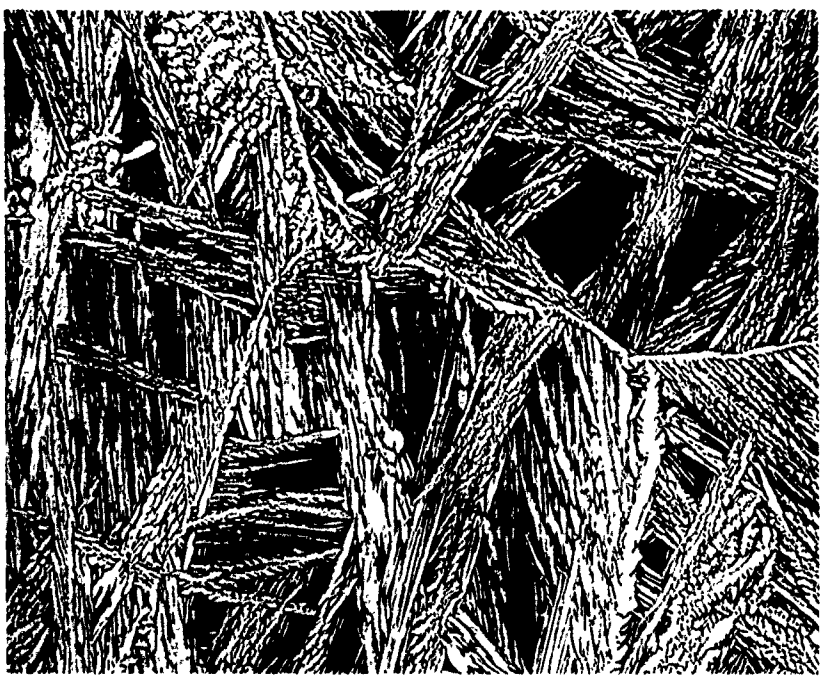

2000°F Mold - G 6299

Figure 56. Ti-6Al-2Sn-4Zr-2Mo Alloy As-Cast .090" Thick Sections from Molds Preheated to Indicated Temperatures. Etchant 2HF:2HNO_3:96H_2O. 100X

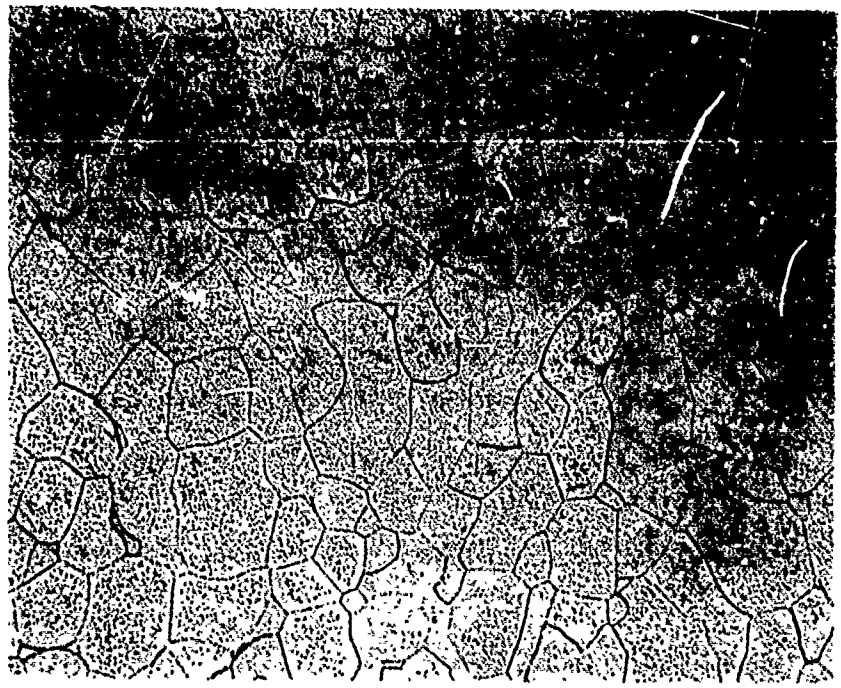

1000°F Mold - G 6065

2000°F Mold - G 6095

Figure 57. 3Al-8V-6Cr-4Zr-4Mo Alloy As-Cast .090" Thick Sections from Molds Preheated to Indicated Temperatures. Etchant $2HF:2HNO_3:96H_2O$.

100X

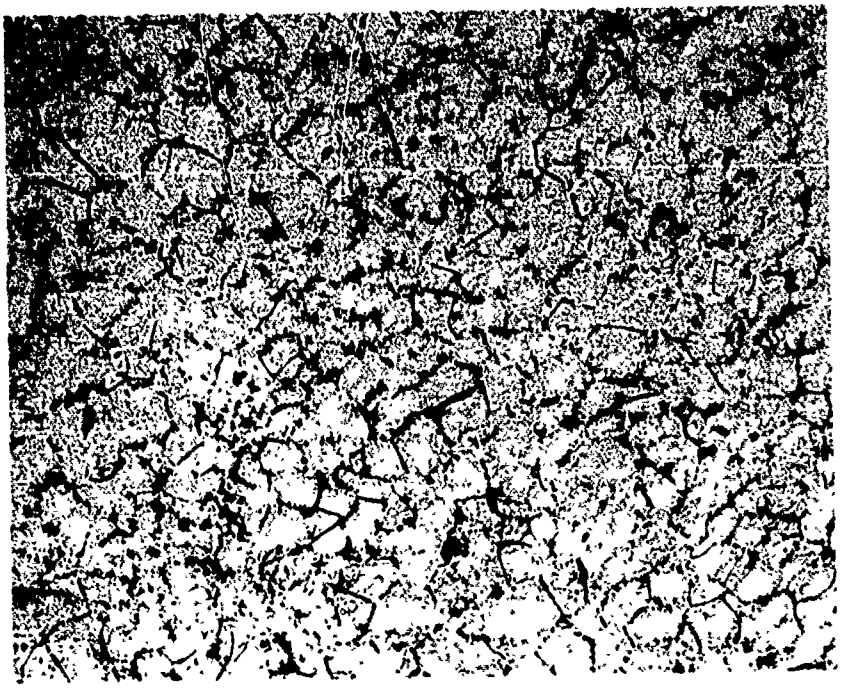

1000°F - G 6329

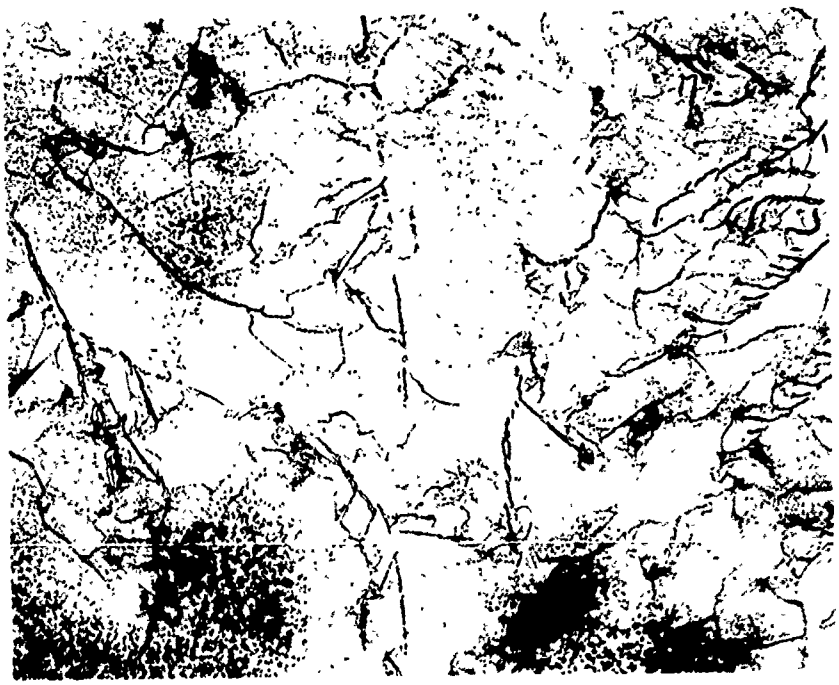

2000°F - G 6331

Figure 58. Beta III Alloy As-Cast .090" Thick Sections from Molds Preheated to Indicated Temperatures. Etchant $3HF:12HNO_3:85H_2O$. 100X

alloys also show higher carbon contents than the alpha beta alloys for similar casting conditions probably as a result of more contact with the graphite crucible during melting as a result of the more sluggish behavior noted earlier. The carbides can be seen in both alloys as grain boundary and internal particles. The lower mold temperature and the attendant more rapid cooling rate result in a significantly smaller grain size in both alloys. The darkened areas in the Beta III alloy cast into the 2000°F mold are thought to be fine alpha grains from the transformation of the metastable beta during the longer cooling time as the mold and casting cooled from 2000°F.

The microstructures of sections of a Ti 6242 bearing housing casting representing thin (1/8") and thick (3/4") sections are shown in Figure 59. This casting (G 6608) was made in a mold preheated to 1250°F. The microstructure is very similar in these two sections showing a slightly larger grain size in the thicker section.

One of the persistent problems in producing titanium castings is the presence of gas porosity and shrinkage. Typical examples of these types of defects are shown in Figure 60. The defects are characteristic and are unrelated to the type of alloy. No composition variations are evident in either alloy with either type of solidification defect. This subject is discussed in detail in the preceding section.

The evaluation of carbon pickup and its effect on castability of the two alpha-beta alloys provided further opportunity to compare the microstructures of the two alloys. In the high carbon Ti 6Al-4V alloy, as shown in Figure 61, alpha plates are considerably larger than in the high carbon Ti 6Al-2Sn-4Zr-2Mo alloy, Figure 62. A very fine grain boundary precipitate of TiC can be seen in the microstructures of the three castings (G 6927, G 6928, G 6930). They are more apparent in the unetched state as shown in Figure 63. No TiC was evident in G 6939 which is consistent with the analytical results which indicated 0.13% carbon in the latter casting. The other three castings in this group were determined to be at 0.20% carbon levels.

In evaluating the tensile properties of the bearing housing casting it was noted that some variability of tensile ductility was obtained. In seeking to explain the variability on the basis of microstructure it was observed that the specimens having lower ductility also had some large alpha phase particles. For example, in Figure 64 the broader than usual alpha phase at the grain boundary was observed. It is thought, therefore, that the lower ductility is associated with porosity, as has been discussed separately, and with microstructures containing fairly massive alpha grains. No attempt was made to analyze these grains but it is possible that they represent microsegregation of alpha stabilizing elements which can be detrimental to the ductility.

Thin Section

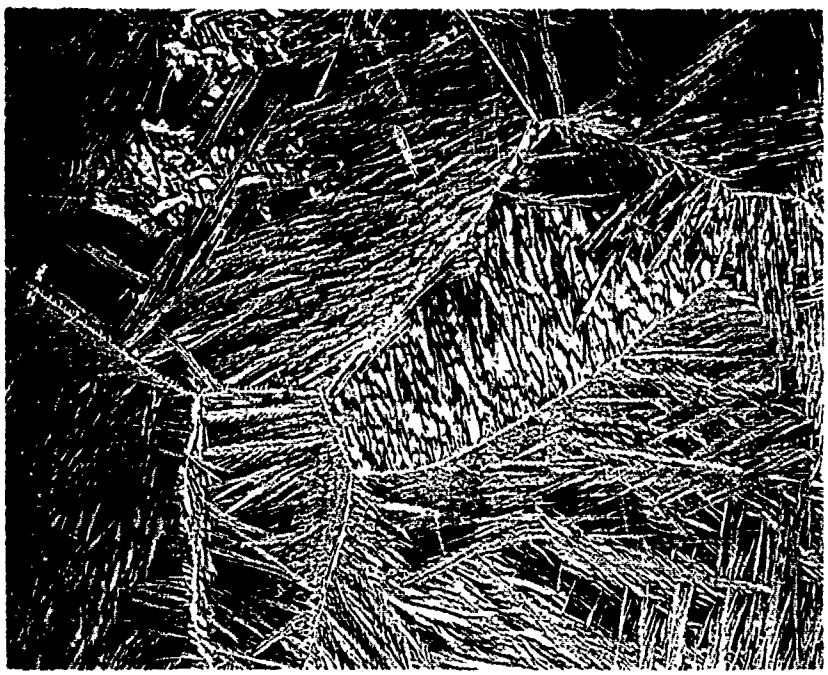

Thick Section

Figure 59. Ti-6Al-2Sn-4Zr-2Mo Bearing Housing Casting As-Cast. Etchant $2HF:2HNO_3:96H_2O$. 100X

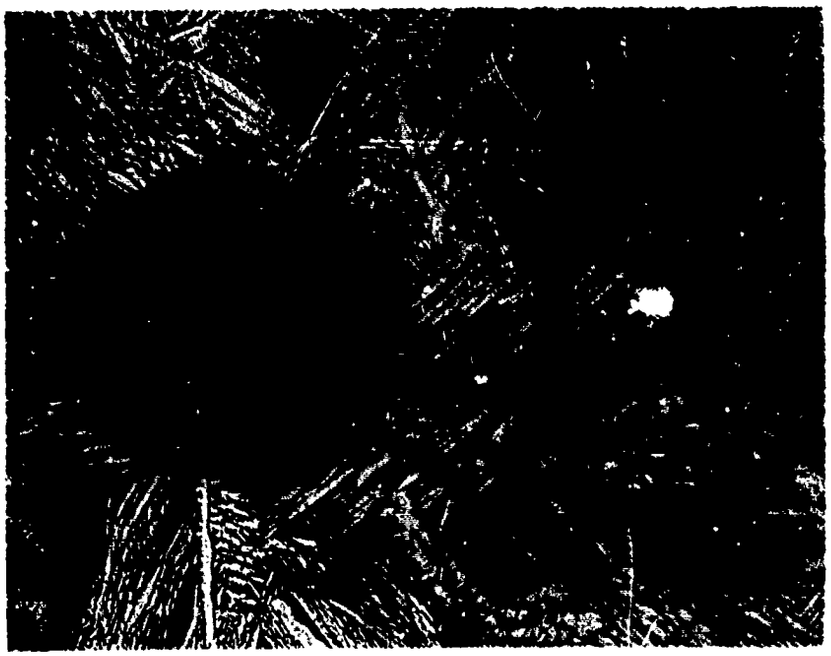

Ti-6Al-4Zr-2Mo

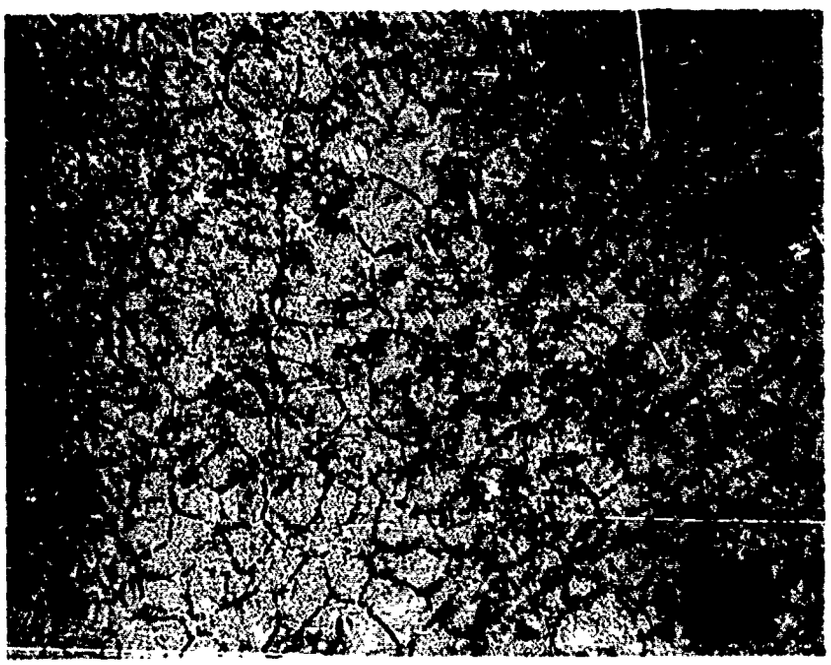

Beta III Titanium

Figure 60. Gas Porosity in Titanium Alloy Casting. Etchant $2HF:2HNO_3:96H_2O$. 100X

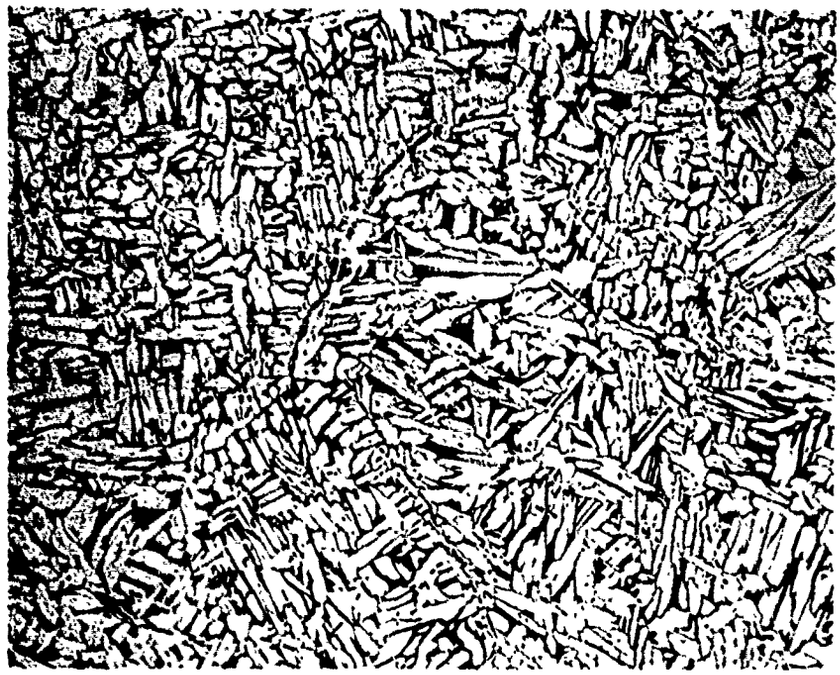

G 6928

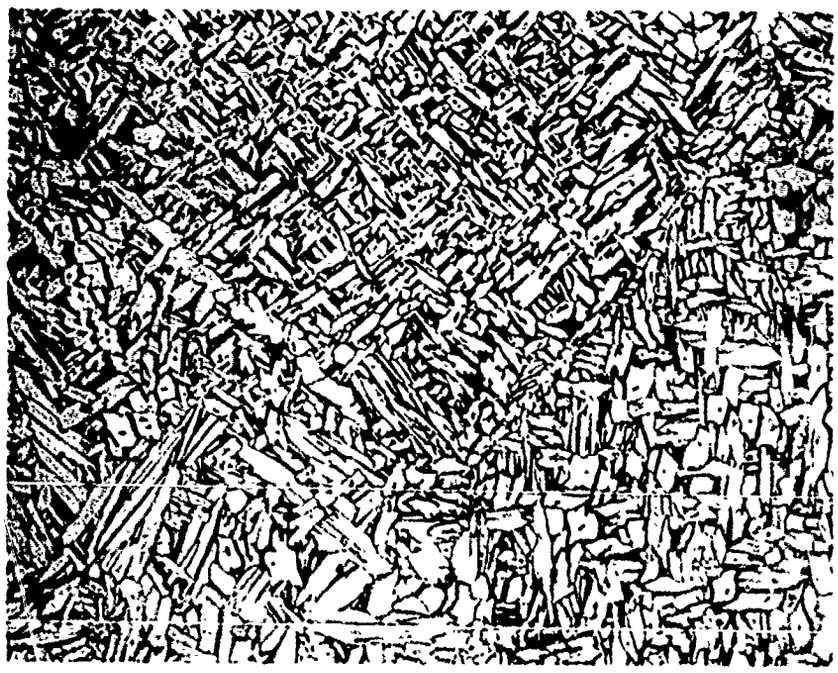

G 6930

Figure 61 Ti-6Al-4V Alloy High Carbon Castability Casting Microstructures As-Cast. Etchant $2HF:2HNO_3:96H_2O$. 250X

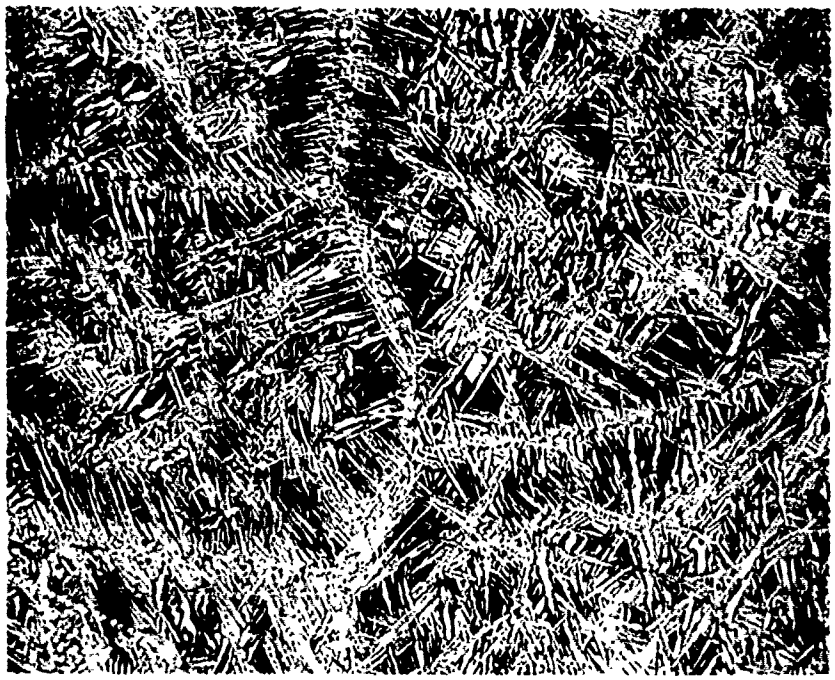

G 6927

G 6929

Figure 62. Ti-6Al-2Sn-4Zr-2Mo Alloy Castability Casting Microstructures As-Cast. Etchant $2HF:2HNO_3:96H_2O$. 250X

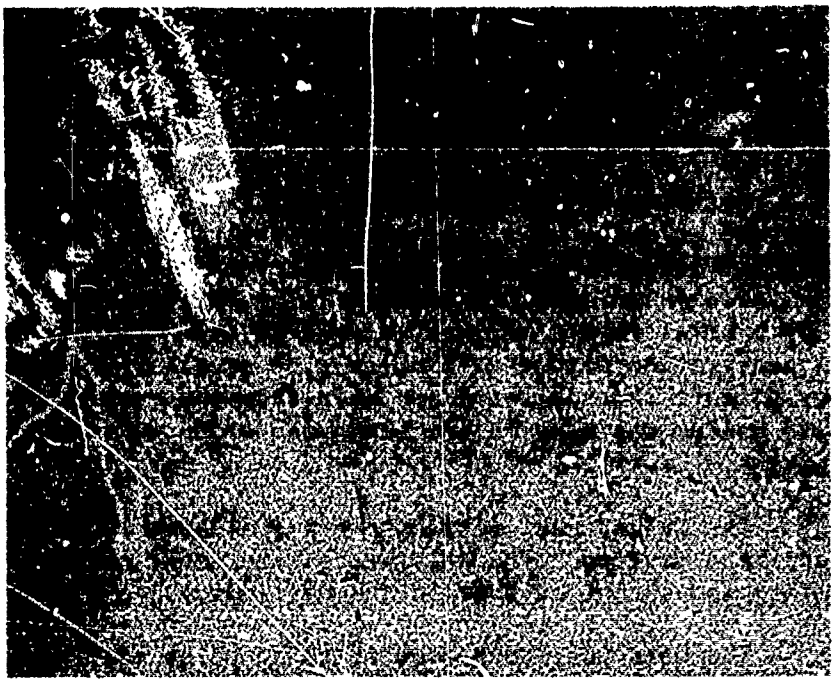

Figure 63. Ti-6Al-4V Alloy Castability Casting. Unetched. 250X

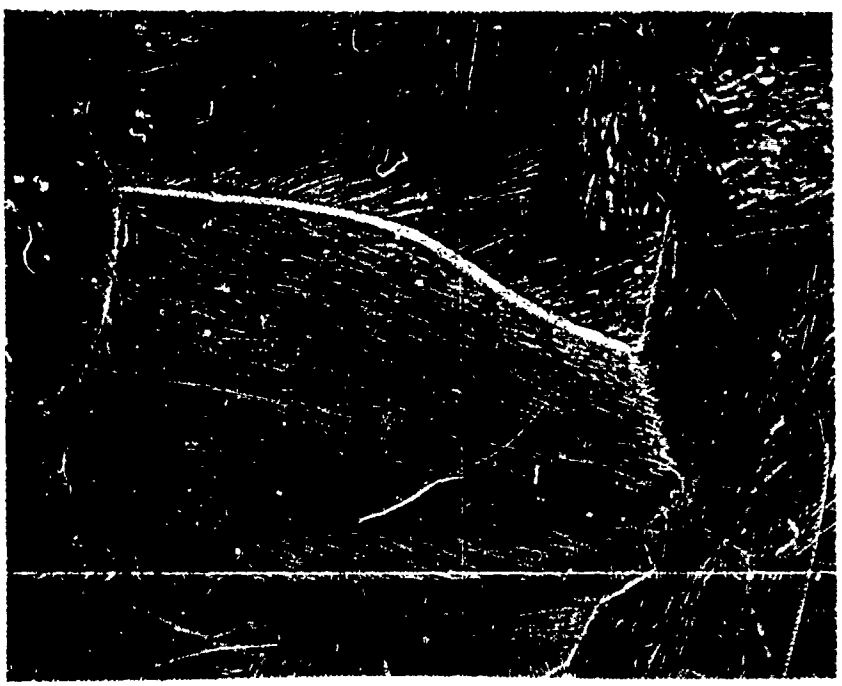

Figure 64. Ti-6Al-2Sn-4Zr-2Mo Bearing Housing. Casting G 6608 Microstructure. Etchant $2HF:2HNO_3:96H_2O$. 100X

3. Welding Evaluation

One area of interest in evaluating castings is the amenability of the material for joining by welding and for repair of defects by welding. A brief study was conducted on the weldability of castings of the four alloys as produced by this process.

Sections of the castability castings were joined by tungsten inert gas welding. Two sections of each alloy, .090" thick x 0.60" wide x 3.5" long were joined along the lengths using 2% thoriated tungsten 3/32" wire in an automatic welder. The sections were prepared for welding by a brief immersion in 5% HF:45%HNO_3:50% H_2O. In order to achieve full penetration with the 14 volts - 80 amperes welding current it was necessary to turn the specimens and weld from the reverse side after the initial pass. Helium was used in the torch and argon for the trailing shield and backup gas.

The welded cast sections were evaluated by radiographic inspection and bend testing. The weld beads were sound even though there was gas porosity and shrink evident in the castings.

The bend test consisted of three point loading as a beam supported on 1/4" rods with a 2" span. The tests were conducted at room temperature at a loading rate of 0.05 inches per minute. The bending was continued until fracture was initiated as indicated by the drop in load on the recorder. The welded specimens exhibited the following bending response:

	Max. Bend Degrees	Max. Load Lbs.
Ti 6Al-2Sn-4Zr-2Mo	23°	985
Ti 6Al-4V	29°	850
Ti 3Al-8V-6Cr-4Zr-4Mo	28°	770
Ti 11.5Mo-4.5Sn-6Zr	13°	660

The alpha beta alloys showed ductile fractures while the beta alloys fractured in a brittle manner. The specimens of Ti 6Al-4V as bend tested before and after welding are shown in Figure 65. The as-cast Ti 6Al-4V specimen bent 71° prior to fracture. Both specimens as shown exhibit lesser bends than the maximum achieved as they relaxed when the load was removed.

These results have shown that the cast titanium alloys can be welded to yield sound welds. The ductility of the alpha beta alloys as welded was superior to the beta alloys; however, the ductility was decreased significantly by the TIG welding process indicating the advisability of a post welding heat treatment to restore the ductility.

Figure 65. Bend Tests of Ti-6Al-4V As-Cast and as TIG Welded. Plates are 0.090" Thick Castability Specimens.

THIS
PAGE
IS
MISSING
IN
ORIGINAL
DOCUMENT

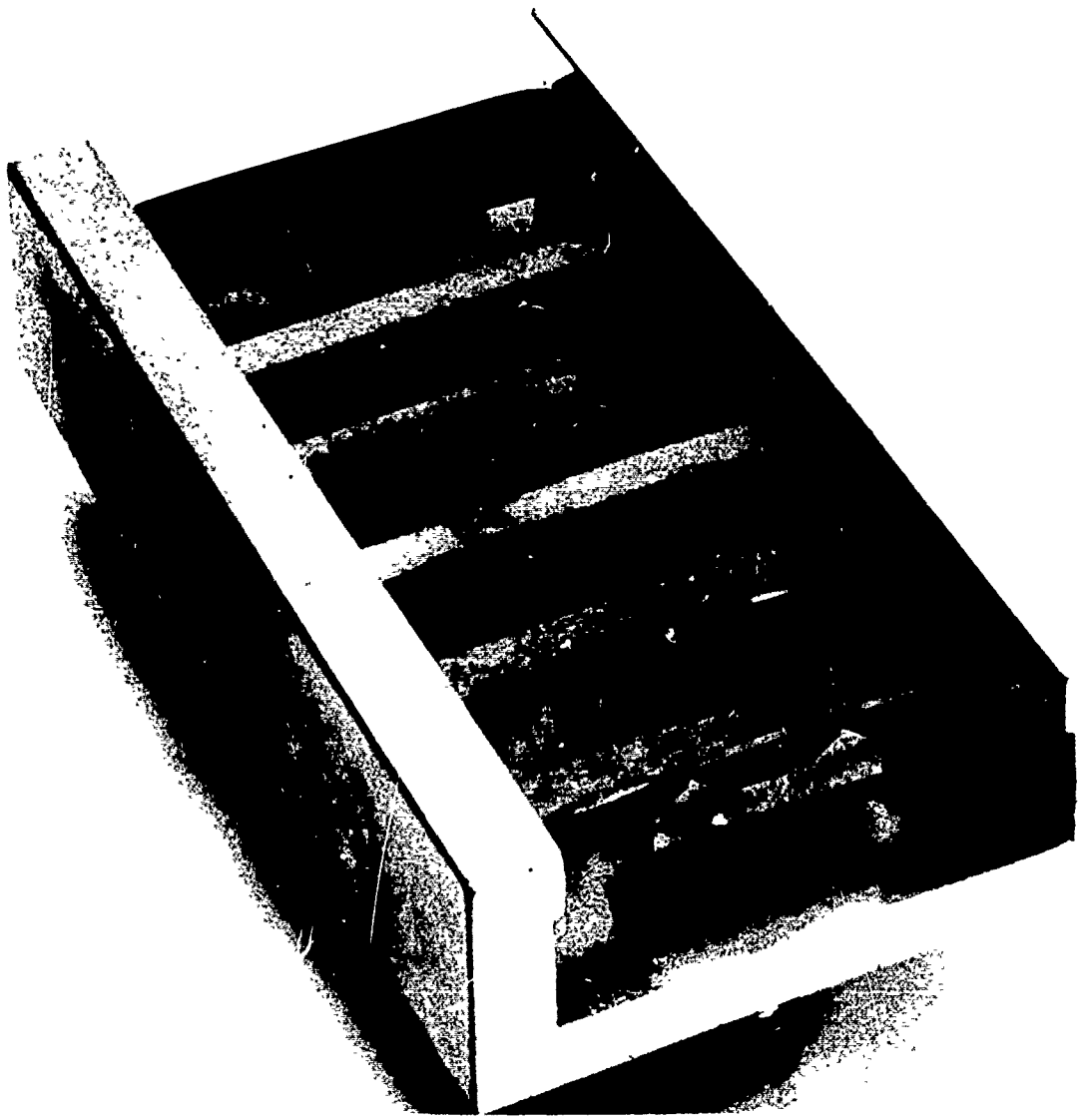

Figure 66. Stress Corrosion Test Fixture and Specimens for NaCl Environment.

TABLE VIII

Results of Stress Corrosion Tests

	Exposure Conditions				Post Exposure Bend Test at R.T.	
Specimen	Temp. (°F)	Stress (ksi)	Time (hrs)	Condition	Max. Deflection (in)	Ult. Load (lbs)
T		Unexposed - as stress relieved.			.214	69.6
B		"	"	" "	.154	68.0
T 1	95	104.8	1000	No exposure to sol'n	.277	74.2
T 5	"	none	"	Aerated 5% NaCl sol'n	.325	77.8
T 4	"	104.8	"	" " " "	.125	63.6
B 1	"	"	"	" " " "	.127	67.6
T 2	"	"	"	" " " "	.148	67.4
T 9	"	"	"	" " " "	.165	68.6
B 4	500	67.6	"	No exposure to NaCl	.098	64.2
B 5	"	none	"	NaCl coated	.098	61.6
T 7	"	67.6	"	" "	.084	56.2
T 8	"	"	"	" "	.109	65.8
T 3	"	"	"	" "	.170	66.6
B 2	"	"	"	" "	.085	56.6

Stress levels are 80% of the yield strengths of the Ti 6Al-2Sn-4Zr-2Mo alloy casting at exposure temperatures.

Post exposure bend tests at room temperature are performed at 0.100 in/min. crosshead speed, 1" span, .250" radius penetrator.

Temperatures were held at 95° ± 1/2°F and at 500° ± 3°F.

III CONCLUSIONS

The following conclusions have been drawn from the work performed in this program:

1. Pyrolytic coating of lost wax ceramic shell molds produces molds suitable for use with titanium alloys in the manufacture of precision investment castings. These molds may be preheated to 1500°F without producing reaction layers with the molten alloy that cannot be removed by surface grit blasting. Molds must be carefully prepared to avoid entrapment of mold inclusions within the casting, and must be carefully designed to avoid formation of hot tears during cooling.

2. Induction melting using semi-levitation techniques and bottom pouring in a machined graphite crucible gives constant, uniform, reproducible pouring temperatures. The process increases the carbon content of the alloy .10 to .15% in 6 to 10 pound melts.

3. Casting fluidity of alpha-beta alloys Ti-6Al-4V and Ti-6Al-2Sn-4Zr-2Mo is superior to beta alloys Ti-3Al-8V-6Cr-4Zr-4Mo and Ti-11.5Mo-4.5Sn-6Zr (Beta III).

4. Tensile properties of the alpha-beta alloys poured using this system were acceptable in strength, ductility, and notch sensitivity. Beta alloys showed excellent strengths but low ductilities, which were caused by formation of a carbide phase during melting. Induction melting in graphite crucibles is thus not recommended for beta alloys.

5. Castings made using this system were subject to unacceptable amounts of porosity with respect to present specifications. This porosity was caused by exsolution of dissolved gas contained in the charge material. Use of heavy gating systems or nonstatic pouring methods is recommended to reduce gas porosity in titanium casting.

6. Induction melted alloys may be successfully welded. Post welding heat treatment is recommended to develop full ductility.

APPENDIX A

Summary of Heats Poured

Heat No.	Alloy	Mold Type	Mold No.	Mold Preheat Time (hrs)	Preheat Temp. (°F)	Maximum Pressure (μ)	Crucible Preheat Time (hrs)	Crucible Preheat Temp. (°F)
G 6010	6-4	C	103	0.5	1000	10	-	-
G 6011	6-4	C	106	0.5	1000	10	-	-
G 6012	6-4	C	104	0.5	1500	2	-	-
G 6013	6-4	C	107	0.5	1500	8	-	-
G 6027	6-4	C	120	0.5	1500	19	-	-
G 6028	6-4	C	112	0.5	2000	12	-	-
G 6048	6-4	C	117	0.5	2000	20	-	-
G 6049	6242	C	108	0.5	1000	12	-	-
G 6050	6242	C	110	0.5	1000	12	-	-
G 6051	6242	C	115	0.5	1500	11	-	-
G 6052	6252	C	NA	0.5	1500	9	-	-
G 6053	6242	C	122	0.5	2000	13	-	-
G 6054	6242	C	116	0.5	2000	13	-	-
G 6055	6-4	T	121	0.5	2000	12	-	-
G 6064	38644	C	130	0.5	1000	15	-	-
G 6065	38644	C	131	0.5	1000	10	-	-
G 6080	38644	C	129	0.5	1500	15	-	-
G 6081	38644	C	134	0.5	1500	10	-	-
G 6082	38644	C	127	0.5	2000	Crucible run out prior to pour		
G 6094	38644	C	133	0.5	2000	10		
F 7367	6242	T	148	0.5	2000	80	-	-
G 6230	6-4	T	161	0.5	2000	2000	Argon added prior to pour	
G 6231	38644	T	163	0.5	2000	2000	Argon added prior to pour	
G 6232	6-4	QBH	NA	0.5	2000	2000	Argon added prior to pour	
G 6299	6242	C	NA	3.5	2000	56		

(continued)

APPENDIX A (cont'd)

Summary of Heats Poured

Heat No.	Alloy	Mold Type	Mold No.	Mold Preheat Time (hrs)	Preheat Temp. (°F)	Maximum Pressure (μ)	Crucible Preheat Time (hrs)	Crucible Preheat Temp. (°F)
G 6300	38644	C	123	6.0	2000	2000	Argon added prior to melt	
G 6325	Beta III	C	155	0.5	1000	42		
G 6326	Beta III	C	158	0.5	1500	10		
G 6327	Beta III	C	144	0.5	2000	Crucible run out prior to pour		
G 6328	Beta III	C	135	0.5	1500	6	-	-
G 6329	Beta III	C	143	0.5	1000	7	-	-
G 6330	Beta III	C	159	0.5	2000	8	-	-
G 6331	Beta III	C	160	0.5	2000	8	-	-
F 7617	6-4	T	140	6.5	1750	53	-	-
F 7618	6-4	T	138	0.5	1750	30	-	-
F 7619	6242	T	154	0.5	1750	29	-	-
F 7620	6242	T	142	0.5	1750	22	-	-
F 7621	Beta III	T	137	0.5	1750	16	-	-
F 7634	Beta III	T	153	0.5	1750	23	-	-
F 7635	38644	T	147	0.5	1750	40	-	-
F 7636	38644	T	149	0.5	1750	15	-	-
F 7642	6242	QBH	197	0.5	1750	44	-	-
G 6373	38644	T	151	0.5	1500	9	-	-
G 6374	6-4	T	156	0.5	1500	6	-	-
G 6375	6242	T	167	0.5	1500	6	-	-
G 6376	Beta III	T	157	0.5	1500	4	-	-
G 6509	6242	QBH	NA	4.0	1500	35	1.0	1800
G 6510	6242	QBH	NA	4.0	1500	15	1.0	1800
G 6543	6242	QBH	202	3.75	1250	10	2.0	1500
G 6544	6242	QBH	201	3.0	1000	5	2.0	1500

(continued)

APPENDIX A (cont'd)

Summary of Heats Poured

Heat No.	Alloy	Mold Type	Mold No.	Mold Preheat Time (hrs)	Preheat Temp. (°F)	Maximum Pressure (μ)	Crucible Preheat Time (hrs)	Crucible Preheat Temp. (°F)
G 6607	6242	QBH	206	2.7	1000	16	1.5	2500
G 6608	6242	QBH	205	2.7	1250	9	2.0	2400
G 6818	6-4	T	165	0.5	1000	NA	-	-
G 6826	6242	SB	-	12.0 (air)	400	47	-	-
G 6827	6242	SB	-	4.0	400	6	4.0	>2400
G 6828	6242	SB	-	4.0	400	5	4.0	>2400
G 6829	6-4	Cup	-	1.0	400	4	1.0	>2400
G 6852	6-4	Cup	-	1.0	400	10	1.0	>2400
G 6853	6242	Cup	-	1.0	400	5	1	>2400
G 6854	6242	Cup	-	1.0	400	4	1.0	>2400
G 6884	6242	SB	-	4.0	400	5	4.0	>2400
G 6885	6242	SB	-	4.0	400	2	4.0	>2400
G 6910	6242	T	211	2-4	2500-400	4	0.5	>2400
G 6911	6242	T	210	0.5	400	NA	0.5	>2400
G 6912	6242	T	216	2-4	2500-400	NA	0.5	>2400
G 6913	6242	T	215	0.5	400	4	0.5	>2400
G 6927	6242	C	228	0.5	1000	4	0.1	2500
G 6928	6-4	C	226	0.5	1000	5	0.1	2500
G 6929	6242	C	229	0.5	1000	NA	0.1	2500
G 6930	6-4	C	227	6.5	1000	5	0.1	2500
G 6934	6242	T	233	1.0	2000	30	0.5	2500
G 6935	6242	T	232	1.0	2000	4	0.5	2500
G 6936	6242	T	224	1.0	400	2	0.5	2500
G 6937	CP	T	222	1.0	1250	2	0.5	2500

C = Castability
T = Tensile Cluster
QBH = Quarter Bearing Housing
SB = Steel Bottle

APPENDIX B

Process Specification - Induction Melting and Casting of Titanium Alloys

This specification shall define the process steps and controls required for the production of shaped casting in pyrolytic graphite molds by induction melting.

1. Flow Chart

The flow chart is given in Figure 67.

2.0 Molds

2.1 Molds shall be formed by low wax ceramic shell techniques. Either ethyl silicate or aqueous silica sols may be employed as binders. Particle size of stucco shall be that which permits the attainment of acceptable casting surface.

2.2 The use of preformed ceramic cores is permitted.

2.3 Molds shall be fired after conventional wax pattern removal operations to complete pattern removal.

2.3.1 Molds shall be thoroughly cleaned prior to coating. All loose particles of ceramic shall be removed from the mold.

2.4 Molds shall be coated in accordance with U.S. Patent No. 3,284,862.

2.4.1 Thickness of pyrolytic graphite shall be limited to 0.002".

2.4.2 Molds shall be properly vented to assure that there is no stagnation of the gas stream within the mold cavity.

2.5 Molds shall be degassed prior to pouring.

2.5.1 Degassing procedure shall be as follows:

2.5.1.1 Heat 24 hours at 400°F prior to placing in vacuum chamber.

2.5.1.2 Place the mold in the vacuum chamber. Evaluate chamber to 10^{-2} torr or below.

2.5.1.3 Preheat mold to 1000°F minimum. Hold 30 minutes minimum at temperature under vacuum. Preheat temperatures above 1500°F are not recommended.

2.5.2 Molds are not to be removed from high vacuum environment between degassing and pouring.

3.0 Crucibles

3.1 Crucibles are to be machined from Graphitite G grade graphite, product of the Carborundum Co.) or its equivalent, or are to be formed from pyrolytic graphite.

3.2 Crucible wall thickness shall be 0.100" + .025" - .0".

3.3 Crucibles shall have an orifice in the crucible bottom appropriately sized for the charge weight and pour rate desired. This orifice shall have a nozzle attached to direct the pour stream.

3.4 Crucibles shall be degassed prior to pouring.

3.4.1 Degassing procedure shall be as follows:

3.4.1.1 Heat crucibles 24 hours at 400°F prior to placing in vacuum chamber.

3.4.1.2 Place crucible in vacuum chamber. Evacuate chamber to 10^{-2} torr or below.

3.4.1.3 Preheat crucible to 2400°F minimum. Hold 20 minutes at temperature under vacuum.

3.4.2 Crucibles are not to be removed from high vacuum environment between degassing and melting.

4.0 Charge

4.1 Charge chemistry shall conform to specifications established by end users of castings. Melting of beta alloy composition is not recommended.

4.2 The charge shall consist of three pieces, a rod, a charge slug, and a melt-out disk.

4.2.1 The purpose of the rod is to support the charge slug. The rod shall be 1" diameter maximum. It is affixed by welding to the center of the charge slug.

4.2.2 The charge slug contains the bulk of the charge weight. It shall be cylindrical in shape, and is to be sized such that there is a minimum clearance between the slug and the crucible of 0.125 inch.

4.2.3 The purpose of the melt-out disk is to retain the molten charge during superheat. It should have a minimum clearance between itself and the crucible of 0.025" and a maximum clearance of 0.050". The disk is to be flat on the bottom and may be dished on the top.

4.3 Charge materials shall be degassed before pouring.

4.4 Degassing procedure shall be as follows:

4.4.1 Place charge assembly (disks, and rod and slug assemblies) in vacuum furnace chamber.

4.4.2 Evacuate chamber to below 1×10^{-5} torr.

4.4.3 Heat charge materials to 1800°F. Hold four hours at temperature under vacuum.

4.4.4 Furnace cool under vacuum to below 200°F before removing from furnace.

5.0 Melt Procedure

5.1 Place the disk in the bottom of the crucible.

5.2 Suspend the charge slug from the roof of the vacuum chamber.

5.3 Arrange the crucible such that there is at least 1" clearance between the bottom of the charge slug and the top of the disk. The crucible should be long enough to come up over the top of the charge.

5.4 Arrange the mold beneath the crucible so that the pour cup is directly beneath (on the same axis) the pouring orifice in the crucible.

5.5 Evacuate the furnace to a pressure of less than 10^{-2} torr. If the furnace is not equipped for continuous operation, perform mold and crucible degassing operations at this time.

5.6 When degassing and mold preheating is completed, apply power to charge at the rate of 3 to 4 KW per pound of cnarge. Maintain power level until charge begins to melt around sides. It may be necessary to increase the power to 5 KW per pound to achieve melting.

5.7 When melting begins, increase power to 10 KW per pound of charge. Maintain this power level until charge melts through the disk and discharges into the mold.

5.8 When the melt has discharged into the mold, turn off the power. The furnace may be filled with inert gas to speed cooling of the cast cluster.

5.9 The casting may be removed to the atmosphere as soon after pouring as convenient.

6.0 Finishing and Inspection

Castings shall be finished and inspected according to procedures agreed upon by the casting vendor and the manufacturer.

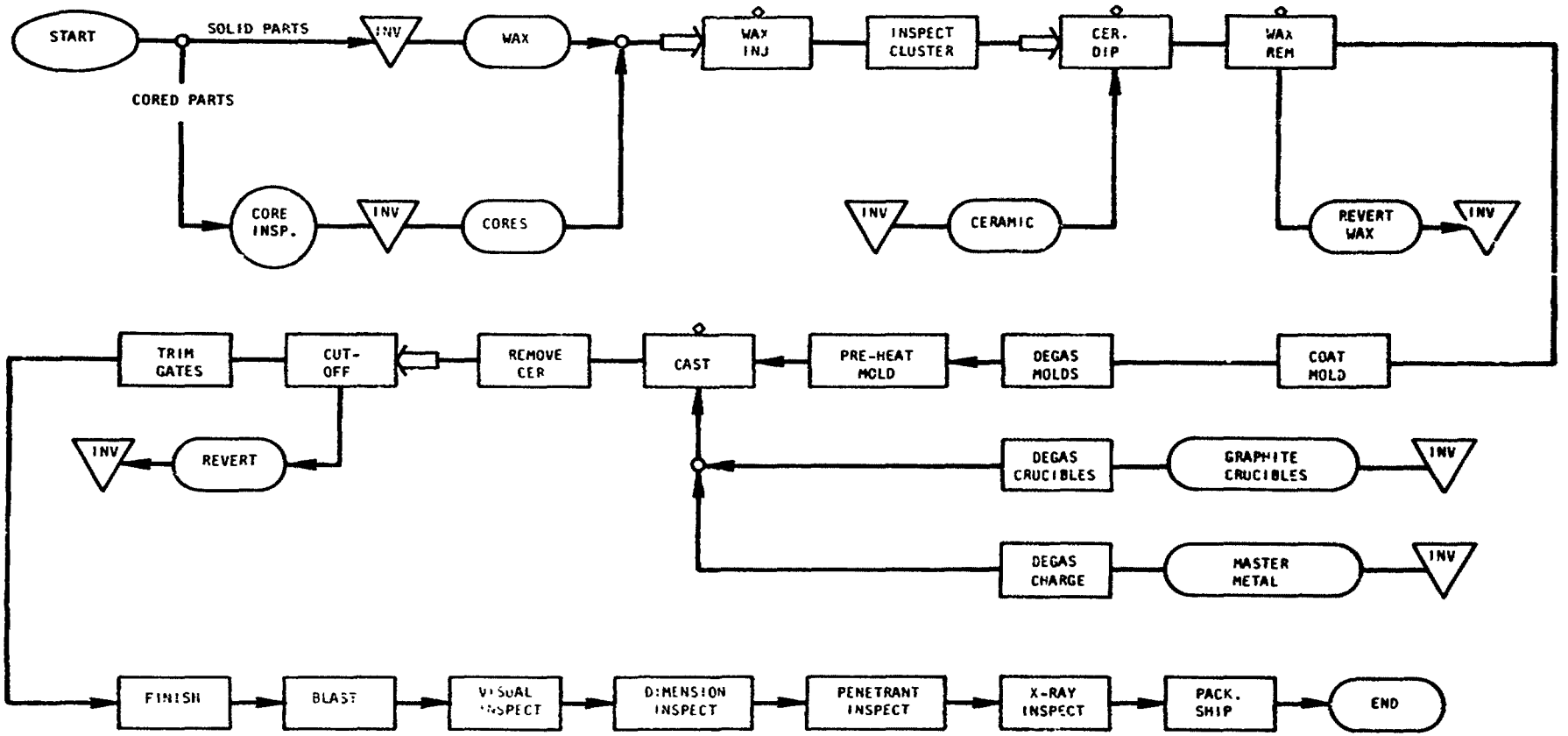

Figure 67. Process Flow Chart for Induction Melting and Casting of Titanium Alloys into Pyrolytic Graphite Coated Molds.

REFERENCES

1. I. Cadoff and J.P. Nielsen, Trans AIME, Feb. 1953, p 248.
2. M. Hansen, Constitution of Binary Alloys, 2nd ed. McGraw-Hill, New York, 1958, p 1019.
3. Product Engineering, Dec. 21, 1970, p 6.
4. B.C. Weber, W.M. Thompson, H.O. Bielstein, and M.A. Schwartz, J. Am. Cer. Soc., 40, 1957, p 363.
5. M. Garfinkle and H.M. Davis, Trans. ASM, 58, 1965, p 520.
6. G.V. Samsonov, G.A. Yasinkaya, and E.A. Shiller, Ogneupory, 1, 1961, p 335.
7. W.A. Pfeifer, J. Metals, May 1965, p 487.
8. P.J. Ahearn, C.F. Frey, and J.F. Wallace, TMS-AIME, Apr. 1958, p 274.
9. J. Zotos, P.J. Ahearn, and H.M. Green, Trans AFS, 66, 1958, p 225.
10. E. Fromm and H. Jehn, Z. Metallkune, 56, 1965, p 599.
11. E.M. Grala, Final Report, Naval App. Sci. Lab., project N00140-69-C-240, March 1970.
12. T.C. Tsareff and U.L. Hellman, Six Month Tech Mgt Report, 15 June - 31 Dec. 1969, AFML project F33615-69-C-1608.
13. T.C. Goel and B.A. Unvala, Rev. Int Hautes Temper. et Refract., 7, 1970, p 197.
14. H.C. Child and A.L. Dalton, Brit. Pat. #1,049,624, 1966.
15. C.E. Shamblen, ASM Titanium Metallurgy Course, New York University, 1969.
16. W.H. Schweikert, U.S. Patent #3,284,862, 1966.
17. R.P. Elliott, Constitution of Binary Alloys, First Supplement, McGraw-Hill, New York, 1965, p 232.
18. H.G. Poole, Titanium Metallurgy Course, New York University, 1965.
19. T.S. Piwonka and M.C. Flemings, TMS-AIME, 236, 1966, p 1157.
20. R.L. Coble and M.C. Flemings, Met. Trans, 2, 1972, p 409.
21. L.A. Elagina, Metall ovedi Term. Obrabotka Metall, 6, 1964, p 23.
22. O.N. Magnitskiy, Casting Properties of Titanium Alloys, Translation by Foreign Tech. Div., WPAFB, Trans No. FTD-HT-386-69, Apr. 1970.
23. E. Ya. Kukkonen, G.A. Kaplunovskii, A.A. Demidova, O.N. Magnitskiy, and B.B. Gulyaev, Gases in Cast Metals, Translation by Consultants Bureau, New York, 1965, p 145.
24. O.N. Magnitskiy, ibid, p 149.
25. H.R. Gray, Corrosion - NACS, May 1972, p 186.

REFERENCES (cont'd)

26. H.B. Dexter, NASA TN D-3299.

27. S.W. McClaren, O.H. Cook, and G. Pascador, AFML-TR-68-264, AFML, WPAFB, Oh. April 1969, p 117.

DISTRIBUTION LIST

Contract F33615-70-C-1409

AFAPL/TBP
Wright-Patterson AFB, Ohio 45433

AFFDL/FBS
Wright-Patterson AFB, Ohio 45433

AFML/LAM (Library)
Wright-Patterson AFB, Ohio 45433

AFML/MXE (Mr. C.L. Harmsworth)
Wright-Patterson AFB, Ohio 45433

AFML/LLN (Mr. T.C. Cooper)
Wright-Patterson AFB, Ohio 45433

AFFDL/DA/Mr. S. Inouye)
Wright-Patterson AFB, Ohio 45433

AFML/LLP (Mr. P.L. Hendricks)
Wright-Patterson AFB, Ohio 45433

AFML/LLP (Mr. I. Perlmutter)
Wright-Patterson AFB, Ohio 45433

AFML/LLP (Dr. C.M. Pierce)
Wright-Patterson AFB, Ohio 45433

AFML/LTM (Mr. K.L. Love)
Wright-Patterson AFB, Ohio 45433

ASD/INH
Wright-Patterson AFB, Ohio 45433

AFML/MXA (Mr. C. Lombard)
Wright-Patterson AFB, Ohio 45433

ASD/ENJET (Mr. J.R. Rhodehamel)
Wright-Patterson AFB, Ohio 45433

FTD/PDTI
Wright-Patterson AFB, Ohio 45433

AFRPL (RPMCH)
Edwards AFB, California 93523

Hq. USAF (AFSPI/Mr. W. Martin
ThePentagon
Washington, D.C. 20330

OCAMA (OCRM)
Tinker AFB, Oklahoma 73145

SAMSO (SMT/AFML)
AF Unit Post Office
Los Angeles, California 90045

(ARMY)

Army Materials Research Agency
Attn: Mr. S.V. Arnold
Watertown, Massachusetts 02172

Army Production Equipment Agency
Attn: Chief, Manufacturing
Technology Division
Rock Island Arsenal
Rock Island, Illinois 61202

Army Research Office
3045 Columbia Pike
Arlington Virginia 22214

Frankford Arsenal
Pittman Dunn Laboratory
Attn: Mr. Harold Markus
Philadelphia, Pennsylvania 19137

(NAVY)

Commander
Naval Ordnance Test Station
Attn: Code P80931
Pasadena Annex
3202 E. Foothill Boulevard
Pasadena, California 91107

Department of the Navy
Naval Air Systems Command
Materials Research & Technology
RRMA-2/Mr. R.F. Kearns
Washington, D.C. 20330

DISTRIBUTION LIST (cont'd)

Contract F33615-70-C-1409

(NAVY)

Mr. Frank Lengenfelder
U.S. Naval Ship Research
and Development Laboratories
Code A934
Annapolis, Maryland 24102

(NASA)

NASA
Attn: R.H. Raring
DUZ-7026, Code RRM
Washington, D.C. 20036

National Aeronautics & Space
Administration
Lewis Research Center
Attn: Mr. John L. Shannon, Jr. MS 105-1
Cleveland, Ohio 44135

(OTHER)

Bureau of Mines
Albany Metallurgy Research Center
Metals Processing Projects
P.O. Box 70
Albany, Oregon 97321

Defense Documentation Center (DDC)
Cameron Station (2 cys)
Alexandria, Virginia 22314

National Academy of Science
National Research Council
Materials Advisory Board
Attn: Dr. Joseph Lane
2101 Constitution Avenue
Washington, D.C. 20036

Abex Corporation
Research Center
Mahwah, N.J. 07340

Amsted Research Laboratories
Attn: C. Robert Lillie
340 County Line Road
P.O. Box 567
Bensenville, Illinois 60106

Arwood Corporation
Groton Plant
Poquonnock Road
Groton, Connecticut 06340

Avco Corporation
Lycoming Division
Attn: Manager, Manufacturing Res.
350 S. Main Street
Stratford, Connecticut 06497

Avco Corporation
Lycoming Division
Attn: Director
Materials Laboratory
550 S. Main Street
Stratford, Connecticut 06497

Boeing Company
Aerospace Group
Technical Library
Mail Stop K-38
P.O. Box 3996
Seattle, Washington 98124

Boeing Company
Commercial Airplane Division
Technical Library
Mail Stop 74-60
Seattle, Washington 98124

Boeing Company
Vertol Division
Technical Library
P.O. Box 16858
Philadelphia, Pennsylvania 19142

Boeing Company
Wichita Division
Technical Library
3801 South Oliver
Wichita, Kansas 67210

Continental Aviation & Eng. Corp.
Attn: Mr. T. Weidig
Research & Advanced Div.
12700 Kercheval Avenue
Detroit, Michigan 48215

DISTRIBUTION LIST (cont'd)

Contract F33615-70-C-1409

Crucible Steel Company
Attn: Mr. E.J. Dulis
Director of Research
P.O. Box 7257
Pittsburgh, Pennsylvania 15213

Eaton, Yale & Towne, Inc.
Research Center
26201 Northwestern Highway
Southfield, Michigan 48075

Ford Motor Company
Process Development Department
Manufacturing Development Office
Attn: Mr. L. Martin, Jr.
24500 Glendale Avenue
Detroit, Michigan 48239

The Garrett Corporation
333 W. First Street
Dayton, Ohio 45402

General Dynamics Corporation
Convair Division
Attn: Mr. A. Hurlich
Manager, Materials & Processes
P.O. Box 1128
San Diego, California 92112

General Electric Company
Aircraft Engine Group
Attn: Mr. R. Peebles
Mail Drop M-76
Cincinnati, Ohio 45115

General Motor Corporation
Allison Division
224 N. Wilkinson Street
Dayton, Ohio 45402

General Motors Corporation
Research Center
Metallurgy Department
Attn: Mr. S. Willner
Twelve Mile & Mound Roads
Warren, Michigan 48090

Howmet Corporation
Reactive Metals Products Div.
555 Benston Road
Whitehall, Michigan 49461

IIT Research Institute
Director of Metals Research
10 West 35th Street
Chicago, Illinois 60616

Investment Casting Corp.
Attn: Mr. Joseph Levine
60 Brown Avenue
Springfield, New Jersey 07081

Lockheed-Georgia Company
Attn: Mr. H. Stemme
86 S. Cobb Drive
Marietta, Georgia 30060

LTV, Inc.
Vought Aeronautics Division
Attn: Library
P.O. Box 5907
Dallas, Texas 75222

LTV, Inc.
Vought Aeronautics Division
Attn: Mr. O. Cook
P.O. Box 5907
Dallas, Texas 75222

McDonnell Douglas Corporation
McDonnell Aircraft Company
General Engineering Division
Material & Process Development
Attn: Mr. Robert E. Newcomer
Technical Specialist
St. Louis, Missouri 63166

Mitron Research & Development Corp.
Attn: Dr. R.A. Rosenberg
8999 Main Street
Waltham, Massachusetts 02154

DISTRIBUTION LIST (cont'd)

Contract F33615-70-C-1409

North American Rockwell Corp.
Columbus Division
Attn: Mr. J.E. Bellitt
1104 Talbott Tower
Dayton, Ohio 45402

Northrop Corporation
Norair Division
Attn: Technical Library
3901 West Broadway
Hawthorne, California 90250

Oregon Metallurgical Corporation
Attn: Director of Research
P.O. Box 484
Albany, Oregon 97321

Precision Castparts Corporation
4600 S.E. Harney Drive
Portland, Oregon 97206

Reactive Metals, Inc.
Attn: Technical Director
Niles, Ohio 44446

REM Metals Corporation
P.O. Box 829
Albany, Oregon 97321

Research Enterprises Corporation
Attn: Mr. C.R. Wheeler
222 S. Ball Park Plaza
Scottsdale, Arizona 85251

TILINE, Inc.
150 W. Queen Avenue
Albany, Oregon 97321

Titanium Technology Corporation
P.O. Box 60
Pomona, California 91769

Titanium West, Inc.
Attn: President
P.O. Box 3056
Reno, Nevada 89505

TMCA
Application Development Center
Attn: Mr. R.G. Broadwell
195 Clinton Road
West Caldwell, New Jersey 07006

TRW Inc.
Materials Technology Group
Attn: Mr. C.R. Cook, T/M 2968
23555 Euclid Avenue
Cleveland, Ohio 44117

United Aircraft Corporation
Pratt & Whitney Division
Attn: Field Representative
Suite 1311, Talbott Tower
Dayton, Ohio 45401

Universal-Cyclops Specialty
Steel Division
Technical Information Center
Mayer Street
Bridgeville, Pennsylvania 15017

Westinghouse Electric Corp.
Power Circuit Breaker Div.
Attn: Mr. Ronald R. Akers
Department 11L13
East Pittsburgh, Pennsylvania 15112

Whittaker Corporation
Nuclear Metals Division
Attn: Librarian
West Concord, Massachusetts 01781

Williams Research Corporation
Attn: Mr. W.P. Schimmel
2280 W. Maple Road
Walled Lake, Michigan 48088

DISTRIBUTION LIST (cont'd)

Contract F33615-70-C-1409

Crucible Steel Company
Attn: Mr. E.J. Dulis
Director of Research
P.O. Box 7257
Pittsburgh, Pennsylvania 15213

Eaton, Yale & Towne, Inc.
Research Center
26201 Northwestern Highway
Southfield, Michigan 48075

Ford Motor Company
Process Development Department
Manufacturing Development Office
Attn: Mr. L. Martin, Jr.
24500 Glendale Avenue
Detroit, Michigan 48239

The Garrett Corporation
333 W. First Street
Dayton, Ohio 45402

General Dynamics Corporation
Convair Division
Attn: Mr. A. Hurlich
Manager, Materials & Processes
P.O. Box 1128
San Diego, California 92112

General Electric Company
Aircraft Engine Group
Attn: Mr. R. Peebles
Mail Drop M-76
Cincinnati, Ohio 45115

General Motor Corporation
Allison Division
224 N. Wilkinson Street
Dayton, Ohio 45402

General Motors Corporation
Research Center
Metallurgy Department
Attn: Mr. S. Willner
Twelve Mile & Mound Roads
Warren, Michigan 48090

Howmet Corporation
Reactive Metals Products Div.
555 Benston Road
Whitehall, Michigan 49461

IIT Research Institute
Director of Metals Research
10 West 35th Street
Chicago, Illinois 60616

Investment Casting Corp.
Attn: Mr. Joseph Levine
60 Brown Avenue
Springfield, New Jersey 07081

Lockheed-Georgia Company
Attn: Mr. H. Stemme
86 S. Cobb Drive
Marietta, Georgia 30060

LTV, Inc.
Vought Aeronautics Division
Attn: Library
P.O. Box 5907
Dallas, Texas 75222

LTV, Inc.
Vought Aeronautics Division
Attn: Mr. O. Cook
P.O. Box 5907
Dallas, Texas 75222

McDonnell Douglas Corporation
McDonnell Aircraft Company
General Engineering Division
Material & Process Development
Attn: Mr. Robert E. Newcomer
Technical Specialist
St. Louis, Missouri 63166

Mitron Research & Development Corp.
Attn: Dr. R.A. Rosenberg
8999 Main Street
Waltham, Massachusetts 02154

Unclassified
Security Classification

DOCUMENT CONTROL DATA - R & D

(Security classification of title, body of abstract and indexing annotation must be entered when the overall report is classified)

1 ORIGINATING ACTIVITY (Corporate author) TRW Materials Development Department - TRW Inc.	2a. REPORT SECURITY CLASSIFICATION Unclassified 2b. GROUP

3 REPORT TITLE

Manufacturing Method for Precision Casting Titanium Alloy Aircraft Components

4. DESCRIPTIVE NOTES (Type of report and, inclusive dates)

5. AUTHOR(S) (First name, middle initial, last name)

T.S. Piwonka and C.R. Cook

6 REPORT DATE July 1972	7a. TOTAL NO. OF PAGES	7b. NO. OF REFS 27
8a. CONTRACT OR GRANT NO. b. PROJECT NO. F33615-70-C-1409 164-0 c. d.	9a. ORIGINATOR'S REPORT NUMBER(S) ER-7468-8 9b. OTHER REPORT NO(S) (Any other numbers that may be assigned this report) AFML-TR-72-	

10. DISTRIBUTION STATEMENT

This document is subject to special export controls and each transmittal to foreign governments or foreign nationals may be made only with prior approval of the Manufacturing Technology Division, Air Force Materials Laboratory, AFB, Ohio 45433

11. SUPPLEMENTARY NOTES	12. SPONSORING MILITARY ACTIVITY Air Force Materials Laboratory/LTP Wright-Patterson AFB, Ohio 45433

13 ABSTRACT

Induction melting of titanium alloys using a semi-levitation technique and bottom pouring in a graphite crucible was evaluated for four titanium alloys. Ti-6Al-4V, Ti-6Al-2Sn-4Zr-2Mo, Ti-3Al-8V-6Cr-4Mo-4Zr (Beta C), and Ti-11Mo-4.5Sn-6Zr (Beta III). Precision investment (lost wax) casting molds coated with pyrolytic graphite were used with the melting technique to make castability, tensile specimen, and bearing housing segment castings. Castability and tensile properties of the alloys were characterized. Bearing housing segments were subject to porosity which was extensively studied. Process capabilities and limitations were investigated for induction melting and the pyrolytic graphite coated mold. Properties of castings were determined, and weldability of the four cast alloys evaluated. Effects of the casting process on microstructure were investigated.

Unclassified
Security Classification

14 KEY WORDS	LINK A		LINK B		LINK C	
	ROLE	WT	ROLE	WT	ROLE	WT
Titanium Alloys						
Investment Casting						
Vacuum Induction Melting						
Aircraft Engine Casting						
Pyrolytic Graphite Molds						

DD FORM 1 NOV 68 1473 (BACK)
S/N 0101-807-6821

Unclassified
Security Classification